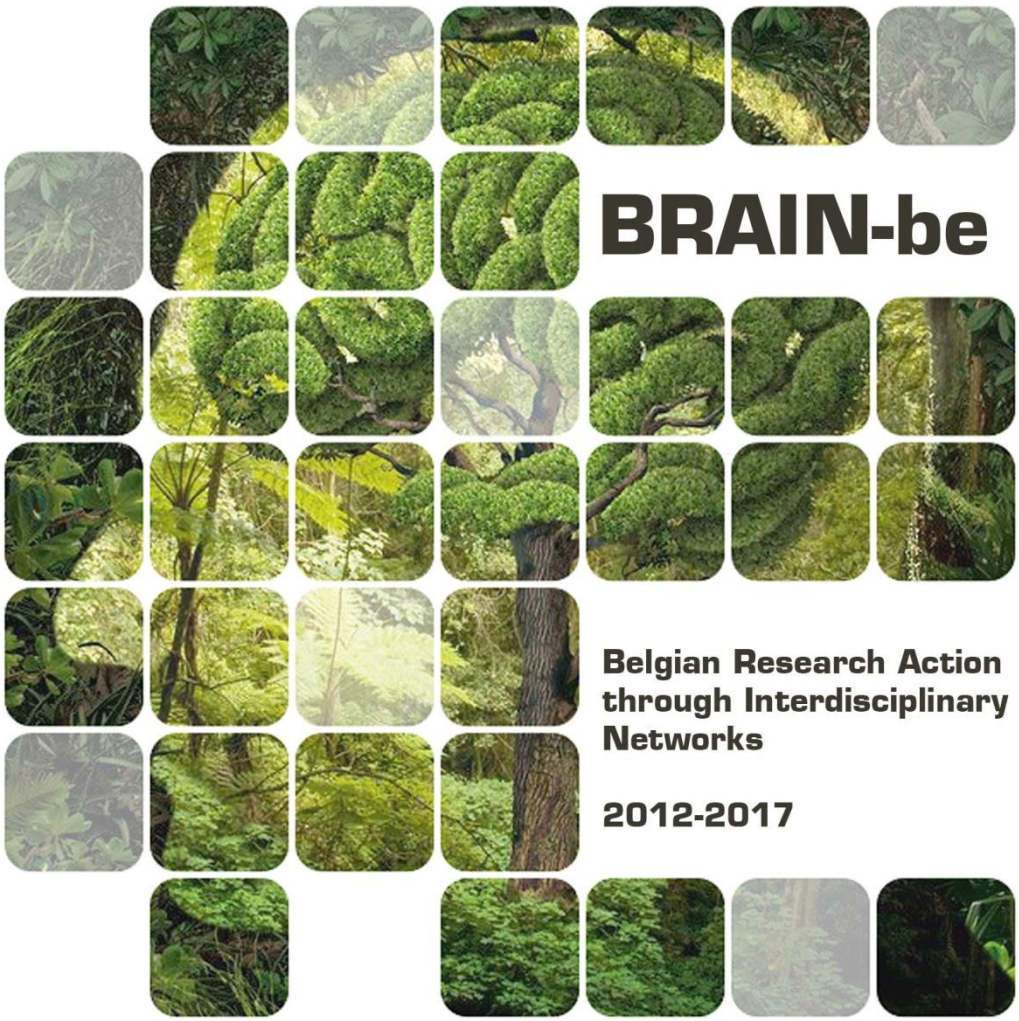

To^{2}DeNano

Towards a toxicologically relevant definition of nanomaterials

Peter Hoet (KU Leuven) – Lode Godderis (KU Leuven) – Sivakumar Murugadoss (KU Leuven) – Jan Mast (Sciensano) – Frederic Brasinne (Sciensano) – Dominique Lison (UCL) – Sybille van den Brule (UCL) –Jasmine Petry (FPS Economy) – Noham Sebaihi (FPS Economy)

Axis 4: Federal public strategies

belspo .be

NETWORK PROJECT

To^{2}DeNano

Towards a toxicologically relevant definition of nanomaterials

Contract - BR/154/A4/To^{2}DeNano

FINAL REPORT

Date:12/04/2019

PROMOTORS: Peter Hoet and Lode Godderis (KU Leuven, Leuven)
Dominique Lison (UCL, Brussels)
Jan Mast (Sciensano, Brussels)
Jasmine Petry (FPS Economy, Brussels)

AUTHORS: Peter Hoet, Lode Godderis and Sivakumar Murugadoss (KU Leuven)
Jan Mast and Frederic Brassinne (Sciensano)
Dominique Lison and Sybille van den Brule (UCL)
Jasmine Petry and Noham Sebaihi (FPS Economy)

KU LEUVEN UCL Université catholique de Louvain sciensano economie belspo .be

Published in 2019 by the Belgian Science Policy Office
WTC III
Simon Bolivarlaan 30
Boulevard Simon Bolivar 30
B-1000 Brussels
Belgium
Tel: +32 (0)2 238 34 11 - Fax: +32 (0)2 230 59 12
http://www.belspo.be
http://www.belspo.be/brain-be

Contact person: BOURGEOIS Emmanuèle
Tel: +32 (0)2 238 34 94

Hoet P., Godderis L., Mast J., Lison D., Petry J., Murugadoss S., Brassinne, F., van den Brule, S. & Sebaihi, N. ***Towards a toxicologically relevant definition of nanomaterials***. Final Report. Brussels : Belgian Science Policy Office 2019 – 71 p. (BRAIN-be - Belgian Research Action through Interdisciplinary Networks)

TABLE OF CONTENTS

ABSTRACT

Context: The current European Union (EU) definition of manufactured nanomaterial (MNM) covers "*particles, in an unbound state, or as an aggregate or as an agglomerate and where, for 50 % or more of the particles in the number size distribution, one or more external dimensions is in the size range 1 nm - 100 nm*"(EU 2011). In this definition, the size threshold 100 nm was adopted for regulatory purposes but its toxicological relevance has not been assessed in detail.

Objective: The main objective of To^{2}DeNano project was to provide scientific insight on how to consider MNM size distribution and agglomeration/aggregation (AA) status in a regulatory context, with regard to hazard.

Conclusion: (1) AA and particle size distributions of MNM influence their toxicity/biological activity. (2) we conclude that the 100 nm threshold in the current EU definition may not be appropriate to classify MNM with regard to hazard.

Keywords: nanomaterials, EU definition, exposure, aggregation/agglomeration, hazard.

1 INTRODUCTION

Agglomeration/aggregation of MNM is an ubiquitous phenomenon and its dynamic behaviour throughout their life cycle poses the greatest challenge in assessing human health impacts. This is clearly recognised in the EU recommended definition of nanomaterials stating "*particles, in an unbound state, or as an **aggregate or as an agglomerate** and where, for **50 % or more** of the particles in the number size distribution, one or more external dimensions is in the size range **1 nm - 100 nm***" (EU 2011). The toxicological relevance of this definition has, however, not been assessed in detail. In particular, a sound justification for considering equally unbound, aggregated and/or agglomerated particles is not available. The issue of size distribution is also not well settled on a toxicological basis. These issues have been the sources of a lingering debate in the regulatory context, hampering the application of regulations and the development of guidelines to monitor NM in products and goods. The To^{2}DeNano project was built on a multidisciplinary group of researchers to address these questions scientifically; and contribute to support (or not) the toxicological relevance of the regulatory definition of MNMs, in particular in the context of the Belgian (nano)register, Royal Decree of May 27, 2014 (Belgisch Staadsblad 2014), implementing a mandatory registry of products/applications containing "substances in nanoparticulate status". Moreover, it will contribute to traceability of MNM and the protection of workers and consumers.

2 STATE OF THE ART AND OBJECTIVES

Currently, over a thousand consumer products worldwide with very diverse applications contain MNM. Despite the bright outlooks for the future of nanotechnology, there also exist concerns that intentional or unintentional human exposure to some types of MNM may lead to significant adverse health effects (Drobne 2007). The unique physico-chemical characteristics of MNM provide technological advances, but their small size implicates an

increased reactivity at the surface, which determines their biological behavior (Hoet et al. 2004)(Oberdörster et al. 2005). The nanoscale size of these particles also implies that they can distribute to the smallest biological structures, to access and interact with fine cellular and molecular structures, indicating the need for a careful toxicological evaluation and a thorough risk assessment. Generally, researchers agree that the smaller the size, the more toxic the particle (Luyts et al. 2013) (Napierska et al. 2009). The importance of MNM characterization has been largely highlighted and efforts are being made to understand the behavior of MNM in the used preparations (Bouwmeester et al. 2011)(Warheit et al. 2008)(Lison et al. 2014). There is a great need for high-throughput protocols that are benchmarked, validated and cost-efficient to screen those potential hazards (Maynard 2007).

In view of the Royal Decree of May 27, 2014 (Belgisch Staadsblad 2014)implementing a mandatory registry of products / applications containing “substances in nanoparticulate status”, it is of major importance to precisely define MNM for the correct assessment of human exposure and possible health risks. The current EU definition, as stated above, includes size (1-100 nm), aggregation and agglomeration (AA) and poly-dispersity (50 % or more of the particles) as important parameters. From a toxicological perspective, next to size, two additional issues about particle dispersion stand out from this definition. It remains unclear whether particles with similar mean size, but with a significantly different size distribution, also differ significantly in toxic activity. Secondly, the AA raises a lot of debate as it is currently not known how this exactly affects the toxic activity of MNM. Consequently, it remains unclear whether it is toxicologically relevant to consider unbound and AA MNM equally for regulatory purposes.

The main *aim* of **To^{2}DeNano** was to provide the scientific insight on how to consider MNM size distribution and AA status in a regulatory context.

Therefore, the main objective of this project was to address the influence of nanoparticle (NP) dispersion (AA and size distribution) on the toxic activity of MNM and how these parameters can be characterized analytically in a precise, repeatable and operational manner. A strategic program was developed to adequately characterize MNM AA and size distribution in samples, and to study the effect of these MNM dispersion parameters in relevant toxicological models (*in vivo* and *in vitro*). The contributing research groups are all actively involved in different aspects of societal effects of nanotechnologies.

The project was structured in 4 work packages (WP):

WP1: Physico-chemical characterization of MNM - Defining the most appropriate metrics and measurement protocols

WP2 : Assessment of impact of AA and size distribution on biodistribution.

WP3 : Study of the impact of AA and size distribution on toxicity

WP4 : Data integration and dissemination.

3 WORK PACKAGE 1: PHYSICO-CHEMICAL CHARACTERIZATION OF MNM - DEFINING THE MOST APPROPRIATE METRICS AND MEASUREMENT PROTOCOLS

3.1 METHODOLOGY

The MNM examined in this project were characterized in detail according to the OECD guidance manual for the testing of MNM (OECD 2010) by a combination of methods including electron microscopy (EM), particle tracking analysis (PTA), and atomic force microscopy (AFM). The MNM were characterized in their pristine state, in the stock dispersion and in the exposure media for *in vivo* and *in vitro* assays. Where required, the MNM were brought in dispersion from their pristine state by sonication-based protocols developed in the FP7 ENPRA, NanoDefine and NanoREG projects.

3.1.1 TEM analysis of NM

The MNM were characterized by transmission electron microscopy (TEM) using procedures proposed in the OECD guidelines (OECD 2010)(Nel et al. 2006) that are derived from those applied in Sciensano. TEM remains one of the few methodologies (Linsinger et al. 2012) that allow measuring particles in line with the new EU law on food information to consumers [28] and the EU definition of a MNM (Potočnik 2011). It covers the full nano-range (1-100 nm) and distinguishes primary particles from AA (De Temmerman et al. 2014). TEM yields number-based results of multiple size and shape parameters. A detailed overview of the (dis)advantages of TEM based approaches is provided in the book chapter “Physical characterization of nanomaterials in dispersion by transmission electron microscopy in a regulatory framework”(Mast et al. 2015). The particles are recovered from the dispersion such that a representative and homogeneous distribution of the particles on the EM-grid is obtained (De Temmerman et al. 2012).

In this project, conventional bright field (BF) TEM was applied to visualize and describe the MNMs (qualitative TEM) and to measure their size and shape distributions (quantitative TEM). The qualitative TEM analysis describes the general physical characteristics of a MNMs supported by (Kreyling et al. 2010) and (2008). Based on information extracted from representative and selected BF TEM images, the MNMs properties of toxicological relevance were determined (SCENIHR 2010).

The MNMs were characterized quantitatively and in detail by estimating the number-based distributions of their particle size and shape properties using a semi-automatic analysis of TEM micrographs. The shape and minimal dimension of primary particles in AA were estimated as described in (De Temmerman et al. 2014). A series of size, shape and surface topology estimates of AA were estimated, represented and classified as described in (De Temmerman et al. 2012).

3.1.2 TEM specimen preparation

TEM specimens were pre-treated with 1% Alcian blue and using the grid on drop method.

3.1.3 Assessment of the VSSA and the 3D morphology of AA

The three-dimensional morphology of particles is an important factor that determines their interaction with cells. For (primary) particles with simple morphologies, this morphology can

be inferred directly from quantitative TEM results. To objectify the morphology of structures with irregular geometries such as aggregates and agglomerates, fractal theory will be applied. It provides a method to compute e.g. a number – the fractal dimension (Df) – that describes how irregular, porous or agglomerated the surface or the structure is. In this project, the fractal properties of aggregated and agglomerated MNM were determined from their projected images by a modification (De Temmerman et al. 2014) of the method of (Brasil et al. 1999)(Brasil et al. 2001) . This modification by De Temmerman et al. (2014) allows to derive the number of primary particles per aggregate and the (calculated) specific surface area of nanoparticle (NP) by analyzing TEM images, from the size of the primary particles, their overlap coefficient and maximal dimension size of the AA.

3.1.4 Dynamic light scattering (DLS)

DLS was applied to verify the quality of the dispersions applied in in vivo and in vitro toxicological tests. DLS has been identified as one of the most robust and accessible instruments for characterization of hydrodynamic sizes of particles in liquid dispersions. DLS is also one of the instruments with the widest range in concentration and hydrodynamic sizes.

3.1.5 Powder electron diffraction

The Bragg diffraction of the electron bean was applied to obtain information about the phase and crystal structure of NM. MNM with crystalline and amorphous phases are differentiated, and the recorded ring-shaped electron diffraction patterns of crystalline MNM are indexed using the Atom Work diffraction database (Xu et al. 2011), which allows determining the possible structure and composition or phase of the material.

3.1.6 Atomic force microscopy

The samples were 00000000 characterized using an Asylum Research (Oxford Instruments) MFP3D Infinity atomic force microscope. The measurements were carried out in air under ambient laboratory conditions in tapping mode. This operating mode is common and allows to measure samples with no damaging. PPP-NCHR AFM probes with a small tip apex (curvature radius < 10 nm) have been used for the measurements.

Poly-L-Lysine coated mica (PL-mica) discs have been used as substrates for the measurement. A few µL of the prepared nanoparticle dispersions were deposited on the PL-mica for 15 minutes before gentle rinsing with DI water and drying under nitrogen flow. PL-mica allows to firmly capture the nanoparticles on a flat surface (RMS roughness < 0.3 nm).

The measurand selected to characterize the nanoparticles is the maximum height of the particles relative to the substrate (Zmax). As schematized on the Figure 3.1.1, Zmax corresponds to the diameter of a spherical primary particle and for an AA the Zmax provides the out of plane dimension that is complementary to the 2D in-plane TEM measurements.

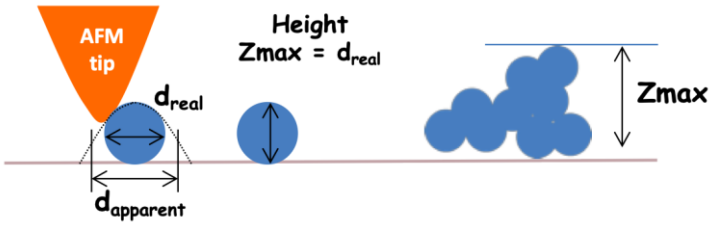

Figure 3.1.1: Schematization of the measurand (Zmax) extracted from the AFM characterization of a spherical nanoparticle and an AA of nanoparticles

3.1.7 Particle tracking analysis

Disadvantages of TEM, are that they require recovering particles from dispersion, coating them on an appropriate support and drying (Linsinger et al. 2012). This can induce artifacts. Although AFM can be performed in liquid, the sample preparation can have an impact on the MNM. To be able to evaluate artifacts, the on-line sizing method of particle tracking analysis (PTA), which analyzes the MNM size in dispersion, was applied in parallel, where feasible.

3.2 SCIENTIFIC RESULTS AND RECOMMENDATIONS

3.2.1 TASK 1.1: Optimization of the dispersion conditions to reproducibly obtain dispersed AA.

3.2.1.1 Selection of NM

Titanium-di-oxide (TiO_2) test nanomaterials and silica nanomaterials were chosen as models for this project due to their extensive use in commercial and industrial applications.

3.2.1.2 Assessment of the influence of agglomerates/aggregates (AA) and size distribution for TiO_2

Two TiO_2 NMs of different sizes were selected from the JRC repository, as TiO_2 NMs are well known for agglomeration. The primary particle size of smaller (JRCNM10202a) TiO_2 NMs **(indicated as SM)** and larger (JRCNM10200a) material **(indicated as LA)** were previously determined as 17 and as 117 nm (Rasmussen et al. 2014).

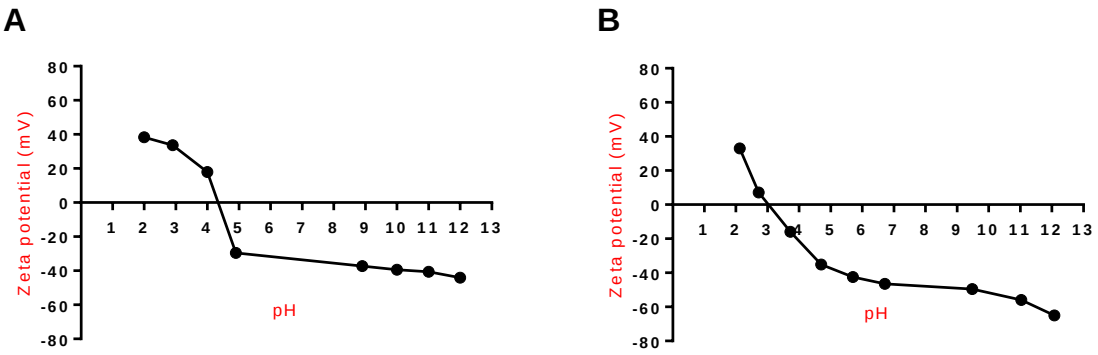

Figure 3.2.1: pH vs Zeta potential curve. SM (A) and LA (B)

A modified Guiot and Spalla method (Guiot and Spalla 2013) was used to generate two differently agglomerated dispersions of the same material. Figure 3.2.1 shows the zeta potential of TiO_2 NMs as a function of pH. Zeta potential and pH are the key players in this protocol as they determine the electrostatic interaction of particles with other particles and with the surrounding medium. In other words, stable dispersions are obtained for a zeta potential higher or lower than, respectively, 20 mV or -20 mV. Based on this principle, dispersion state over a range of pH (2-12) was analysed for each particle type. SM at pH 2 (0.01 M HCl-ultrapure water) was determined to be relatively well dispersed and predominantly exist as primary/unbound particles **(indicated as SM-PP)** compared to suspension at pH 7.5 (pH adjusted ultrapure water), in which particles were strongly agglomerated **(SM-AGG)**. In contrast, LA was found to be well dispersed at pH 7.5 **(LA-PP)** and exist as agglomerates at pH 2 solution **(LA-AGG)**. Table 3.2.1 shows the stability of TiO_2 dispersions according to pH.

Table 3.2.1: Summary of the dispersion conditions selected for both TiO_2 SM and LA

pH	SM	LA
2	Most dispersed condition (SM-PP)	Metastable dispersion (LA-AGG)
7.5	Metastable dispersion (SM-AGG)	Most stable condition (LA-PP)

Figure 3.2.2 shows the schematic diagram of the modified Guiot and Spalla protocol to prepare stock suspensions for biological experiments. After dispersing the particles in respective pH solutions, the particles were sonicated to deliver an energy of 7056 J (calibrated by calorimetric calibration) and stabilized using 1% bovine serum albumin (BSA) to sterically stabilize the particles. Afterwards, the pH 2 solutions were brought back to working biological pH (7-7.5) by slowly adding NaOH (pH was monitored by pH meter). Figure 3.2.3 shows representative pictures of different TiO_2 dispersions.

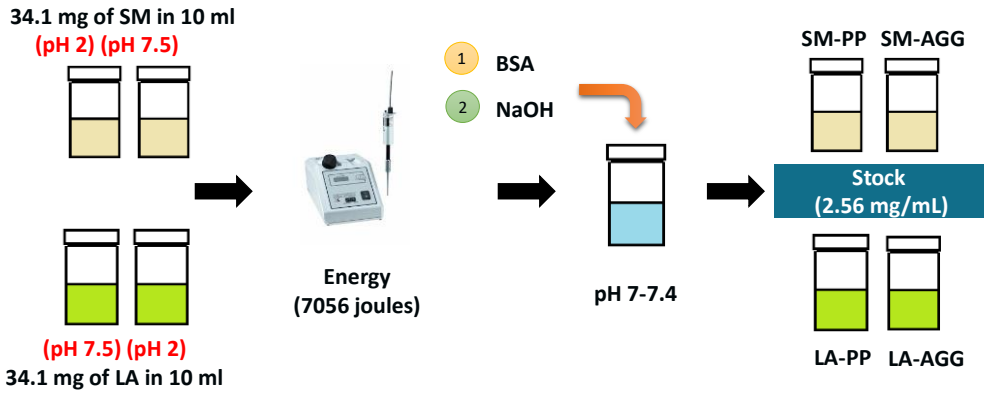

Figure 3.2.2: Scheme of modified Guiot and Spalla protocol

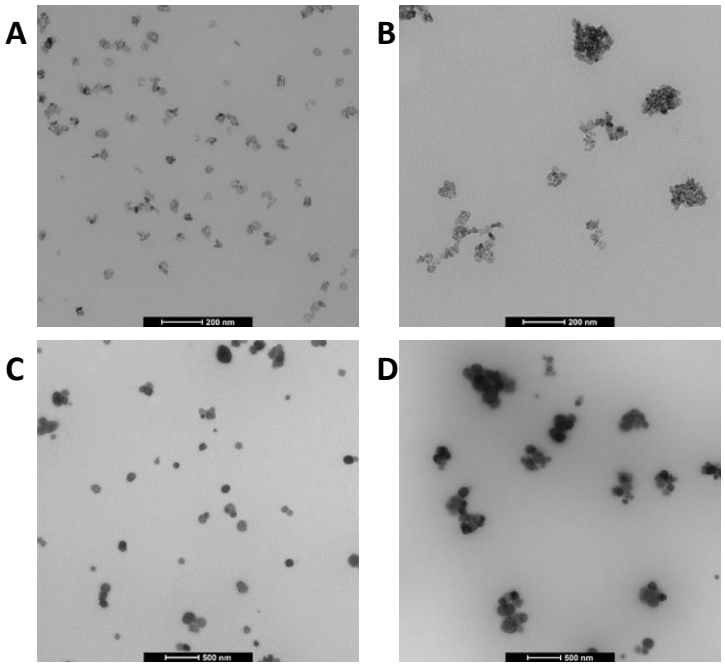

Figure 3.2.3: Representative TEM pictures of TiO_2 dispersions. SM-PP (A), SM-AGG (B), LA-PP (C) and LA-AGG (D). Scale bar: 200 nm (A and B) and 500 nm (C and D).

3.2.1.3 Assessment of the influence of agglomerates/aggregates (AA) and size distribution for silica NMs

The first set of Ludox silica batches provided by the KU Leuven were analyzed by descriptive TEM and DLS and compared. TEM analyses showed no significant differences between the samples supposed to contain different aggregated states (primary particles, small aggregates and large aggregates, data not shown). After several attempts to obtain proper silica dispersions, this strategy was abandoned. As an alternative approach, silica NMs (JRCNM02000a) were chosen as a model as they are well known for aggregation in their manufactured form. The primary particle size of this JRCNM02000a silica NMs was previously determined as 15-20 nm (Rasmussen et al. 2013).

Figure 3.2.4 shows schematically how the four different suspensions of JRCNM02000a silica NMs were freshly prepared during every independent experiment.

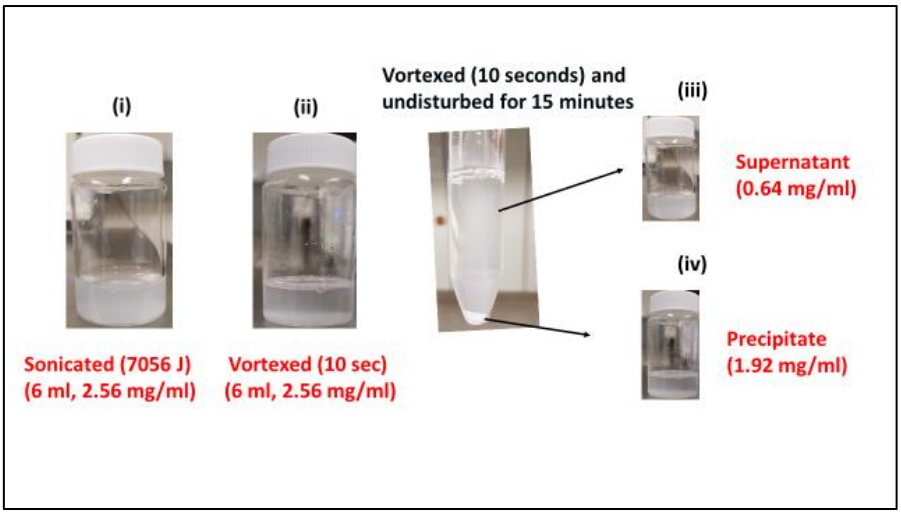

Figure 3.2.4: Stock suspension preparation using JRCNM02000a silica NMs

A first suspension of de-aggregated JRCNM02000a silica NMs was prepared using the generic NANOGENOTOX dispersion protocol: 2.56 mg/ml of silica powder was pre-wetted with 30 µl of ethanol and suspended in 5.970 ml water containing 0.05% of Bovine Serum Albumin (BSA) to achieve the final stock concentration of 2.56 mg/ml. Then the suspension was sonicated in order to deliver an energy of 7 kJ (by applying the settings defined during the sonicator calibration) - this suspension is indicated as **DE-AGGR,**

A second suspension was made by stirring: 15.36 mg of silica NMs was pre-wetted with 30 µL of ethanol and suspended in 5.970 mL water containing 0.05% of BSA and was stirred using a vortex shaker for 10 seconds, silica NMs in this suspension remain aggregated - this suspension is indicated as **AGGR**,

We found that AGGR suspensions contain two different size fractions. Therefore, third and the forth suspension were obtained from the stirred suspension by leaving it undisturbed for 15 minutes: the supernatant (5.8 mL) was removed and 200 µL of 0.05% BSA-water was added to make it to 6 mL - suspension indicated as supernatant '**SuperN**';

and the forth suspension was prepared from the precipitate (200 µL) by resuspension in 5.8 mL of 0.05% BSA-water - suspension indicated as precipitate '**PREC**'. Using ICP-MS, the concentration of SuperN and PREC were determined as 0.64 mg/ml (25% of AGGR) and 1.92 mg/ml (75% of AGGR) respectively. Figure 3.2.5 shows the representative pictures of different silica dispersions.

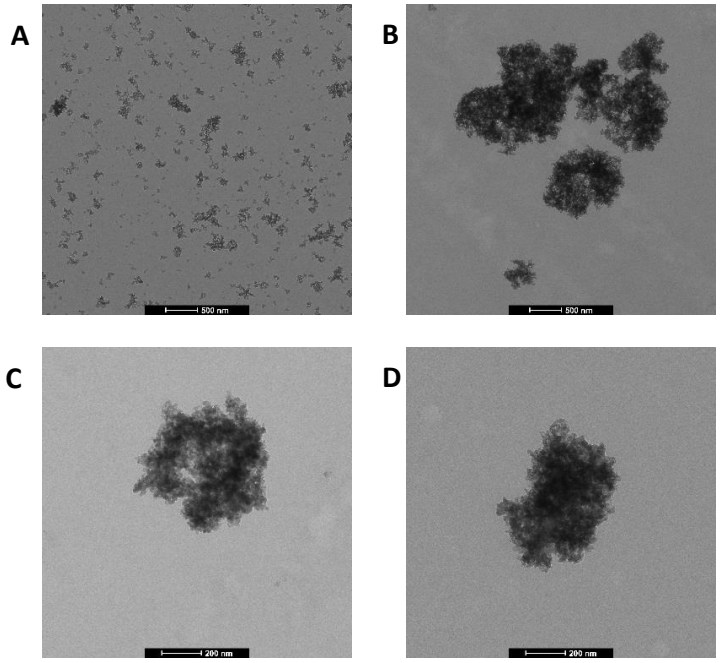

Figure 3.2.5: Representative TEM pictures of JRCNM02000a silica suspensions. DE-AGGR (A), AGGR (B), SuperN (C), PREC (D); Scale bar:500 nm (A and B) and 200 nm (C and D).

3.2.1.4 Optimization of the dispersion conditions to reproducibly obtain dispersed AA.

KU Leuven, UCL and FPS economy calibrated the performance of their sonicating conditions by the calorimetric calibration and by benchmarking the DLS measurements of the Z-average and Pdi of a NM200 (silica) suspension.

3.2.2 Task 1.2: Optimization and intra-laboratory validation of TEM for characterizing the MNM applied in the in vivo and in vitro toxicity tests

3.2.2.1 Methodology development

Based on the work achieved in task 1.1, the protocols were optimized and following standard operation procedures (SOPs) were developed:

- Sonicator calibration : “SOP – Sonicator calibration”
- Sample preparation:
  - TiO2: SOP “Nanomaterial dispersion through pH adjustment” based on the approach of Guiot and Spalla (5).
  - JRCNM02000a silica: generic Nanogenotox dispersion protocol (3) followed by ….
- TEM:
  - Specimen preparation: SOP/NANoREG/D2.10/TEMSpePrep “Preparation of EM-grids containing a representative sample of a dispersed NM” (6)
  - Imaging: SOP/NANoREG/D2.10/TEMIma “Transmission electron microscopic imaging of nanomaterials” (6)

- Image analysis: SOP "Validation of the measurement of the minimal external dimension of the primary particles of particulate materials from TEM images by the NanoDefine Particle Sizer software"

- DLS:
  - SOP "SOP – Sample preparation for zetapotential measurement"
  - SOP "SOP – DLS"

3.2.2.2 Methodology validation

The proposed methodology consists of the above mentioned combination of several SOPs. These were validated simultaneously. The measurement uncertainties associated to the repeatability and the intermediate precision were estimated based on a top down validation approach with triplicate measurements on five days within one week. The calibration and the trueness uncertainties were estimated using a bottom-up approach.

The validations of the quantitative TEM measurement of size, shape and surface properties of primary particles and of aggregates/agglomerates were made for the two selected conditions (stable and metastable), for both SM and LA TiO_2 (Figure 3.2.6). The dispersion and analysis of JRCNM02000a was validated for the 7056 J sonicated (DE-AGGR) condition only. The vortexed (AGGR) condition was not analysed since the material was unstable and precipitated quickly due to the very large particle size. Concerning the Ludox samples, only the characterization of the primary particle fraction was validated since no differences were observed between the different samples supposed to contain different aggregated states (primary particles, small aggregates and large aggregates).

In parallel to the TEM validation, the complementary techniques dynamic light scattering (DLS) and particle tracking analysis (PTA) were validated on the same samples. To achieve a complete characterization of the NMs using TEM, the volume specific surface area analysis (VSSA) was calculated and diffraction analysis was performed using the images from the validation studies of TiO_2 in their most dispersed state.

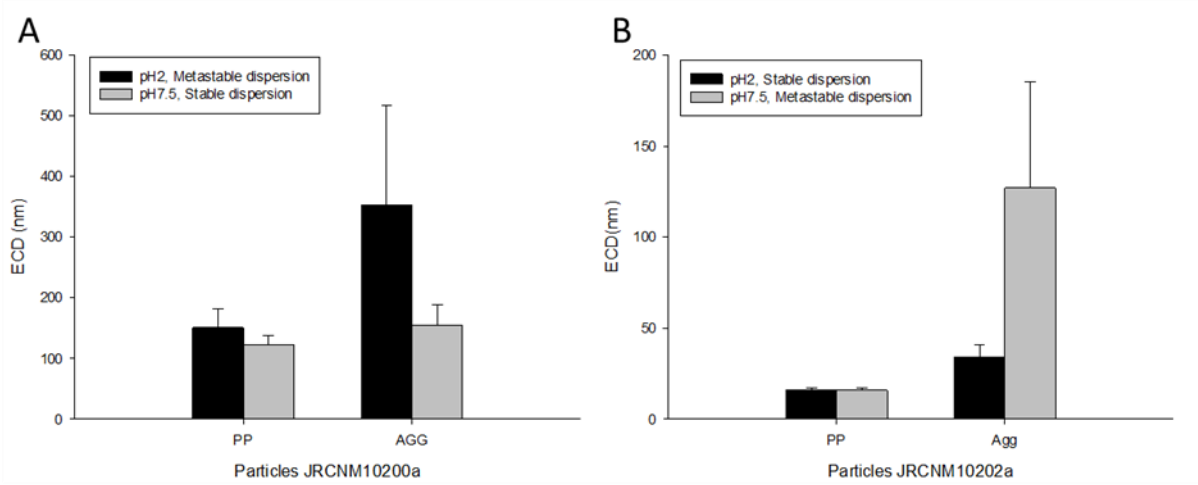

Figure 3.2.6: Equivalent Circular Diameter (ECD) and 95% expanded uncertainties measured in the validation studies of primary particles and aggregates/agglomerates using TEM for both TiO_2 LA (A) and SM (B) in the selected stable dispersions (PP) and in metastable conditions (AGG).

3.2.3 Task1.3 Optimization of the AFM classical methods for characterizing the AA applied in *in vivo* and *in vitro* toxicity tests

The two selected specimens of TiO_2 nanoparticles, namely JRCNM10202a (SM) and JRCNM10200a (LA), were prepared following the modified Spalla and Guiot protocol to obtained two sample dispersions of each specimen. The obtained samples were deposited on PL-mica and characterized by AFM. Representative 3D AFM images of the topography of these samples are presented in Figure 3.2.7: a. and c. are 5 x 5 µm^2 images of SM specimen and b. and d. are 10 x 10 µm^2 images of LA specimen. Each image shows particles well dispersed on a flat substrate. The grey scale on the right hand side corresponds to the z-scale of the 3D-images. An example of PP (dotted arrow) and AA (solid arrow) are shown in Figure 3.2.7.c. The PP are isolated round shaped particles and AA consist of big clusters of PP with various geometries. PP and AA are observed on each sample, meaning the agglomerated samples also contain a non-negligible fraction of primary particles.

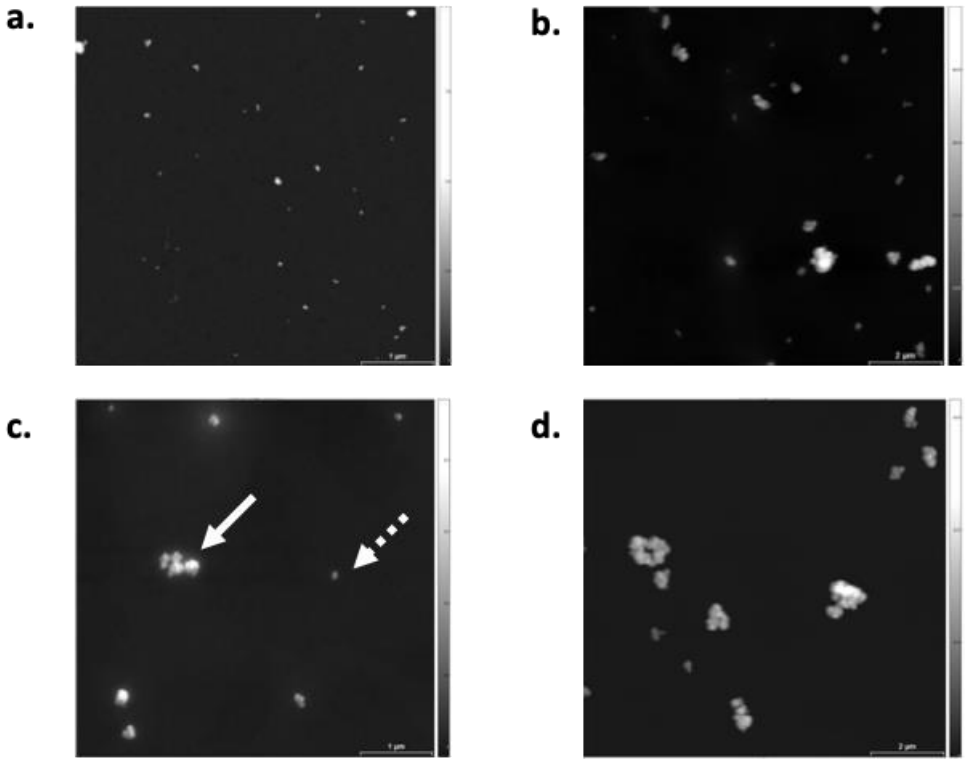

Figure 3.2.7: Representative AFM images of the topography of TiO2 samples deposited on PL-mica substrate. Left images represents the 2 dispersions of JRCNM10202a (SM) specimen: SM-PP (a.) and SM-AGG (c.), while the right images represent the 2 dispersions based on the JRCNM10200a (LA): LA-AGG (b.) and LA-PP (d.). Images a. and c. are 5 x 5 µm2 with a Z color scale of 100 nm while images b. and d. are 10 x 10 µm2 with a Z color scale of 600 nm. Solid line arrow and dotted line arrow on figure c. point out an example of AA and a PP, respectively**.**

Figure 3.2.7.a. shows that the SM-PP dispersion is mainly composed of PP compared to the LA-AGG dispersion (c.) which shows a majority of AA. Samples based on LA specimen (right images) show bigger PP. The LA-AGG dispersion (Figure 3.2.7.b.) consists of a mixture of PP and AA. The number and size of the AA increase when the samples are prepared at pH2 (LA-AGG, d.).

a.

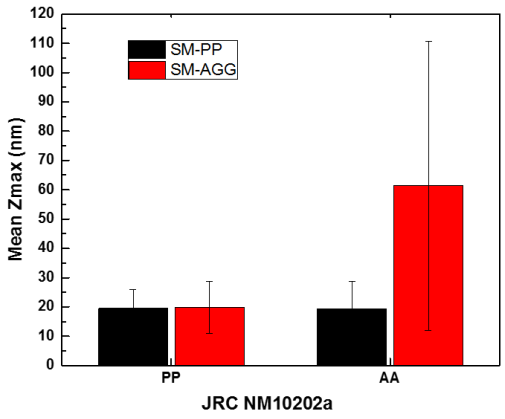

b.

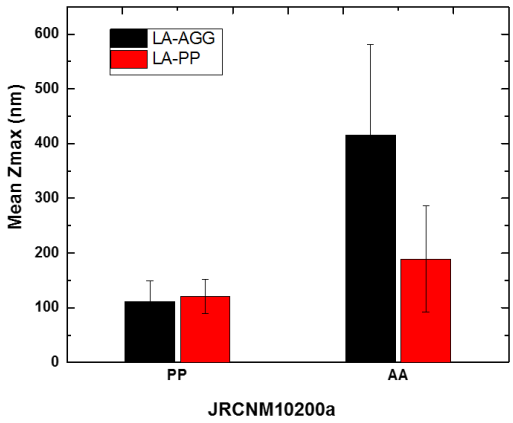

c.

Zmax	Sample	# np	Mean (nm)	Median (nm)	SD (nm)	Uncert. 95% CI
TiO_2 SM	PP	1550	19.5	19.5	6.5	9 %
	AA (SM-PP)	2551	19.4	18.9	9.2	
	AA (SM-AGG)	577	61.4	47.9	49.4	
TiO_2 LA	PP	586	120.5	115.5	31.7	9 %
	AA (LA-AGG)	248	415.5	398.7	175.8	
	AA (LA-PP)	462	188.9	163.4	96.9	

Figure 3.2.8: Comparison of the mean Zmax (error bars represent the standard deviation) of the samples prepared based on the SM TiO2 specimen (a.) and the LA TiO2 specimen (b.). The table (c.) represents the data measurements obtained from several images of each sample.

A summary of the measurements data are presented in Figure 3.2.8. For the statistics on the PP, isolated particles are only considered. Figure 3.2.8.a. and b. show the impact of the dispersion conditions on the two TiO_2 specimen. Both specimen shows similar PP sizes for each preparation condition indicating that the PP are not affected by the preparation procedures. The measured mean Zmax (Figure 3.2.8.c.) of PP of the SM and LA specimens are 19.5 ± 6.5 nm (mean ± SD) and 120.5 ± 31.7 nm, respectively. The measurement uncertainty is 9% with 95% confidence interval, similarly calculated following the accredited procedure of the nanometrology division of the FPS Economy[1].

The mean Zmax of the AA of SM specimen is threefold increased when prepared at pH7.5 (SM-AGG) conditions compared to pH2 (SM-PP), going from 19.4 ± 9.2 nm to 61.4 ± 49.4 nm. It should be noted that the AA at pH2 (SM-PP) show identical Zmax as the PP, indicating that these AA are small flat clusters one nanoparticle high relative to the substrate, flakes-like, and a few nanoparticles wide.

Similarly, the mean Zmax of the AA of LA specimen is almost doubled when prepared at pH2 (LA-AGG) conditions compared to pH7.5 (LA-PP), going from 188.9 ± 96.9 nm to 415.5 ±

[1] J. Pétry, B. De Boeck, N. Sebaihi, M. Coenegrachts, T. Caebergs and M. Dobre, " Uncertainty evaluation through data modelling for dimensional nanoscale measurements", ARXIV:1812.09157, Dec. 2018

175.8 nm. These data measurements confirm the trends qualitatively observed on the AFM images.

Figure 3.2.9 shows the particle density as a function of their height for the TiO_2 small primary particle prepared at a PH of 7.5. We clearly see the presence of small particles at median height of 19.5 nm which correspond to the primary particles and a significant fraction of larger particle with a median height of 47.9 nm. The SM-AGG formed are still nanoparticles according to nano definition. It should be noted that both primary particles and agglomerates are present in the dispersion.

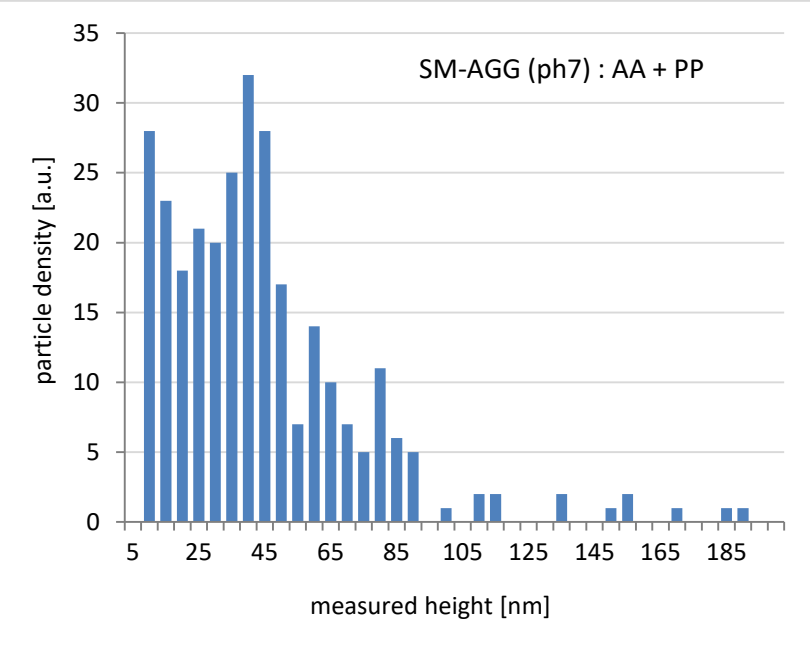

Figure 3.2.9 : Height distribution measured by AFM for small (SM) TiO_2 particles in a solution at PH of 7.5.

From the height measurement data, we can conclude that the agglomerates (AA) of the primary particles both for small size TiO_2 and large size TiO_2 consist of 2 or 3 layers of nanoparticles, at least in the direction perpendicular to the measurement plan.

Information on the shape of the agglomerates can be obtained from the form factor parameter. The measurement in the xy plane are overestimated due to AFM tip-shape effect. The length measurements performed in the xy plane are the convolution of the tip geometry and the particle shape. From SEM images of the tip apex, the tip can reasonably supposed to be symmetrical at its apex such that the tip shape would not affect the form factor. The form factor is defined as the ratio of the particle area and its perimeter. In the case of a perfect disc, it is equal to 1. The table below summarizes the form factor for the 2 agglomerated samples. In both cases, the form factor is high enough to conclude that the agglomerates seems to be rather solid and dense.

	$form\ factor = \frac{area}{4\pi.perimeter}$
SM-AGG (PH7)	0.85 (SD = 0.1)
LA-AGG (PH7)	0.80 (SD = 0.2)

3.2.4 Task 1.4 Detailed physico-chemical characterization of MNM in the stock dispersions and under the applied experimental conditions

3.2.4.1 Characterization in the stock dispersion

The physical properties of the primary and AA in all samples (size, shape and surface properties) were characterized in their most dispersed state using the validated quantitative TEM method (Table 3.2.2), which resulted in precise and accurate size and shape measurements. Accurate and precise estimations of the median primary particle Feret min are presented as the size measurement relevant in the context of the definition of the nanomaterial. Further, all results of physico-chemical characterization of the materials were introduced in the Belgian Nanoregister giving a very complete overview of the different material properties (Figure 3.2.10) including 'General info', 'Chemical identification of the substance', 'Particle shape and size', 'Agglomerates and aggregates', 'Coating', 'Impurities', 'Crystallographic phases', 'Specific surface area' and 'Surface charge'.

Table 3.2.2 Summary of the conditions in which the samples were characterized quantitatively

Nanomaterials	**Condition of the dispersion for characterization**
JRCNM10200a (SM)	Most dispersed state at pH 2 and using 7 kJ of sonication energy
JRCNM10202a (LA)	Most dispersed state at pH 7.5 and using 7 kJ of sonication energy
Ludox PP fraction	Most dispersed state with dilution 10000 times in water
JRCNM02000a	Most dispersed state using 7 kJ of sonication energy

These results are available in the test version of the Nanoregister (https://apps-acc.health.belgium.be/ordsm/02/f?p=NANO) and access can be provided on demand. They are accompanied by a detailed estimation of the measurement uncertainties expressed as expanded uncertainties and they are documented by validation reports and validation plans for TEM, DLS and PTA analyses, when it is relevant. For each property, the choice of relevant techniques was justified. Differences in results between sizing methods are illustrated by comparing TEM, DLS and PTA in the topic "Agglomerates and aggregates". A summary of these results are provided in annexure (annex_work package 1).

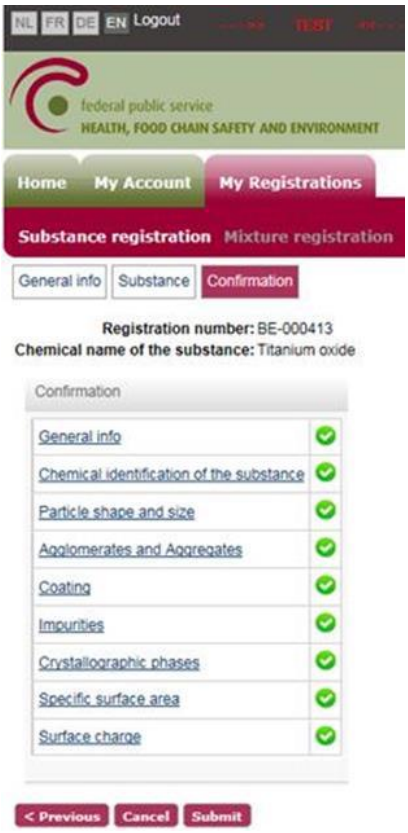

Figure 3.2.10 Topics used to describe the characterization of nanomaterials in the Nanoregister

3.2.4.2 Characterization under the biological conditions

The PP and AGG stock dispersions of SM and LA TiO_2 were tested under experimental conditions *in vivo* and *in vitro*. The stock dispersions were prepared as indicated in Task 1.1 and diluted 10 times in different cell culture media. Similar experiments were performed for the SiO_2 NMs. SuperN and PREC fractions of the AGGR sample were also characterized in the stock dispersion and under the same biological conditions *in vitro*. For the Ludox material, no metastable condition could be obtained, hence biological experiments and characterizations in biological media were not pursued. Table 3.2.3 summarizes the six tested conditions of cell culture media used for the TEM characterization. For each dispersion tested under biological conditions, only qualitative TEM analysis could be performed due to the low amount of particles recovered on the EM grids.

TiO_2 NMs

Table 3.2.3 shows the summary of cell culture media conditions used for the characterization of TiO_2 NM in *in vitro* biological conditions. TiO_2 NM (SM and LA) were analysed by DLS in 4 independent stock suspensions (dispersion conditions previously determined by SCIENSANO, i.e. pH 2 and 7.5 for both SM and LA). These stock suspensions were used in the first *in vivo* experiment because DLS tend to be biased by populations of large particles, we could not show with this method that the pH conditions were able to produce differently agglomerated TiO_2 suspensions. The results of the TEM characterization of both SM and LA in the stock dispersion and under the biological conditions (100 µg/ml) are presented respectively in the Table 3.2.4 and in Table 3.2.5.

Table 3.2.3:Summary of the cell culture media and the conditions used for the characterization of NM under the biological conditions

Cell culture media	Condition 1	Condition 2
HBE	HBE + 0.025% BSA	HBE + 5% serum
Caco2	Caco2 +0.025% BSA	Caco2 + 10% serum
THP1	THP1 + 0.025% BSA	THP1 + 10% serum

Table 3.2.4: Overview of the particle size (smallest-mean-largest) expressed in nm of both SM TiO_2 dispersed at pH2 and pH7.5 samples in stock dispersion and diluted ten times in cell culture medium at time T=0H as assessed by manual measurements.

Medium	Stock dispersion		Diluted 10 times Medium + 0.025% BSA		Diluted 10 times Medium + Serum	
	pH2	pH7.5	pH2	pH7.5	pH2	pH7.5
	PP	AGG	PP	AGG	PP	AGG
Stock Dispersion	35 – 100 – 1500	40 – 200 – 1100	n.a.	n.a.	n.a.	n.a.
HBE	n.a.	n.a.	50 – 150 – 500	40 – 600 – 1100	40 – 100 – 900	90 – 600 – 900
Caco2	n.a.	n.a.	70 – 150 – 500	150 – 600 – 800	70 – 200 – 900	100 – 350 – 1200
THP1	n.a.	n.a.	90 – 100 – 700	250 – 600 – 1300	80 – 200 – 350	90 – 350 – 800

Table 3.2.5:Overview of the particle size (smallest-mean-largest) expressed in nm of both LA TiO_2 dispersed at pH2 and pH7.5 samples in stock dispersion and diluted ten times in cell culture medium at time T=0H as assessed by manual measurements.

Medium	Stock dispersion		Diluted 10 times Medium + 0.025% BSA		Diluted 10 times Medium + Serum	
	pH2	pH7.5	pH2	pH7.5	pH2	pH7.5
	AGG	PP	AGG	PP	AGG	PP
Stock Dispersion	150 – 500 – 1600	100 – 250 – 1800	n.a.	n.a.	n.a.	n.a.
HBE	n.a.	n.a.	200 – 500 – 900	250 – 650 – 1200	300 – 650 – 900	100 – 300 – 1900
Caco2	n.a.	n.a.	150 – 500 – 1100	150 – 300 – 1100	250 – 650 – 1600	150 – 400 – 800
THP1	n.a.	n.a.	200 – 1200 – 1400	200 – 450 – 3500	200 – 600 – 800	200 – 300 – 800

Silica NMs

Silica NMs AGGR and DE-AGGR dispersions were analysed by TEM and DLS in stock suspensions and, at a relevant concentration (100 µg/ml) for in vitro testing, just after dilution in cell culture media. Measurements were repeated after 24 h (in vitro exposure duration). Table 3.2.6 shows size distribution of DE-AGGR and AGGR silica dispersions. The TEM size

measurement results of both DE-AGGR and AGGR silica dispersions are presented in Table 3.2.7.

Table 3.2.6: DLS and TEM characterization of sonicated and vortexed JRCNM02000a suspensions

	TEM (Feret min, nm)	DLS (Z-average, nm)
DE-AGGR	28.8	264
AGGR	600	12530

Table 3.2.7:Overview of the particle size (smallest-mean-largest) expressed in nm of both sonicated and vortexed silica samples in stock dispersion and diluted ten times in cell culture medium at time T=0H as assessed by manual measurements.

Medium	Stock dispersion		Diluted 10 times Medium + 0.025% BSA		Diluted 10 times Medium + Serum	
	DE-AGGR	AGGR	DE-AGGR	AGGR	DE-AGGR	AGGR
Stock Dispersion	20 – 100 – 450	50 – 2000 – 3800	n.a.	n.a.	n.a.	n.a.
HBE	n.a.	n.a.	20 – 150 – 1400	50 – 2000 – 3000	30 – 200 – 1400	1300 – 2700 – 4000
Caco2	n.a.	n.a.	20 – 150 – 600	100 – 1100 – 1300	15 – 150 – 400	15 – 150 – 400
THP1	n.a.	n.a.	20 – 200 – 650	70 – 500 – 1200	20 – 200 – 2700	150 – 2400 – 3300

However, when SuperN and PREC stocks fractions (as described in Task 1.1) were analysed using both drop on grid method or grid on drop method, the results were not conclusive:

- For the SuperN: no particles were observed.
- For the PREC: using the drop on grid method, it was not possible to analyze the grid because it was completely covered by particles. The particles could not be distinguished from each other.

For each repetition of the experiment and for both SuperN and PREC conditions, TEM inspection demonstrated that the particles were highly agglomerated/aggregated, the particles were not evenly distributed over the grid surface and the concentration of particles on the specimen was really low.

However, particles could be distinguished from the background, but the amount of particles on the EM grids was low and they were not evenly distributed on the grid. Therefore, a quantitative TEM analyses was not feasible. The values reported in Table 3.2.8 are estimates for the smallest, mean and largest particles observed in selected micrographs that contained particles. The TEM results of both SuperN and PREC characterized in stock dispersion and under the biological conditions are presented in Table 3.2.9.

Table 3.2.8: Summary of the particle size (smallest-mean*-largest) expressed in nm and the number of particles detected for supernatant and precipitate sample characterization in stock dispersion for each repletion of the experiment

	Repletion 1		Repletion 2		Repletion 3	
	PREC	SuperN	PREC	SuperN	PREC	SuperN
Size (in nm)	60 – 1200 – 3200	30 – 900 – 4400	40 – 600 – 2500	40 – 700 – 2600	70 – 750 – 1600	20 – 600 – 1100
Number of particles measured	32	14	46	20	10	11

* The mean value is calculated from the size measurements.

Table 3.2.9: Overview of the particle size (smallest-mean-largest) expressed in nm of both precipitated and supernatant silica samples in stock dispersion and diluted ten times in cell culture medium at time T=0H as assessed by manual measurements.

Medium	Stock dispersion		Diluted 10 times Medium + 0.005% BSA		Diluted 10 times Medium + Serum	
	PREC	SuperN	PREC	SuperN	PREC	SuperN
Stock Dispersion	70 – 750 – 1600	20 – 600 – 1100	n.a.	n.a.	n.a.	n.a.
HBE	n.a.	n.a.	500 – 800 – 1200	70 – 450 – 1300	No particles found	200 – 400 – 850
Caco2	n.a.	n.a.	350 – 900 – 1500	750 – 950 – 1250	1000 – 1250 – 1500	500 – 750 – 1100
THP1	n.a.	n.a.	800 – 9300 – 22250	200 – 400 – 800	200 – 450 – 650	250 – 450 – 750

Based on the TEM characterization results, the particles in the SuperN and the PREC samples have similar qualitative properties in the stock dispersions. It was not possible to prepare a TEM specimen allowing quantitative analysis and interpretation starting from a non-stable sample.

This similarity of the results could be explained by methodological reasons that may hide difference between samples at three levels:

1. During the sample preparation, while waiting the 15 minutes for “stabilization”, the particles that are in dispersion (mainly aggregates/agglomerates) will precipitate. During precipitation, these particles will create bigger agglomerate with the other precipitating particles. Bringing up the volume to 6 ml for the PREC fraction, can influence the agglomeration state of the particles. The big agglomerates, created with the small AA during the precipitation phase, can break apart and get back to smaller AA state. The biggest particles that did not break apart would again precipitate and the smallest AA could stay in dispersion. Finally, these AA in dispersion could attach to the EM grid, which would give similar results than for the SuperN analysis.
2. During the specimen preparation, sedimentation of large aggregated/agglomerated particles on the grid in the drop on grid method results in a sample containing such a

high amount of material that it is unsuitable for TEM imaging as the beam does not penetrate well enough. Moreover, small particles (PP and AA) cannot be distinguished from the AA bound to the EM-grid. Very large, micrometer-sized particles are known to not representatively attach to the grid. The grid-on-drop method does not allow larger particles to attach to the EM grid representatively since these precipitating rapidly.

3. During imaging, TEM inspection of the grids showed that the particles could be distinguished from the background based on their grey value. The grid inspection demonstrated also that the particles were not evenly distributed over the surface for both SuperN and PREC of each repetition of the experiment. The EM specimen were not representative for both SuperN and PREC samples.

RECOMMENDATIONS

SOPs for NM dispersion and quantitative TEM, DLS and PTA measurements, instrumental to apply the EC definition of NM and for characterizing MNM applied in the *in vivo* and *in vitro* toxicity tests, were successfully developed, validated and implemented in the present project to produce differently agglomerated or aggregated nano- TiO_2 suspensions

Calibration of the sonicator is essential to ensure the reproducibility across different laboratories.

The suspensions of TiO_2 NMs were not stable when prepared using the Nanogenotox protocol but this problem was solved using modifications of the Spalla and Guiot protocol based on the dispersion of NP at different pH and stabilization of the suspensions with BSA.

For silica NMs, the fraction of small particles in the supernatant probably/possibly explains the differences observed in toxicological tests (please refer workpackage 3). Ensemble methods such as DLS and CLS are considered not suitable to differentiate both samples. Their results are biased by the fraction of large particles such that they will miss the fraction of small particles, if present.

Because demonstrating differences in the presence of small particles is important in view of valorisation in publications, we plan to explore a density gradient based separation method to isolate and concentrate this fraction of small particles. A comparison between the SuperN and PREC isolated fractions can be analysed using TEM to see if differences can be observed.

4 WORK PACKAGE 2: ASSESSMENT OF IMPACT OF AA AND SIZE DISTRIBUTION ON BIODISTRIBUTION

4.1 METHODOLOGY

4.1.1 ICP-MS analysis

Measuring Ti from TiO_2 NP by inductively coupled plasma-mass spectrometry (ICP-MS) normally requires the mineralization of the particles with strong acids like hydrofluoric acid (HF) (Gaté et al. 2017)(Pujalté et al. 2017). Since using HF was not an option in any of the partner laboratories because of security reasons, we aimed at developing a methodology to quantify Ti by ICP-MS in biological tissue without using HF.

Ti was quantified on an ICP-MS Agilent 7500 ce Octopole Reaction System according to the following method: method spectrum, analyte 47Ti, internal standard 74Ge, Helium mode, peak pattern maximum (20), integration time 1 sec per point/20 sec per mass, acquisition time: 5 repetitions. Calibration of the measurement was done with serial dilutions of a TraceCERT Titanium Standard for ICP (soluble Ti).

4.2 SCIENTIFIC RESULTS AND RECOMMENDATIONS

4.2.1 Task 2.1: Measurement of MNM in biological samples (organs, blood, urine,…).

Ti was first quantified in serial dilutions of JRCNM10202a (TiO_2 SM) and JRCNM10200a (TiO_2 LA) sonicated suspensions (following the dispersion protocol developed at pH 7.5). The linear regression obtained with the theoretical Ti concentration engaged and the measured concentration indicated a recovery of 69 % for SM TiO_2 and 98 % for LA TiO_2 (figure 4.2.1), indicating that particle size and agglomeration probably influence the quantification of Ti. Given that TiO_2 SM are in a more agglomerated state at pH 7.5, this could explain the lower recovery for TiO_2 SM.

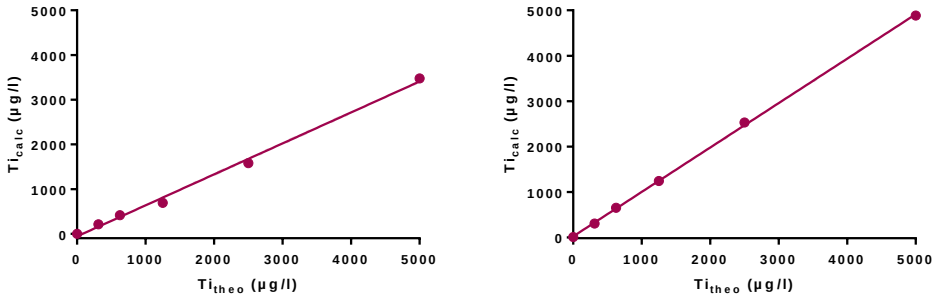

Figure 4.2.1: Ti recovery in SM TiO_2 (left, slope = 0.69, R^2 = 0.99) and LA TiO_2 (right, slope = 0.98, R^2 = 0.99) suspensions measured by ICP-MS. Ti_{theo} is the theoretical Ti concentration engaged according TiO_2 NP weight and Ti_{calc} is the measured concentration calculated from a soluble Ti standard curve.

To assess the effect of the biological matrix, Ti was then measured in TiO_2 dispersions in the presence or not of tissue. Serial dilutions of TiO_2 with or without 200 mg mouse lung tissue

were mineralized with 4.5 ml HNO_3 65 % and 1.5 ml HCl 30 % in a microwave (Multiwave Go, Anton Paar) before ICP-MS measurement. Ti recovery for SM TiO_2 was 50 % and 57 % in the absence and presence of lung tissue, respectively, and 55 % and 57 % for LA TiO_2 (figure 4.2.2), indicating similar recovery for both TiO_2 after HNO_3/HCl treatment. The presence of tissue did, therefore, not significantly influence Ti recovery. Based on these results, it was decided that Ti would be quantified in mouse tissues (task 2.2) from a standard curve established with TiO_2 dispersions treated with HNO_3/HCl (like the organs) in absence of biological tissue.

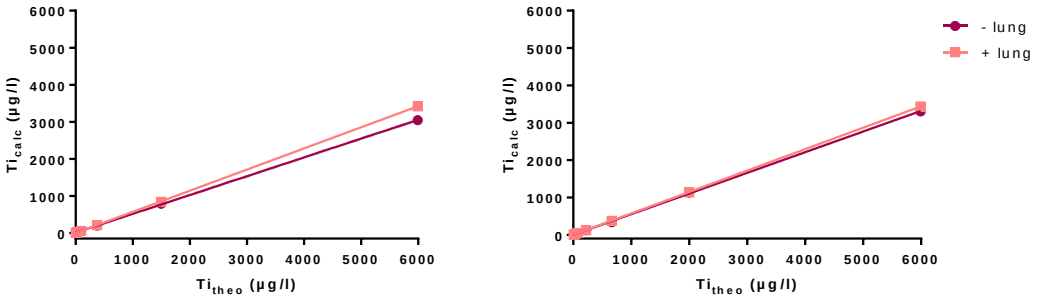

Figure 4.2.2: Ti recovery in TiO_2 SM suspensions (left) in the absence (slope = 0.50, R^2 = 0.99) and presence (slope = 0.57, R^2 = 1) of lung tissue and TiO_2 LA suspensions (right) in the absence (slope = 0.55, R^2 = 0.99) and presence (slope = 0.57, R^2 = 1) of lung tissue measured by ICP-MS.

The <u>standard curves</u> were established with triplicate serial dilutions of sonicated and non sonicated NP suspensions (dispersion protocol at pH 7.5) treated with HNO_3/HCl (figure 4.2.3). Ti recovery was similar for both NP but different in sonicated and non sonicated NP suspensions: 71 and 52 % for SM TiO_2, respectively, and 69 and 48 % for LA TiO_2. Because TiO_2 NP are probably differentially agglomerated in tissues, the standard curve for each TiO_2 was calculated with sonicated and non sonicated NP suspensions. Thus, the mean Ti recovery was 61.7 and 58.5 % for TiO_2 SM and TiO_2 LA, respectively. These values were used to evaluate the Ti/TiO_2 contents in mouse tissues (task 2.2).

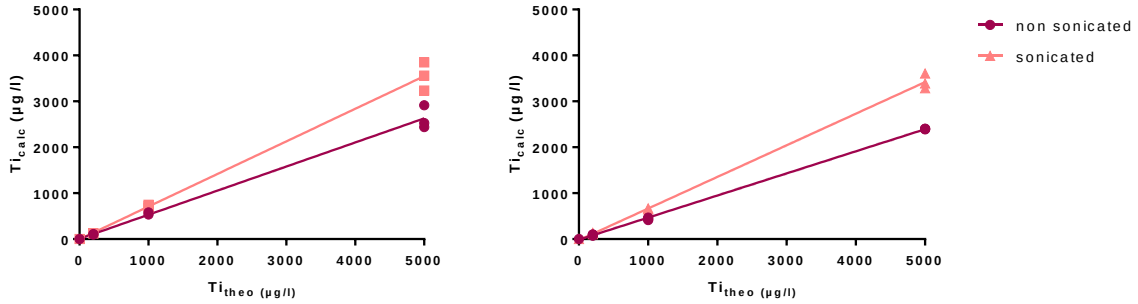

Figure 4.2.3: Ti recovery in TiO_2 SM suspensions (left) after sonication (slope = 0.71, R^2 = 0.99) or no sonication (slope = 0.52, R^2 = 0.99) and TiO_2 LA suspensions (right) after sonication (slope = 0.69, R^2 = 0.99) or no sonication (slope = 0.48, R^2 = 0.99) measured by ICP-MS. NP were prepared at pH 7.5 as described in the dispersion protocol.

A limit of quantification was calculated from Ti concentrations measured in blank samples (treated exactly the same way as mineralized tissues): LOQ = mean (blanks) + 10 x SD (standard deviation) = 14.67 µg Ti/l.

The developed methodology is found to be reliable to quantify the Ti in biological samples (blood, liver, spleen and kidney) without the use of HF.

4.2.2 Task 2.2: Studying how AA and size distribution modulate internal exposure.

Mice were exposed to human relevant doses of each TiO_2 dispersions (SM-PP and AGG, and TiO_2 LA-PP and AGG) by aspiration (2, 10, 50 and 100 µg) or gavage (10, 50, 250 and 500 µg). Three days after exposure, blood and organs were collected for assessing Ti biodistribution. Blood or organs were mineralized and Ti was quantified by ICP-MS according to the protocol described in task 2.1.
TiO_2 dose-dependently accumulated in mouse lungs after aspiration (figure 4.2.4). A two-way ANOVA analysis indicated a significant effect of the dose but no effect of the size/agglomeration state on lung tissue Ti content. Levels of Ti in blood were all below the LOQ.
Ti was also measured in blood, liver, spleen and kidney after gavage. Levels of Ti were all below the LOQ.

Our data suggest that the size/agglomeration has no effect on TiO_2 NP biodistribution in the lung after exposure by aspiration.

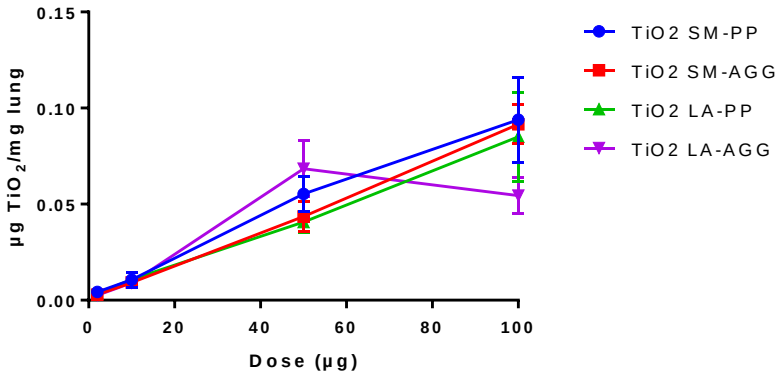

Figure 4.2.4: TiO_2 distribution in lung tissue 3 d after exposure. Mice were exposed to TiO_2 NP (2, 10, 50 and 100 µg/mouse) by aspiration. Ti was measured in lung tissue 3 d after exposure by ICP-MS.

Note: No in vivo experiments was executed for silica NMs (please refer workpackage 1 for the issue) because it is considered ethically unacceptable to use lab-animals in a test that is a priori supposed to be negative. This was discussed in previous meeting and in annual reports, and it was accepted by follow up committee members.

5 WORK PACKAGE 3: STUDY OF THE IMPACT OF AA AND SIZE DISTRIBUTION ON TOXICITY

5.1 METHODOLOGY

5.1.1 Animals and treatments

Animal experiments were performed only with TiO_2 NMs (agglomeration). For aspiration (representative of inhalation exposure), female C57BL/6JRj mice were anaesthetized and 50 µl dispersions of different TiO_2 doses (2, 10, 50,100 µg/mouse) were administered by oro-pharyngeal aspiration. For gavage (representative of oral exposure), mice were administered with 200 µl of dispersions (10, 50, 250, 500 µg/mouse). Control mice were administered with dispersant medium. Animals were sacrificed 3 days after particle administration and samples were collected.

5.1.2 Blood, broncho-alveolar lavage and organ sampling

Blood was collected in EDTA tubes for ICP-MS, hematology and genotoxicity. Cytokines were quantified with Cytokine 23-plex Assay in plasma.

Broncho-alveolar lavage (BAL) was performed by cannulating the trachea and infusing the lungs with 1 ml NaCl 0.9 %. Whole lungs were then perfused with NaCl 0.9 % and excised. Left lobes were placed in 3.65 % paraformaldehyde in phosphate buffered saline (PBS) for later histological analysis, and right lobes were used for ICP-MS, genotoxicity and glutathione (GSH) depletion. BAL were centrifuged 10 min at 4°C (240 *g*). Cell-free supernatant (BALF) was used for biochemical measurements such as lactate dehydrogenase (LDH) activity, total proteins and cytokines. After resuspension of the pellet in PBS, total BAL cells were counted in Turch and cytocentrifuged for differentiation by light microscopy after Diff-Quick staining.

Lung, liver, spleen and kidney were collected after gavage for ICP-MS and GSH measurement (liver). Distal Ileum and proximal colon parts were also placed in paraformaldehyde for histological analysis.

5.1.3 Histology

Paraffin-embedded organ sections were stained with hematoxylin and eosin (HE). The sections were scanned and examined with Tissue Image Analysis.

5.1.4 Cell culture

Inhalation and ingestion are the primary routes of exposure to MNMs during production and use. Therefore, we studied the toxic effects in vitro using human bronchial (HBE) and human colon epithelial (Caco2) cell lines. Further, we used a human monocytic cell line (THP-1) to partly mimic the innate immune response, as they are actively involved in phagocytosis of these particles. HBE cells were cultured in DMEM/F12 supplemented with 5% fetal bovine serum (FBS) while RPMI 1640 supplemented with 10% FBS, was used for THP-1. Caco2 was cultured in DMEM/HG supplemented with 10% FBS. Cells were cultured in T75 flasks at 37°C in a 100% humidified air containing 5% CO_2. Medium was changed every 2 or 3 days

and cells were passaged every week (7 days). Cells from passage 4 to10 were used for the experiments.

5.1.5 Dilution of NM stock dispersions in cell culture medium and *in vitro* exposure conditions

For all experiments except for barrier integrity assessment, HBE, Caco2 and THP-1 cells were seeded at a density of $1.5x10^5$, $1.05x10^5$ and $3x10^5$ cells/cm^2 in 96-well plates or 24 well plates and incubated overnight at 37°C. On the day of exposure, freshly prepared stock dispersions were diluted in 0.25% BSA water to prepare the sub-stocks of different concentrations of TiO_2 (40 µg/mL - 2560 µg/mL) or SiO_2 (20 µg/mL - 1280 µg/mL) and further diluted 10 times in serum-free cell culture medium (CCM) to achieve the final exposure concentrations (4 - 256 µg/mL). Cells were then washed with HBSS (without Ca2+/Mg2+) once and exposed to different concentrations of SiO_2 or TiO_2 NMs. After 24 h, the cell cultures were washed twice with HBSS and the respective assays were performed.

5.1.6 *In vitro* dosimetry

Volume Centrifugation Method (VCM) was used to determine the effective density of SiO_2 and TiO_2 NMs in cell culture medium (100 µg/ml) and to estimate the dose delivered to the cells over 24 h exposure was calculated using the Distorted Grid (DG) model (DeLoid et al. 2017). The doses were presented as mass of the material delivered per unit surface area of the well plate (µg/cm^2).

5.1.7 Repeated low dose exposure

HBE, Caco2 and THP-1 cells were seeded in 6 well plates and repeatedly exposed to 2 µg/mL (0. 76 cm^2 surface area of the plate) of all TiO_2 and silica dispersions diluted in cell culture medium with serum (5-10%, according to cell type). For Silica SuperN and PREC fractions, exposure concentration was 0.5 and 1.5 µg/mL respectively. The cell cultures were then washed and repeatedly exposed to the same concentration for every two days and passaged weekly. The exposure cycle was repeated for three weeks and at the end of every week, samples (cells and supernatants) were collected and cryopreserved at -80°C for further analysis. Cell viability and cell number were determined by an automated cell counter (countless, Invitrogen) and, GSH depletion, interleukin (IL) -8 and IL-6 release. Genotoxicity was analysed as described section below (5.1.13).

5.1.8 WST-1 assay

To determine the effect NMs on the cell metabolic activity, exposed cell cultures were incubated with 120 µL substrate solution WST-1 reagent diluted in medium without phenol red at the ratio of 1:10 for 1 - 2 h. At the end of incubation, the supernatants were centrifuged at 1600 *g* for 10 minutes, then 100 µL was transferred to a new plate and the optical density (OD) was recorded using a micro-plate reader at 450 nm. After subtracting the blank OD values from the sample OD values, the values were normalized to the control (untreated) cells.

5.1.9 LDH assay

The effect on membrane integrity was assessed by a kinetic Lactate dehydrogenase (LDH) assay. At the end of exposure, the supernatants were transferred to a new plate and the cell cultures were incubated with 0.2% triton for 30 minutes. After 30 minutes, the plates were centrifuged at 1600g for 10 minutes. Then the samples were transferred to a new 96-well plate, substrate solution (pyruvate) was added and the absorbance was measured by spectrophotometer at 340 nm for 3 min with 15 s interval. Velocity was calculated according to the standard curve and the cell viability was calculated according to the formulae:

Viability = [slope of leakage/ (slope of lysate+ slope of leakage) *100]

Relative viability = (sample viability /untreated control viability) *100

5.1.10 Glutathione depletion

Glutathione (GSH) was measured using a glutathione detection kit according to the manufacturer's protocol, and the protein content of cell cultures was estimated using bicinchoninic acid (BCA) protein assay kit. GSH was normalized to the total protein content (in vitro) or of lung or liver weight (from animal treatments). The results were expressed as percentage of control (untreated) cells or animals.

5.1.11 Inflammatory cytokine release

IL-8, IL-6, TNF-α and IL1β were IL-1β were quantified using ELISA kits. The cytokines were measured in the supernatants (collected during glutathione measurement experiments and stored at -80°C) according to the manufacturer protocol and normalized to the total protein content. Results were expressed as percentage of control (untreated cells).

5.1.12 Trans Epithelial Electrical Resistance measurements

HBE and Caco2 cells were seeded at a density of $2.0x10^4$ cells per well in 24 well Transwell inserts. The Trans epithelial electrical resistance (TEER) was monitored everyday using a Chopstick electrode and an epithelial voltohmmeter. After 7 days, the cells were exposed to different concentrations of these dispersions for 24 h and TEER was measured. Culture with TEER > 600 ohm.cm^2 were used for the experiments. The results were expressed as percentage of control (untreated cells).

5.1.13 DNA Strand breaks

Cell cultures exposed to silica and TiO_2 dispersions were used to quantify DNA strand breaks using alkaline comet assay kit according to the manufacturer's protocol. Cells treated with 100 µM Methyl Methane Sulfonate (MMS) for 1-2 hour served as a positive control. For in vivo, blood and BAL cells collected from exposed animals were used and untreated animal blood or BAL cell exposed to 100 µM of H_2O_2 for 15 minutes served as positive control. The slides were imaged using microscopy in FITC mode and at 10x magnification. Fifty random comets per well were scored using the Casplab software. The mean percentage of tail DNA was calculated from the median of three independent experiments (*in vitro*) or 4-5 animals per group *in vivo*.

5.1.14 Statistical analysis

For *in vitro*, three independent experiments were performed in triplicate or duplicate and data were presented as mean ± standard deviation (SD). For *in vivo*, mean± standard error mean (SEM) or SD was calculated from 4-5 animals per group. Using GraphPad prism 7 software, the results were analysed with Two-way ANOVA + Bonferroni pairwise comparison test to determine the significance of differences between suspensions at the same mass dose and Two-way ANOVA + Dunnett's multiple comparison test to determine significant difference compared with control.

5.2 SCIENTIFIC RESULTS AND RECOMMENDATIONS

5.2.1 Single exposure in vitro

5.2.1.1 Agglomeration - TiO_2 NMs

Cytotoxicity

Annex figures 1 and 2 represent the results of WST-1 (1A, C, E) and LDH assay (1B, D, F) measured after 24 h exposure to different concentrations of SM (fig.1) and LA (fig.2) TiO_2 respectively. Except a mild increase in metabolic activity observed at some concentrations, none of the dispersions induced noticeable effect on metabolic activity or cell viability, even at the highest concentration tested.

Oxidative stress induction

Figures 5.2.1 and 5.2.2 present the results of GSH measurements measured after 24 h exposure to different concentrations of SM (fig. 5.2.1) and LA (fig. 5.2.2) TiO_2. Significant effects were observed at 256 µg/ml. Dispersions of SM induced stronger decrease of GSH levels compared to LA. This indicates the potential of smaller nanomaterials to induce more severe oxidative stress. However, no significant difference between the PP and AGG dispersions was noticed in HBE and Caco2. Interestingly, SM-AGG, but not the PP, decreased the GSH significantly in THP-1. Such a response could be attributed to size dependent phagocytic nature of THP-1.

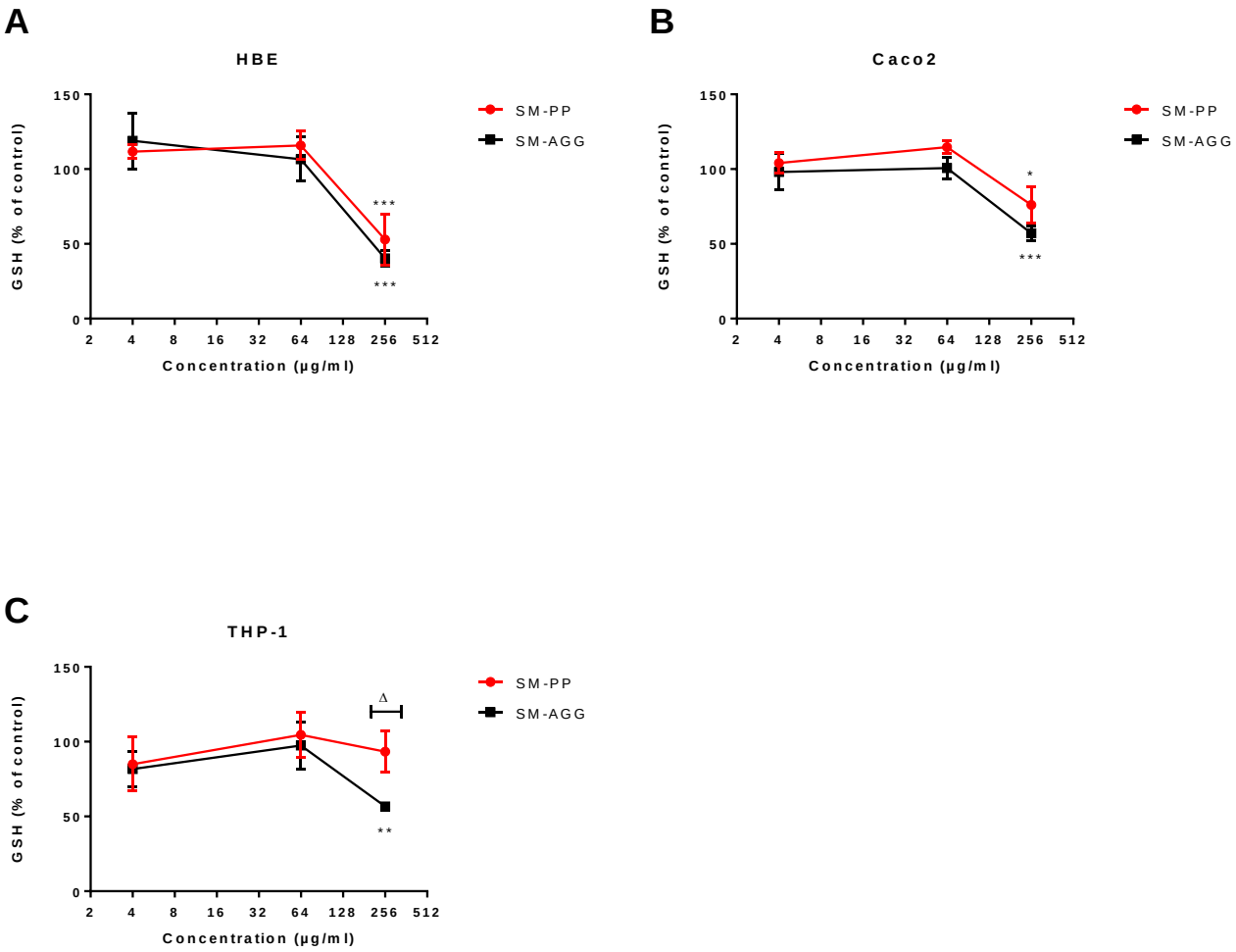

Figure 5.2.1: Effect of SM-TiO_2 NMs on glutathione (GSH) levels. GSH levels were measured in cell cultures (A-HBE; B-Caco2; C-THP1) following 24 h exposure to SM-PP (red line) and SM-AGG (black line). Data are expressed as means ± SD from three independent experiments performed in duplicates. Two-way ANOVA followed by post-hoc tests were performed to determine statistical significances. $p < 0.05$ (*), $p < 0.01$ (**) and $p < 0.001$ (***) represents significant difference compared to control; $p < 0.05$ (Δ) represents significant difference between PP and AGG at the same mass dose.

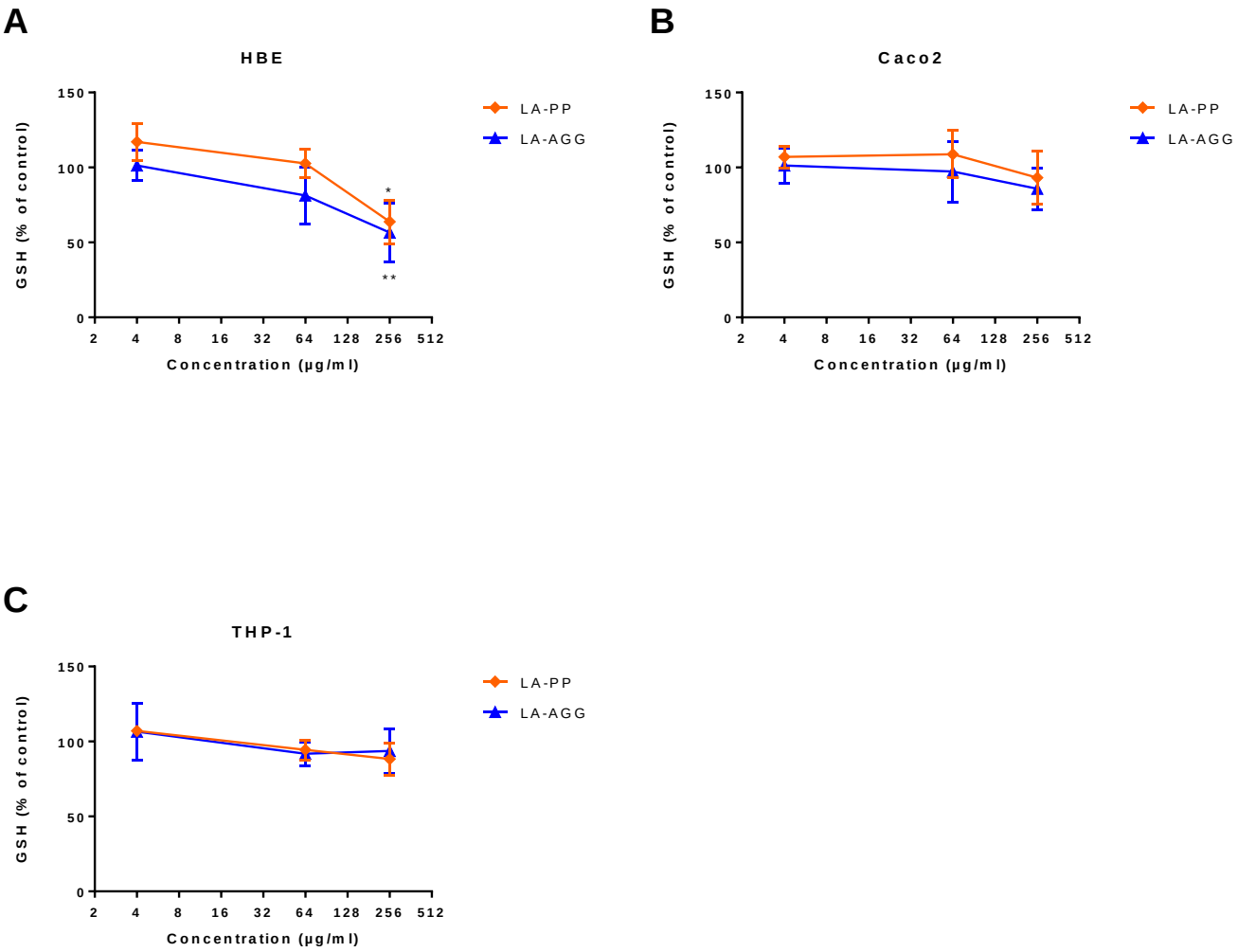

Figure 5.2.2: Effect of LA-TiO_2 NMs on glutathione (GSH) levels. GSH levels were measured in cell cultures (A-HBE; B-Caco2; C-THP1) following 24 h exposure to LA-PP (orange line) and LA-AGG (blue line) dispersions. Data are expressed as means ± SD from three independent experiments performed in duplicates. Two-way ANOVA followed by post-hoc tests were performed to determine statistical significances. $p < 0.05$ (*) and $p < 0.01$ (**) represents significant difference compared to control.

Barrier integrity

Figure 5.2.3 presents the results of TEER measurements after 24 h exposure to different concentrations of SM and LA-TiO_2 NMs. Dispersions of SM and LA dose-dependently decreased the TEER in HBE. Caco2 showed such decrease only for LA and only at the highest concentration tested (256 µg/ml). However, there are no significant difference between PP and AGG.

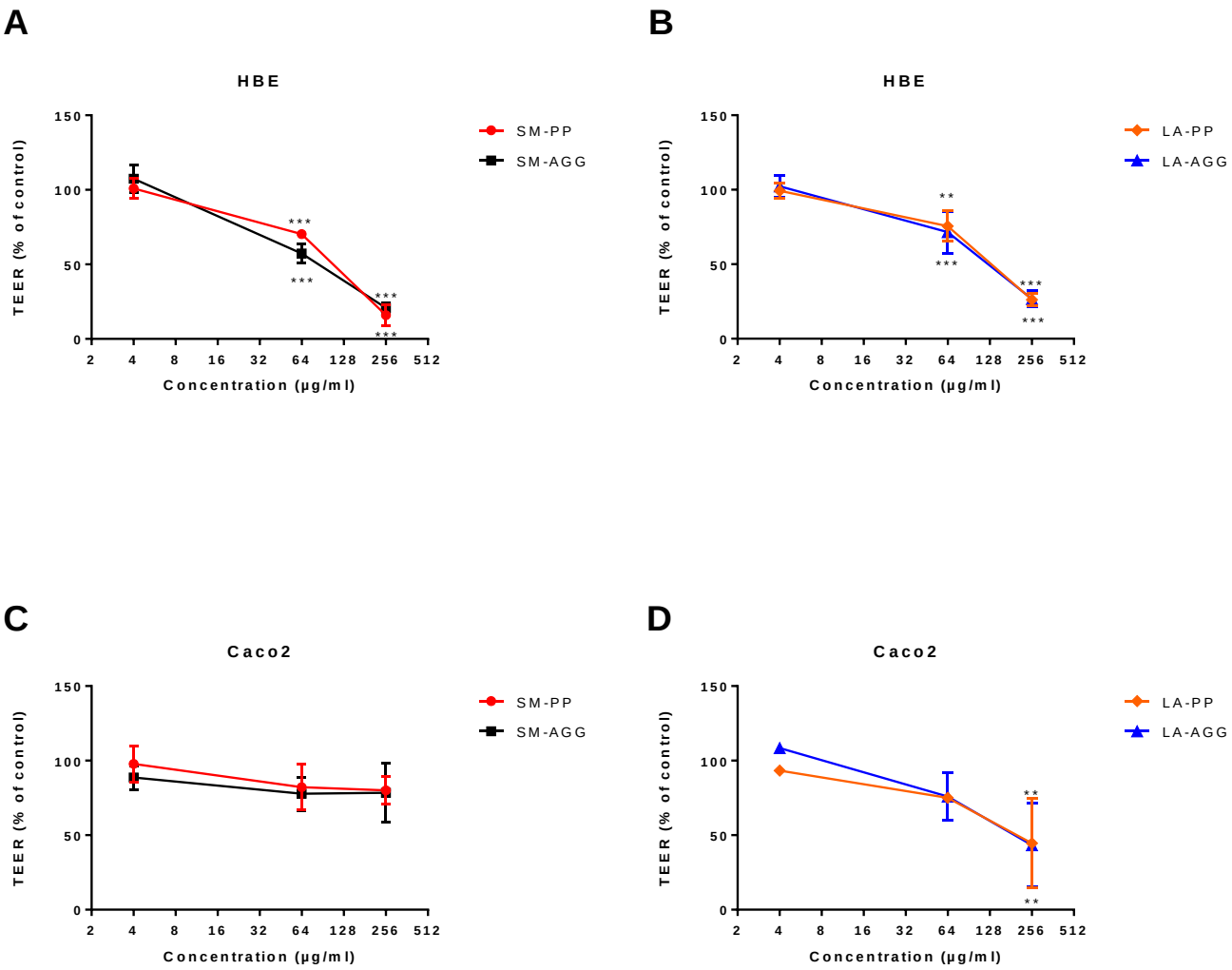

Figure 5.2.3: Effect of TiO_2 NMs on Trans epithelial electrical resistance (TEER). TEER was measured in HBE (A and B) and in Caco2 (C and D) following 24 h exposure to SM-PP (red line), SM-AGG (black line), LA-PP (orange line) and LA-AGG (blue) dispersions. Data are expressed as means ± SD from three independent experiments performed in duplicates. Two-way ANOVA followed by post-hoc tests were performed to determine statistical significances. $p < 0.001$ (***) represents significant difference compared to control.

Pro-inflammatory cytokine release

Annex figures 3, 4, 5 and 6 present the cytokine measurements in different cell lines after 24 h exposure to different concentrations of SM (fig 3 and 4) and LA (fig 5 and 6) TiO_2 NMs. A pronounced effects were seen in THP-1 exposed to SM dispersions. IL-8 and IL-1β were significantly higher for AGG while PP did not show any increase at the same concentrations. Increase of TNF-α was significantly higher compared to control at the highest concentration tested with no difference between PP and AGG. In contrast, LA-PP induced increase of IL-1β only in HBE.

Genotoxicity

Figures 5.2.4 and 5.2.5 illustrate the results of DNA damage measured in different cell lines after 24 h exposure to different concentrations of SM (fig 5.2.4) and LA (fig 5.2.5) TiO_2. For SM, a dose dependent increase of DNA damage was seen in AGG while PP showed a significant effect only at 100 µg/ml. AGG dispersions of SM seem to be potentially genotoxic at low concentrations compared to its PP counterparts, particularly in THP-1. For LA, both dispersions induced similar dose dependent increase of DNA damage in all the cell types.

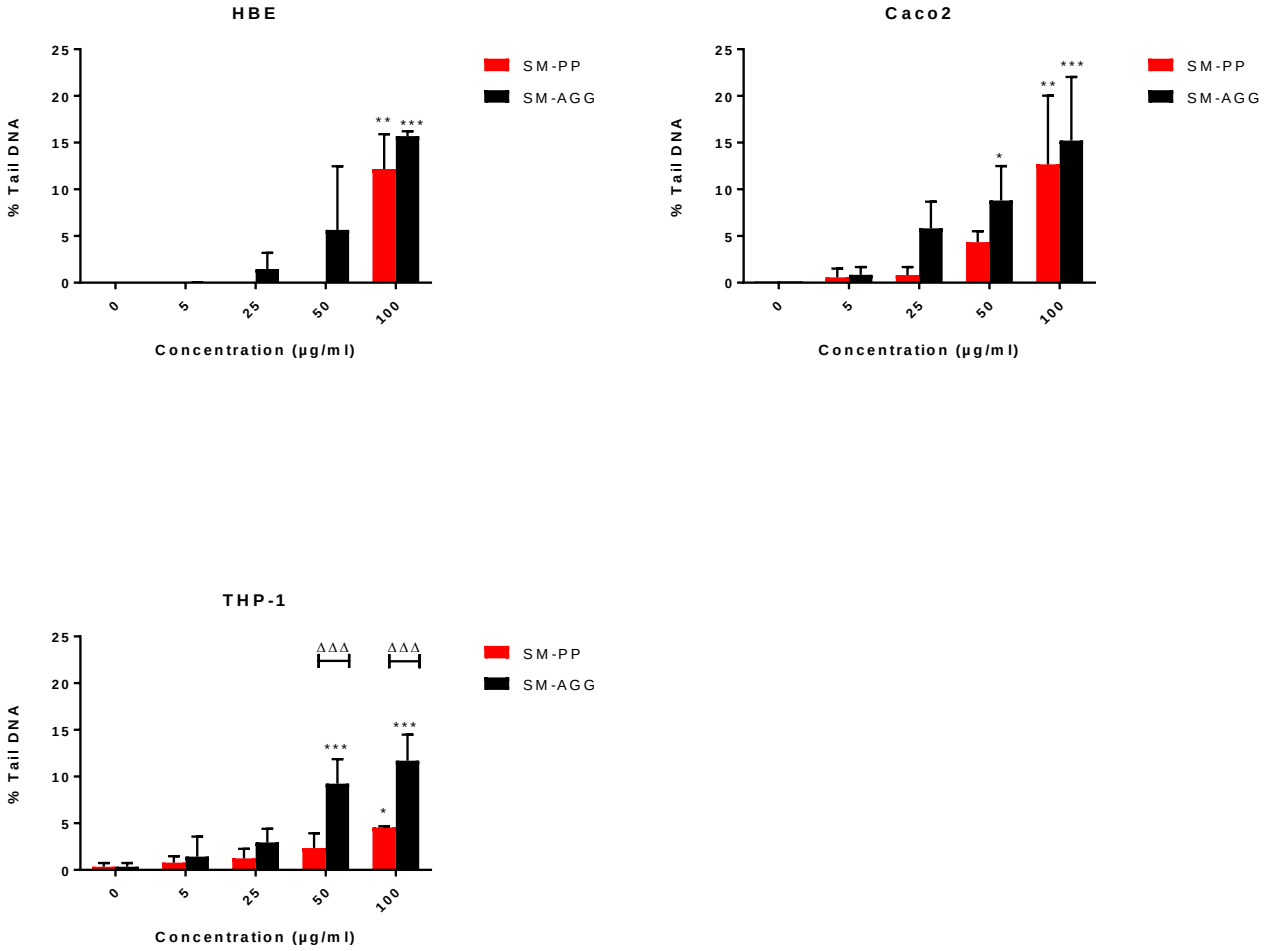

Figure 5.2.4: Effect of TiO_2 NMs on Genotoxicity. DNA damage (A-HBE; B-Caco2; C-THP1) were measured following 24 h exposure to SM-PP (redcolumns) and LA-PP (black columns) suspensions. Data are expressed as means ± SD from three independent experiments performed in duplicates. Two-way ANOVA followed by post-hoc tests were performed to determine statistical significances. $p < 0.05$ (*), $p < 0.01$ (**) and $p < 0.001$ (***) represents significant difference compared to control. $p < 0.001$ (ΔΔΔ) represents significant difference between PP and AGG at the same mass dose.

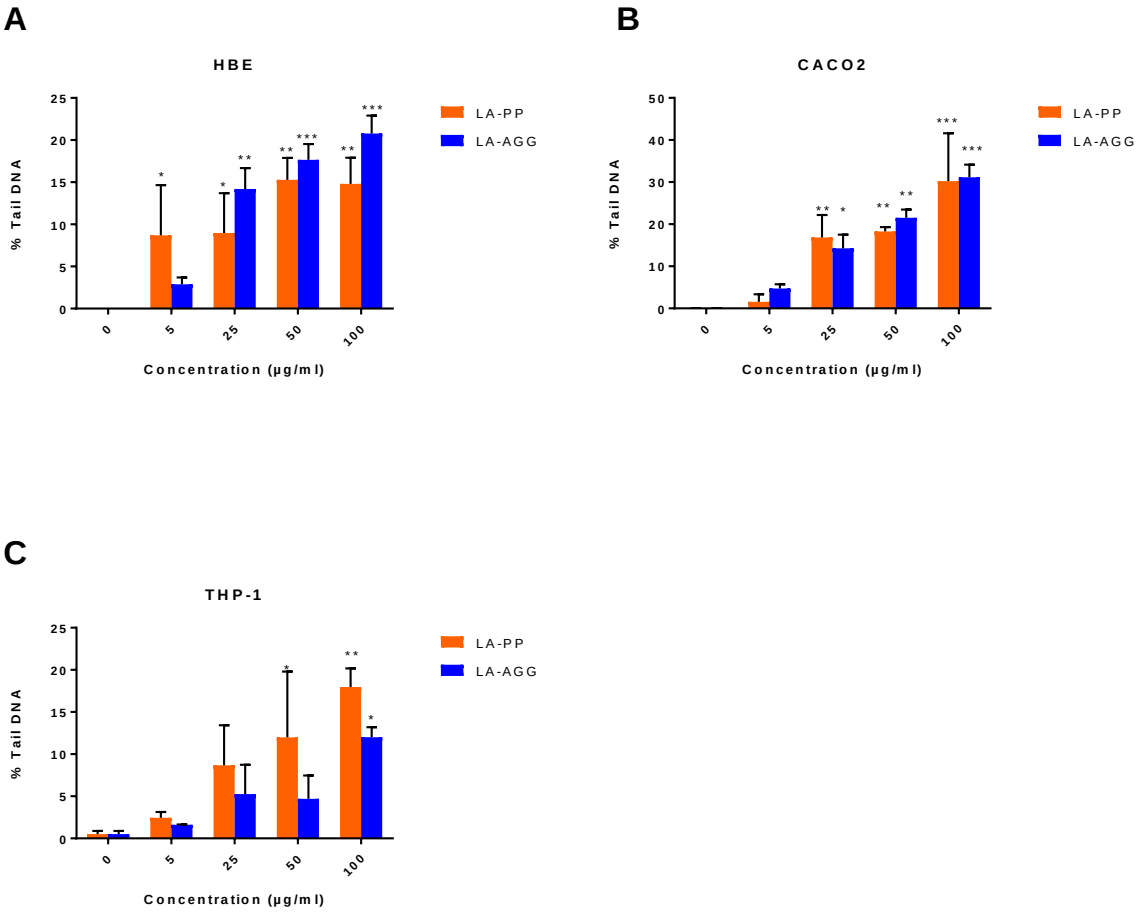

Figure 5.2.5: Effect of TiO_2 NMs on Genotoxicity. DNA damage (A-HBE; B-Caco2; C-THP-1) were measured in the cell cultures following 24 h exposure to LA-PP (orange column) and LA-AGG (blue column) suspensions. Data are expressed as means ± SD from three independent experiments performed in duplicates. Two-way ANOVA followed by post-hoc tests were performed to determine statistical significances. $p < 0.05$ (*), $p < 0.01$ (**) and $p < 0.001$ (***) represents significant difference compared to control.

In vitro dosimetry

In Caco2 cell culture medium, the size of the particles tend to change > 30 % over 24 h incubation in Caco2 cell culture medium and did not meet the criteria (i.e. change in size<30% over 24 h) to perform the dosimetry analysis. Therefore, *in vitro* dosimetry evaluation was performed only for HBE cell cultures. Figure 5.2.6 shows the TiO_2 dose delivered to HBE cell cultures as a function of nominal (applied) dose. The results suggest that the dose delivered to the cells was significantly lower compared to the dose applied, but the dose delivered between dispersions did not or slightly differed. Therefore, the difference in toxicity observed between the dispersions could not be attributed to differential dosimetry contribute.

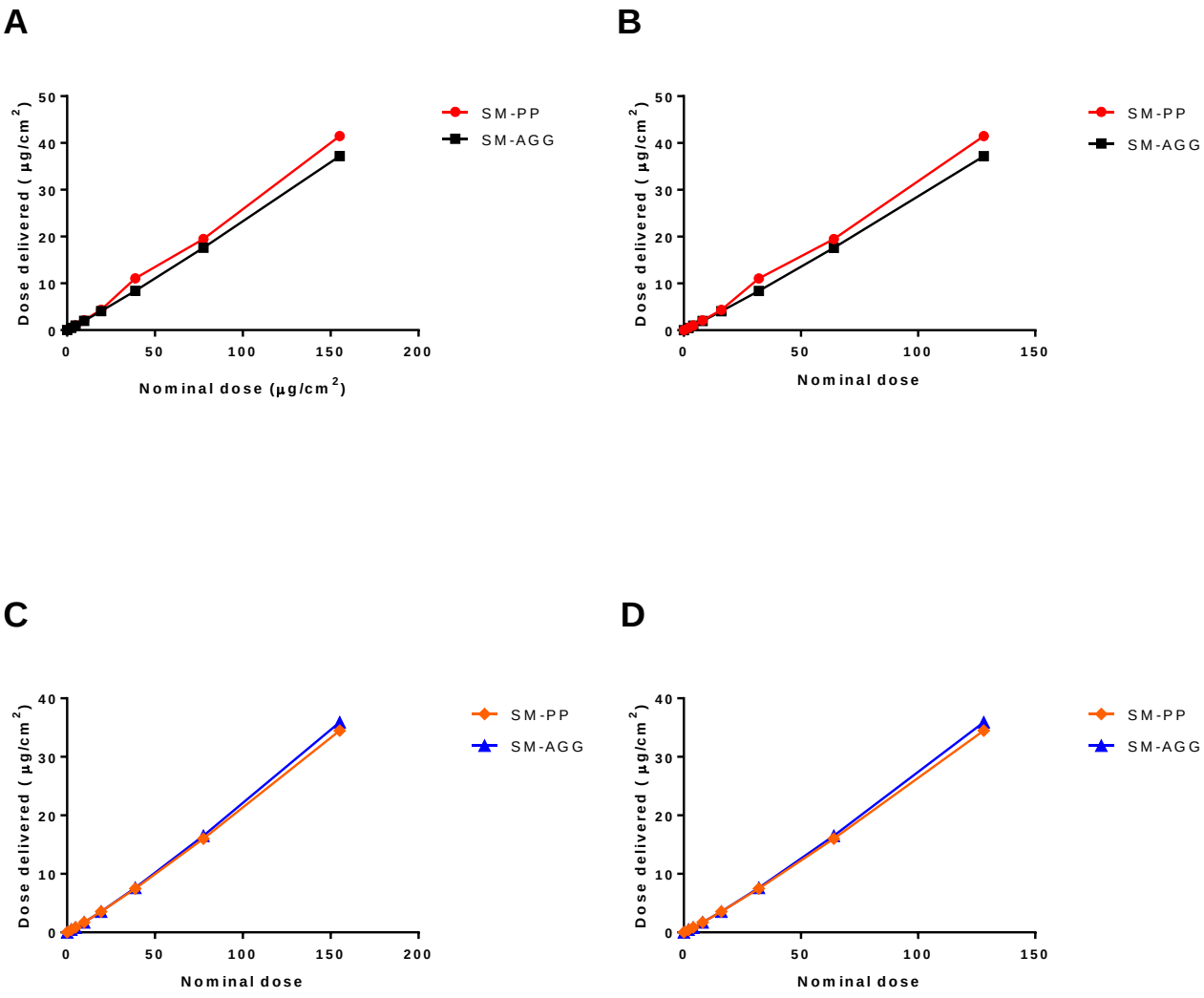

Figure 5.2.6: Dose reaching the HBE cell cultures after 24h (calculated by VCM and distorted grid model) as a function of nominal dose in 96 well plate (A) and in 24 well plate (B).

5.2.1.2 Aggregation - silica NMs

Cytotoxicity

Cytotoxicity was measured using the WST-1 (Figure 5.2.7A, C, E) and LDH assays (Figure 5.2.7B, D, F). DE-AGGR silica strongly reduced the metabolic activity in a dose dependent manner in HBE (64 - 128 µg/mL) and in Caco2 and THP-1 (32 - 128 µg/mL). This decrease was significant compared to AGGR, which caused a mild or no decrease at the same concentrations. The results of the LDH assay showed that DE-AGGR silica strongly affected the cell viability in all the cell lines compared to AGGR, and such differences were significant only in HBE (16 - 128 µg/mL) and in caco2 (64 - 128 µg/mL). In THP1, no significant difference between both dispersions was observed.

Oxidative stress induction

Glutathione (GSH) depletion was measured as an indicator of oxidative stress (Figure 5.2.8). DE-AGGR strongly decreased the GSH levels dose-dependently in all the cell lines compared to AGGR, but the difference between these dispersions was significant only at 64 µg/mL in HBE and at 32 - 64 µg/mL in Caco2 and THP-1. At the highest concentration tested (128 µg/mL), the magnitude of GSH depletion induced by DE-AGGR was not significantly different compared to AGGR in all the cell lines.

Barrier integrity

TEER was measured as an indicator of epithelial barrier integrity (Figure 5.2.9). The TEER was decreased in dependence of dose in HBE and Caco2 monolayers exposed with DE-AGGR. AGGR also affected the TEER in HBE cells in a dose-dependent manner, while such a decrease was noticed in Caco2 cells only at the highest concentration tested (32 µg/mL). Compared to AGGR, HBE and Caco2 cells exposed with DE-AGGR showed a significantly stronger decrease in TEER at concentrations of 8 - 16 µg/mL and 32 µg/mL, respectively.

Pro-inflammatory cytokine release

IL-8 and IL-6 release were measured in the supernatants of exposed cultures using ELISA (Figure 5.2.10)**.** A strong and dose-dependent increase of IL-8 and IL-6 was observed in HBE and Caco2 exposed to DE-AGGR but not in AGGR-exposed cells. In contrast, THP-1 cells showed a ~ 40-fold increase at 32 µg/mL, which dropped to ~20 fold at 128 µg/mL compared to control. No significant increase of IL-6 was noticed in THP-1 for both dispersions.

Genotoxicity

At maximum testable concentration (cell cultures with viability about 70%), assessment of DNA damage in cell cultures indicate that none of the dispersions induced any significant DNA damage in any of the cell lines tested (annex figure 7).

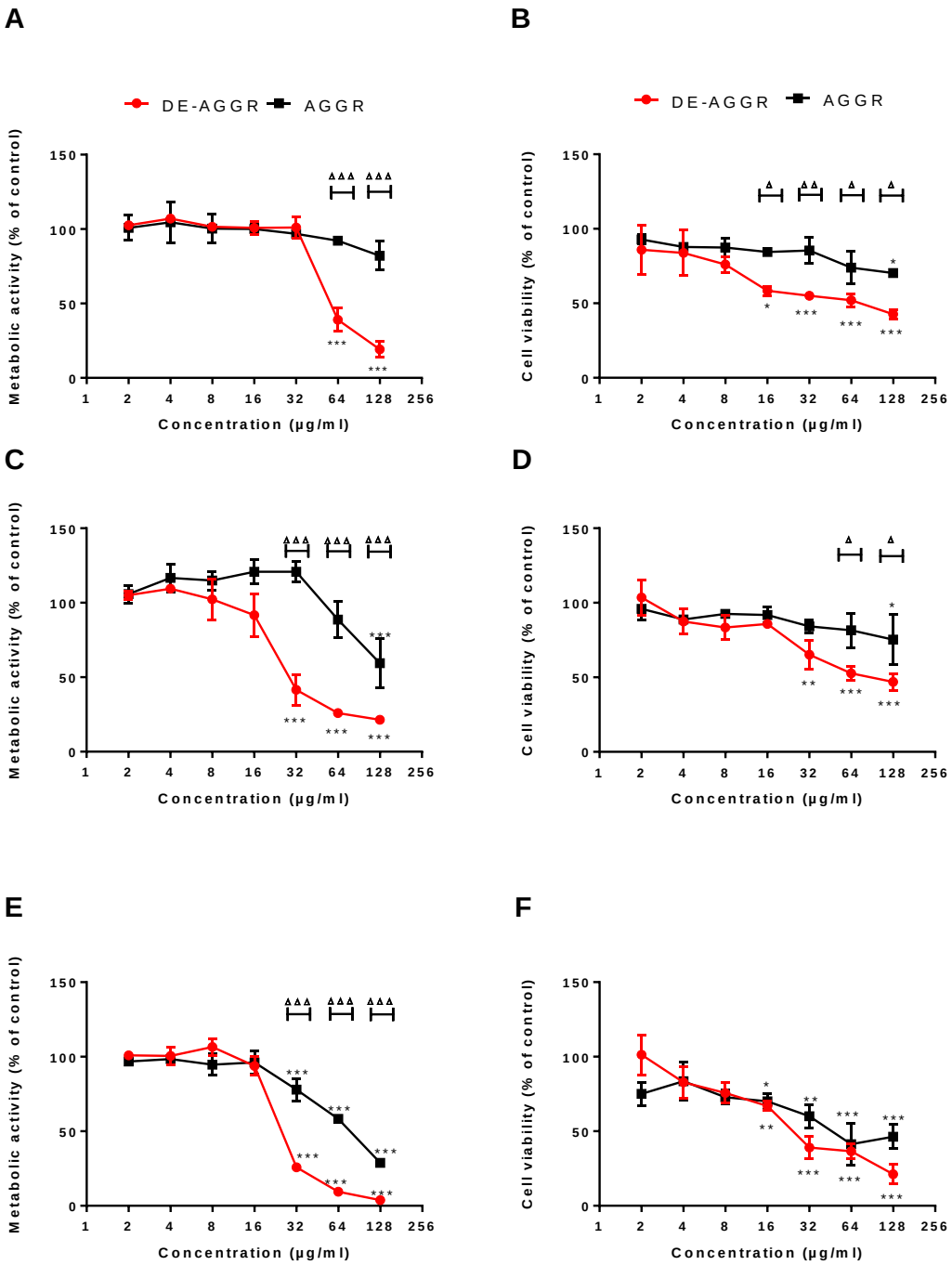

Figure 5.2.7: Effect of silica NMs on cytotoxicity. WST-1 and LDH assay was used to measure the effect on metabolic activity (A-HBE;C-Caco2; E-THP1) and cell viability (B-HBE;D-Caco2; F-THP1) in cell cultures following 24 h exposure to DE-AGGR (red line) and AGGR (black line) dispersions. Data are expressed as means ± SD from three independent experiments performed in triplicates. Two-way ANOVA followed by post-hoc tests were performed to determine statistical significances. $p < 0.05$ (*), $p < 0.01$ (**) and $p < 0.001$ (***) represents significant difference compared to control; $p < 0.05$ (Δ), $p < 0.01$ (ΔΔ) and $p < 0.001$ (ΔΔΔ) represents significant difference between DE-AGGR and AGGR at the same mass dose.

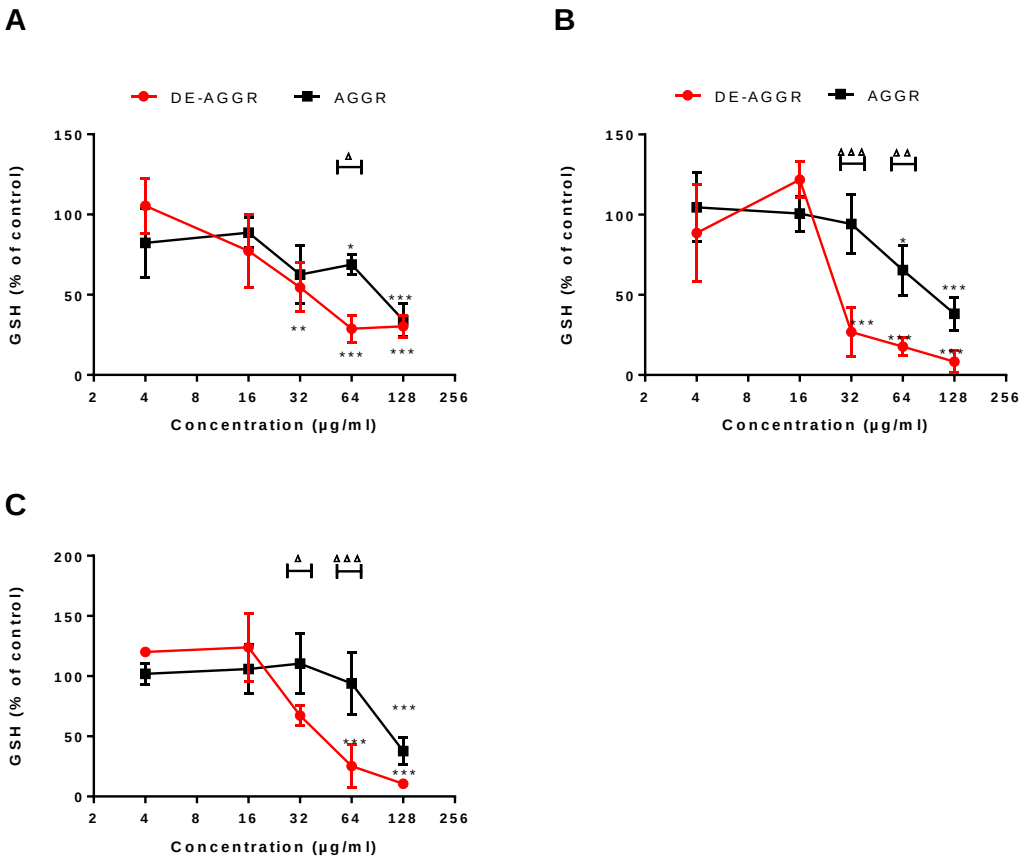

Figure 5.2.8: Effect of silica NMs on glutathione (GSH) levels. GSH levels were measured in cell cultures (A-HBE; B-Caco2; C-THP1) following 24 h exposure to DE-AGGR (red line) and AGGR (black line) dispersions. Data are expressed as means ± SD from three independent experiments performed in duplicates. Two-way ANOVA followed by post-hoc tests were performed to determine statistical significances. $p < 0.05$ (*), $p < 0.01$ (**) and $p < 0.001$ (***) represents significant difference compared to control; $p < 0.05$ (Δ), $p < 0.01$ (ΔΔ) and $p < 0.001$ (ΔΔΔ) represents significant difference between DE-AGGR and AGGR at the same mass dose.

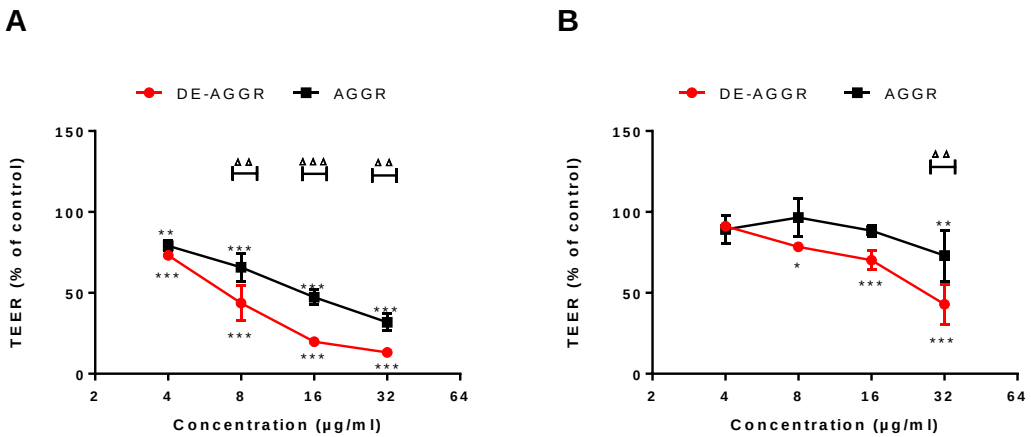

Figure 5.2.9: Effect of silica NMs on Trans epithelial electrical resistance (TEER). TEER was measured in cell cultures (A-HBE;B-Caco2) following 24 h exposure to DE-AGGR (red line) and

AGGR (black line) dispersions. Data are expressed as means ± SD from three independent experiments performed in duplicates. $p < 0.05$ (*), $p < 0.01$ (**) and $p < 0.001$ (***) represents significant difference compared to control. Two-way ANOVA followed by post-hoc tests were performed to determine statistical significances. $p < 0.05$ (Δ), $p < 0.01$ (ΔΔ) and $p < 0.001$ (ΔΔΔ) represents significant difference between DE-AGGR and AGGR at the same mass dose.

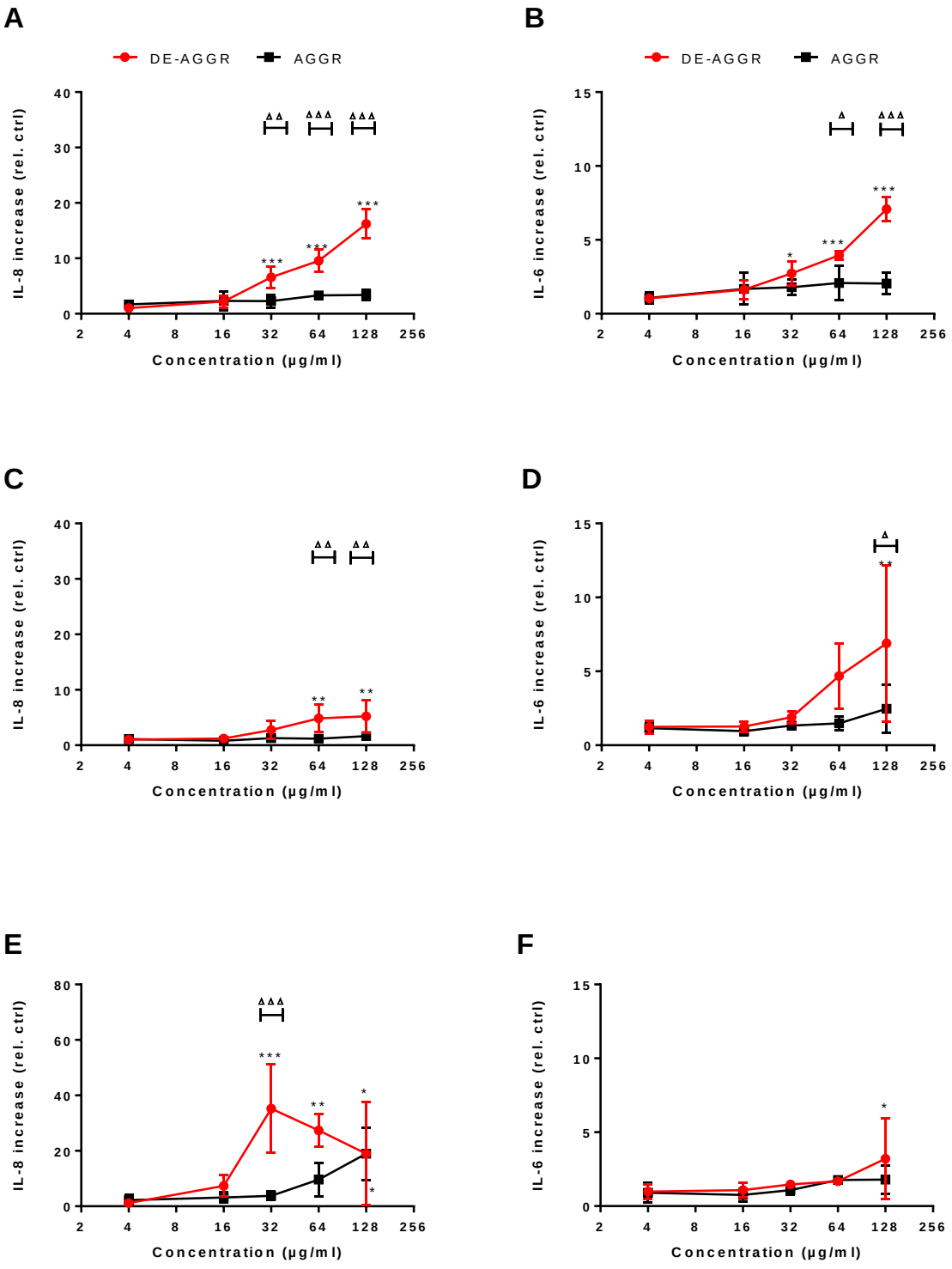

Figure 5.2.10: Effect of silica NMs on cytokine release. IL-8 (A-HBE; C-Caco2; E-THP1) and IL-6 (B-HBE; D-Caco2; F-THP1) levels were measured in the supernatant of the cell cultures following 24 h exposure to DE-AGGR (red line) and AGGR (black line) suspensions. Data are expressed as means ± SD from three independent

experiments performed in duplicates. Two-way ANOVA followed by post-hoc tests were performed to determine statistical significances. $p < 0.05$ (*), $p < 0.01$ (**) and $p < 0.001$ (***) represents significant difference compared to control; $p < 0.05$ (Δ), $p < 0.01$ (ΔΔ) and $p < 0.001$ (ΔΔΔ) represents significant difference between DE-AGGR and AGGR at the same mass dose.

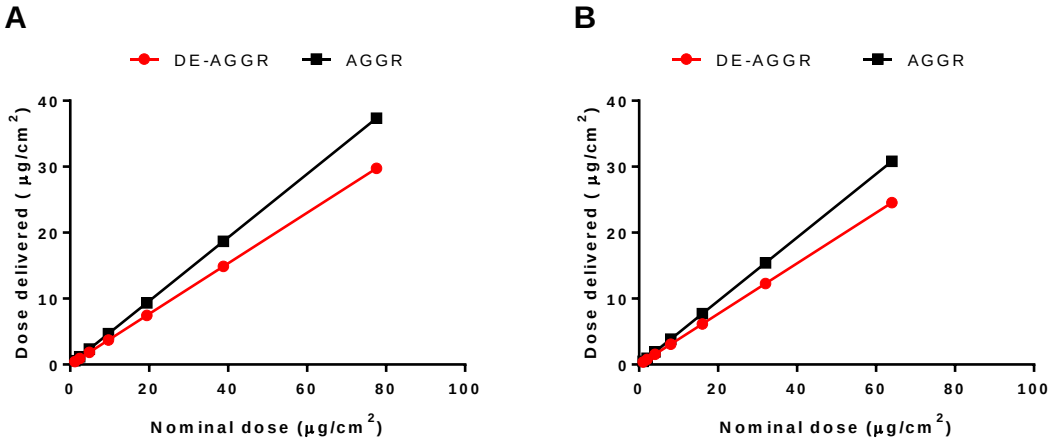

Figure 5.2.11: Dose reaching the HBE cell cultures after 24h estimated by VCM and distorted grid model in 96 well plate (A) and in 24 well plate (B) as a function of nominal dose.

In vitro dosimetry

In Caco2 cell culture medium, the size of the particles tend to change > 30 % over 24 h incubation in Caco2 cell culture medium and did not meet the criteria (i.e. change in size<30% over 24 h) to perform the dosimetry analysis. Therefore, *in vitro* dosimetry evaluation was performed only for HBE cell cultures. Figure 5.2.11 shows the silica dose delivered to HBE cell cultures as a function of nominal (applied) dose. The measurements from *in vitro* dosimetry suggest that the dose delivered to the cells was significantly lower compared to the dose applied, but, the dose delivered did not differ or slightly differed between both dispersions. Therefore, the difference in toxicity observed between the dispersions could not be attributed to differential dosimetry contribute.

We noticed that the AGGR dispersion was composed of two different fractions of aggregates, one that sedimented quickly (PREC) after vortexing and the other remained well dispersed in the supernatant (SuperN).). The quantification of Si by ICP-MS in SuperN and PREC suspensions indicated that Si was distributed in each fraction at a rate of 25 % in SuperN and 75 % in PREC. Therefore, both dispersions were fractionated and tested separately to determine which fraction contributed to AGGR toxicity.

Figure 5.2.12 illustrate the comparison of effects induced by DE-AGGR, SuperN and PREC, both prepared from AGGR dispersion (as a function initial in this figure, mass concentrations were not adapted according to the distribution determined above). The PREC composed of visible large aggregates did not show any biological activity although its mass concentration was 75% of the AGGR dispersion. Further, the quick sedimentation of PREC did not influence the toxicity. However, SuperN composed of smaller aggregates with indicative size ~ 250 nm showed toxicity/biological activity, particularly in THP-1 and HBE cells. The effects

observed with AGGR and SuperN were similar, suggesting that the effects observed with AGGR were predominantly induced by “small” particles in the SuperN fraction (figure 5.2.12). The most interesting is, the comparison between effects induced by DE-AGGR and SuperN dispersions at the same mass doses reveals that both suspensions induced very similar effects (figure 5.2.13).

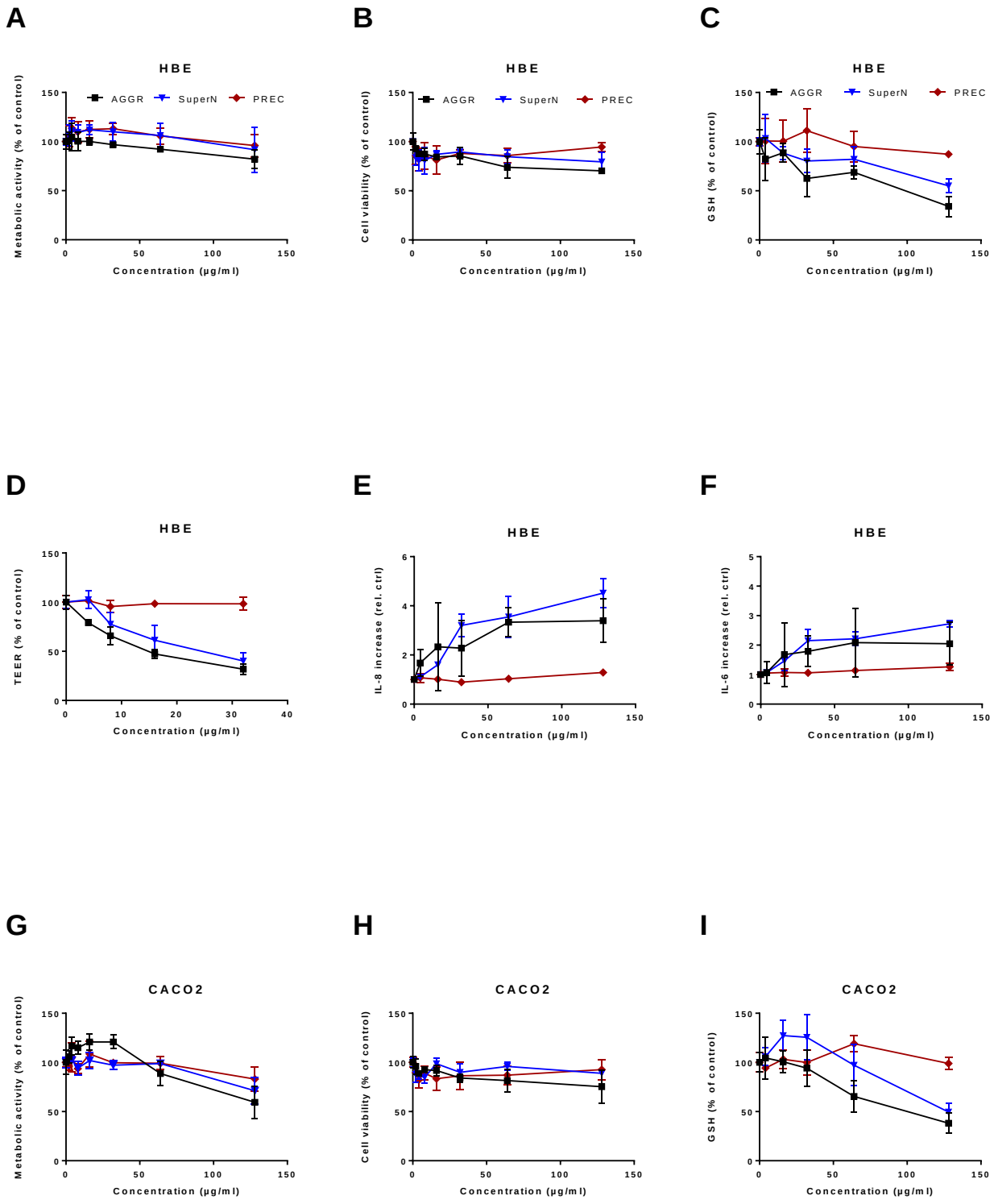

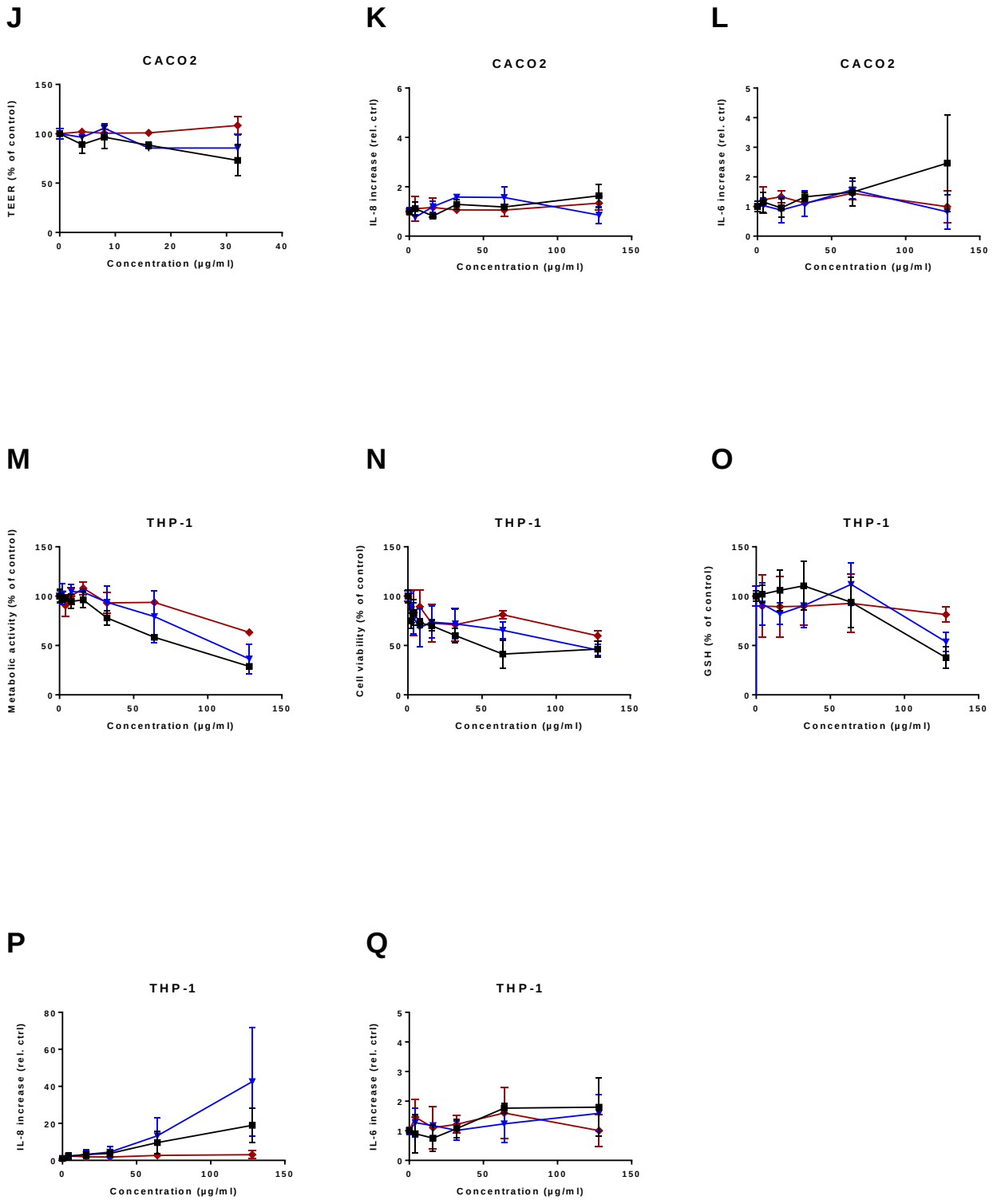

Figure 5.2.12: Comparison of effects induced by different silica dispersions. Toxic and biological effects induced by AGGR (black line) in HBE (A-F), Caco2 (G-L) and THP-1 (M-Q) were compared with SuperN (blue line) and PREC (brown line) as a function of the initial mass doses.

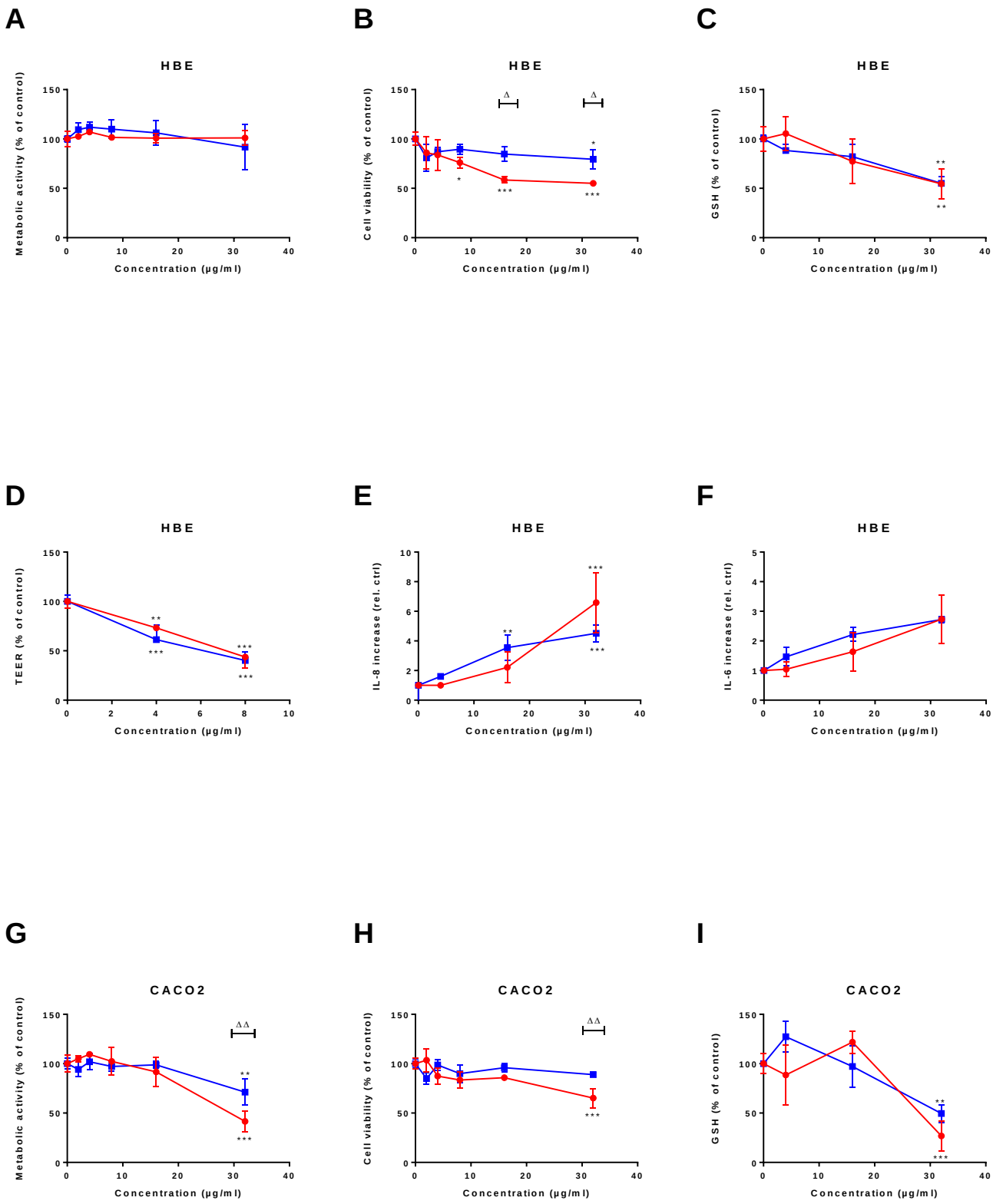
A
HBE
Metabolic activity (% of control)
Concentration (µg/ml)
B
HBE
Cell viability (% of control)
Concentration (µg/ml)
C
HBE
GSH (% of control)
Concentration (µg/ml)
D
HBE
TEER (% of control)
Concentration (µg/ml)
E
HBE
IL-8 increase (rel. ctrl)
Concentration (µg/ml)
F
HBE
IL-6 increase (rel. ctrl)
Concentration (µg/ml)
G
CACO2
Metabolic activity (% of control)
Concentration (µg/ml)
H
CACO2
Cell viability (% of control)
Concentration (µg/ml)
I
CACO2
GSH (% of control)
Concentration (µg/ml)

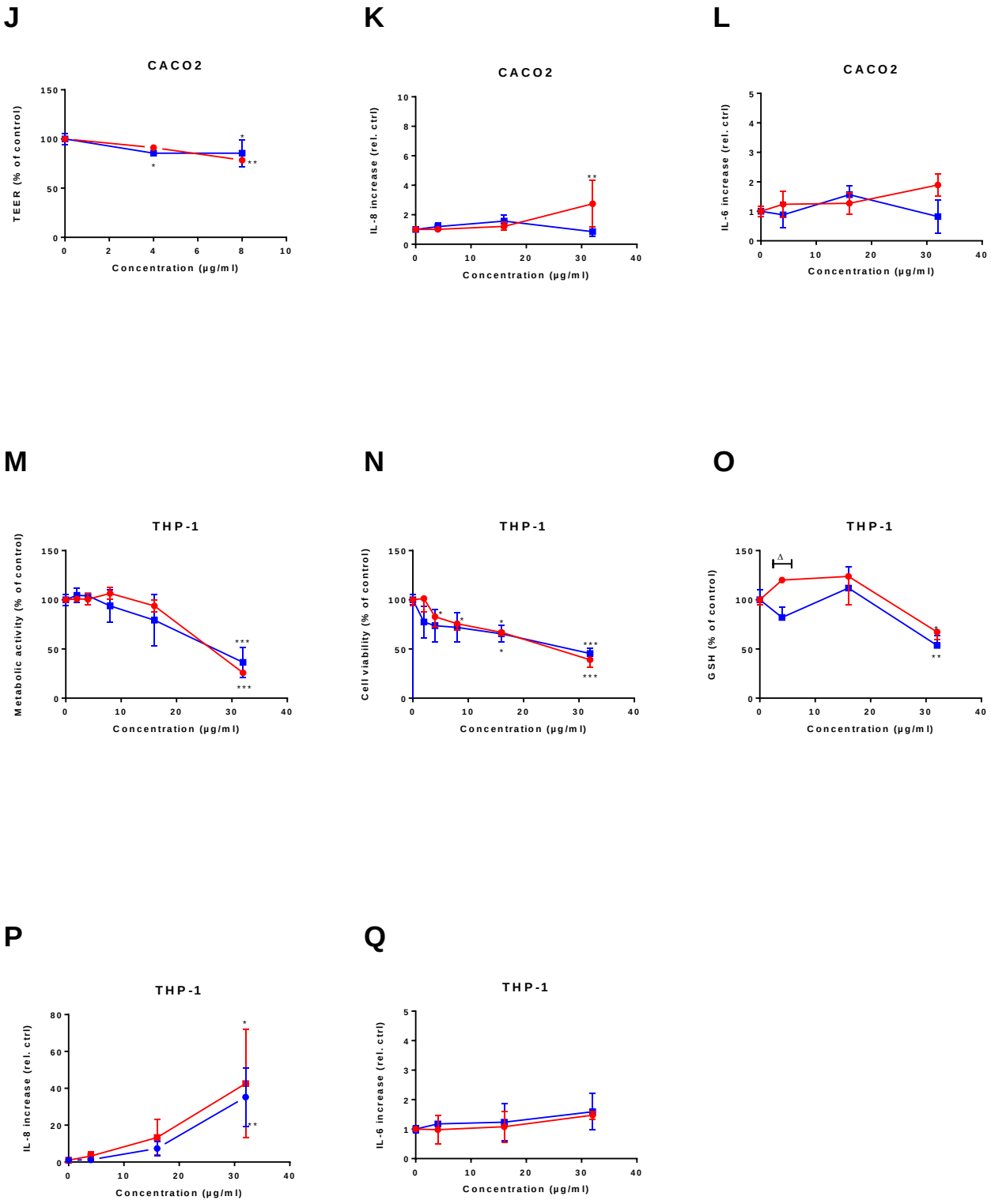

Figure 5.2.13: Comparison of effects induced by different silica dispersions. Toxic and biological effects induced by DE-AGGR (red line) in HBE (A-F), Caco2 (G-L) and THP-1 (M-Q) were compared with SuperN (blue line) at the same mass doses (1-32 µg/mL). The results are presented as mean± SD from three independent experiments. Two-way ANOVA followed by post-hoc tests were performed to determine statistical significances. $p < 0.05$ (*), $p < 0.01$ (**) and $p < 0.001$ (***) represents significant difference compared to control; $p < 0.05$ (Δ), $p < 0.01$ (ΔΔ) and $p < 0.001$ (ΔΔΔ) represents significant difference between DE-AGGR and AGGR at the same mass dose.

5.2.2 Chronic exposure in vitro

5.2.2.1 Agglomeration - TiO_2 NMs

Annex figure 8 presents toxicity and biological responses measured in different cell lines after 3 weeks of repeated exposure to a low concentration. No significant effects were observed for any of the dispersions indicating that the exposure concentration might not be sufficient to induce toxicity/biological responses.

5.2.2.2 Aggregation - silica NMs

Figure 5.2.14 represents the toxic/ biological effects measured induced by low dose repeated exposure to different SiO_2 dispersions. At the end of a three weeks exposure, cell viability and total GSH levels of all the cell lines was not affected by any of these suspensions. Interestingly, DE-AGGR decreased the cell number only in HBE cells compared to the control. A nearly 2.5-fold increase of IL-8 and a 3-fold increase of IL-6 release was found in the supernatant of DE-AGGR and AGGR exposed HBE cells. In contrast to HBE cells, THP-1 and Caco2 did not show any significant effects on cytokine release compared to the control.

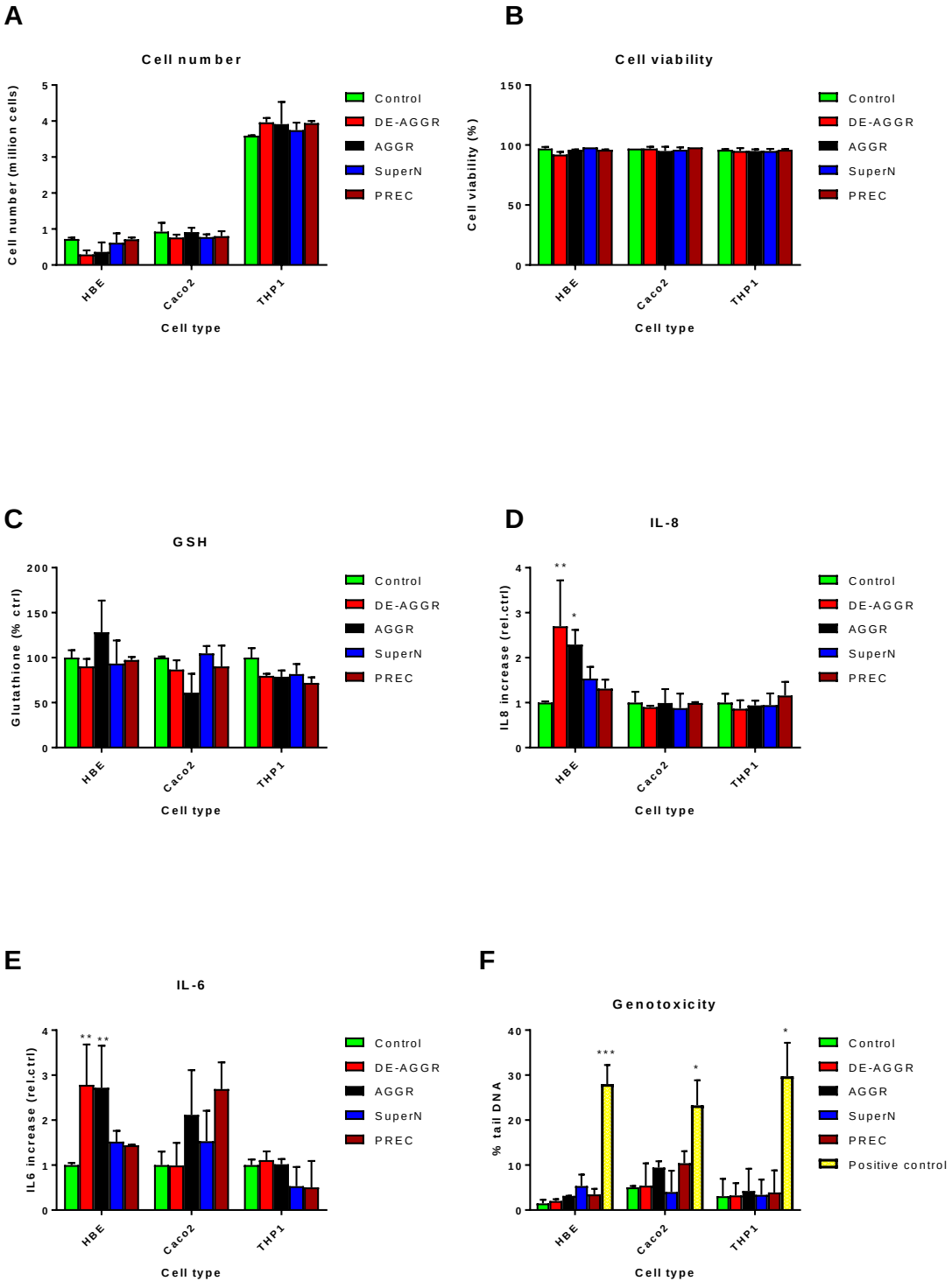

Figure 5.2.14: Effects induced by repeated exposure to a low concentration of silica dispersions. Cell number (A), cell viability (B), GSH levels (C), IL-8 release (D), IL-6 release (E) and DNA damage (F) evaluated in different cell lines after repeated exposure to 2 µg/ml of DE-AGGR and AGGR; 1.5 µg/ml of PREC and 0.5 µg/ml of SuperN dispersions.

5.2.3 Task 3.3: Measurements of effects in tissues obtained in the in vivo study (samples from task 2.2)

5.2.3.1 Short-term exposure: Aspiration

Lung damage and inflammation

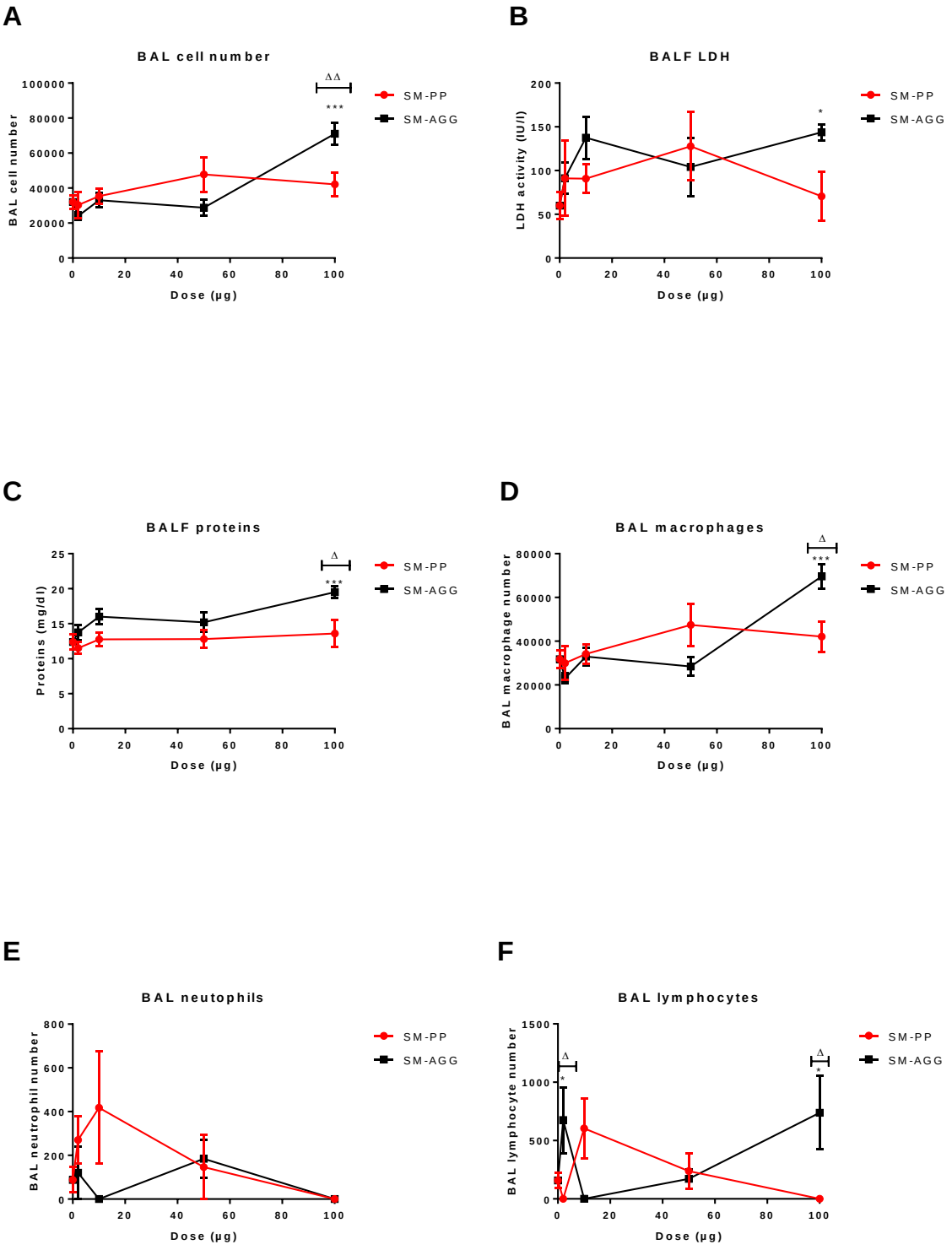

Figure 5.2.15: Effect of SM-TiO_2 dispersions on lung damage and inflammation in mice 3 d after aspiration of increasing doses. cell number(A), LDH activity(B), proteins(C), macrophages(D), neutrophils(E) and lymphocytes(F) measured in the BAL(F) after exposure to SM-PP (red line) or

SM-AGG (black line) suspensions. Data are expressed as means ± SEM from 4-5 mice in each group. $p < 0.05$ (*), $p < 0.01$ (**) and $p < 0.001$ (***) represents significant difference compared to control. Two-way ANOVA followed by post-hoc tests were performed to determine statistical significances. $p < 0.05$ (Δ) and $p < 0.01$ (ΔΔ) represents significant difference between PP and AGG at the same mass dose.

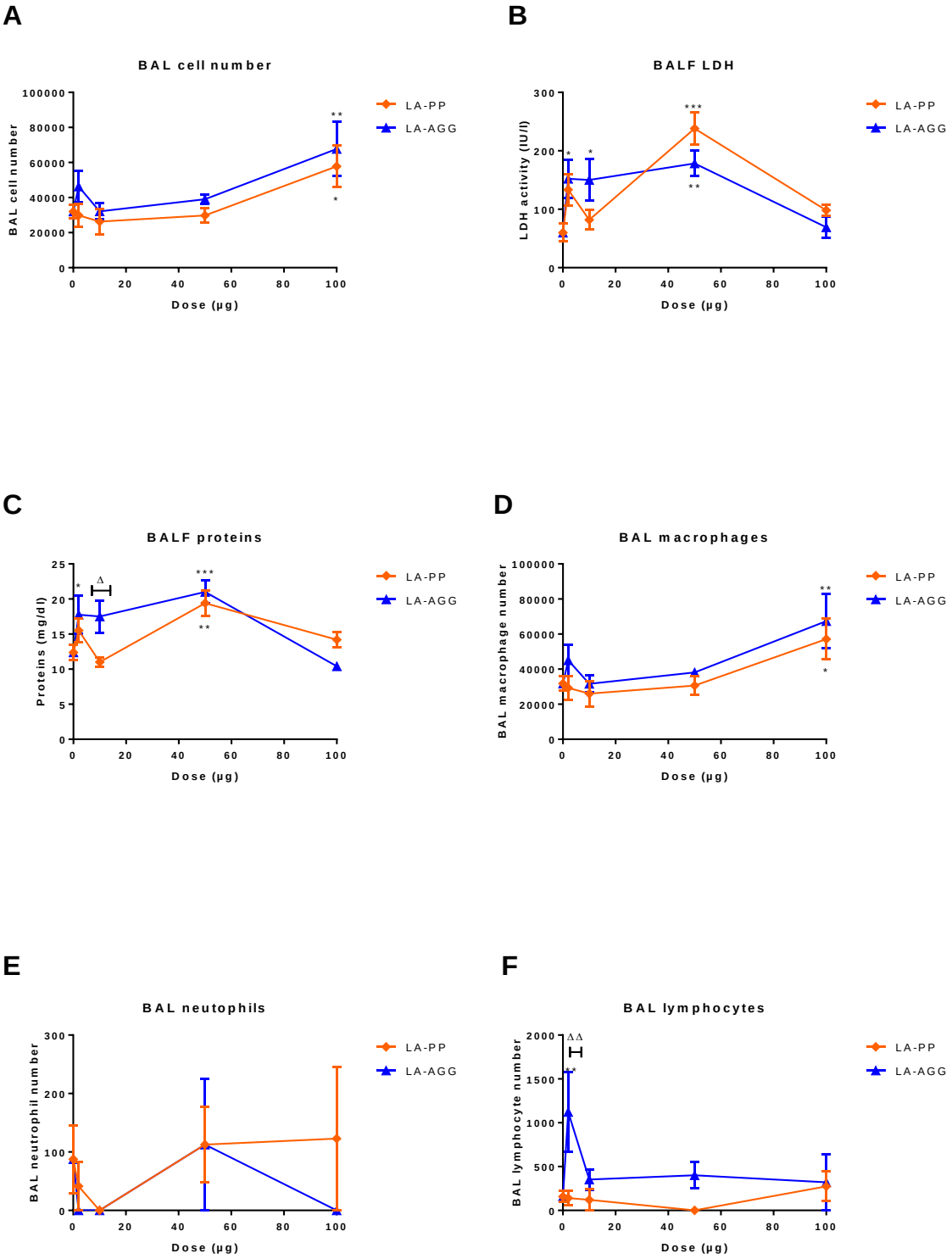

Figure 5.2.16: Effect of LA-TiO_2 dispersions on lung damage and inflammation in mice 3 d after aspiration of increasing doses. cell number(A), LDH activity(B), proteins(C), macrophages(D), neutrophils(E) and lymphocytes(F) measured in the BAL(F) after exposure to SM-PP (red line) or

SM-AGG (black line) suspensions. Data are expressed as means ± SEM from 4-5 mice in each group. $p < 0.05$ (*), $p < 0.01$ (**) and $p < 0.001$ (***) represents significant difference compared to control. Two-way ANOVA followed by post-hoc tests were performed to determine statistical significances. $p < 0.05$ (Δ) and $p < 0.01$ ($\Delta\Delta$) represents significant difference between PP and AGG at the same mass dose.

Figure 5.2.15 and 5.2.16 show the LDH activity, total proteins and inflammatory cells measured after 3 days in the BAL(F) of mice aspirated with SM and LA TiO_2, respectively.

SM-TiO_2: Significant effects were observed only at the highest dose tested. AGG induced significant increase of BALF LDH activity and proteins compared to PP, which induced mild or no effect. Similarly, BAL macrophages and lymphocytes number were significantly higher in AGG exposed mice compared to PP exposed mice. These results suggest that AGG of SM might have a higher potential for lung inflammation compared to its PP counterparts.

LA-TiO_2: AGG and PP showed similar potential for lung damage. However, a dose specific response was seen at 50 µg with an increase in BAL LDH activity and proteins while no significant effect observed at the highest concentration (100 µg). A significant increase in macrophages was observed at 100 µg but no significant difference between PP and AGG was noticed. These results suggest that AGG of SM might have the similar potential for lung inflammation compared to PP its counterparts.

Systemic inflammation

Figure 5.2.17 presents quantification of white blood cells (WBCs) in the blood of mice aspirated with SM and LA TiO_2 respectively. SM-TiO_2 showed a significant effect only at 100 µg; AGG and PP induced similar increase of blood lymphocytes, decrease in monocytes and.granulocytes. A similar trend was observed for LA-TiO_2 except for blood monocytes, whereas PP induced a mild but significant decrease compared to its AGG counterparts.

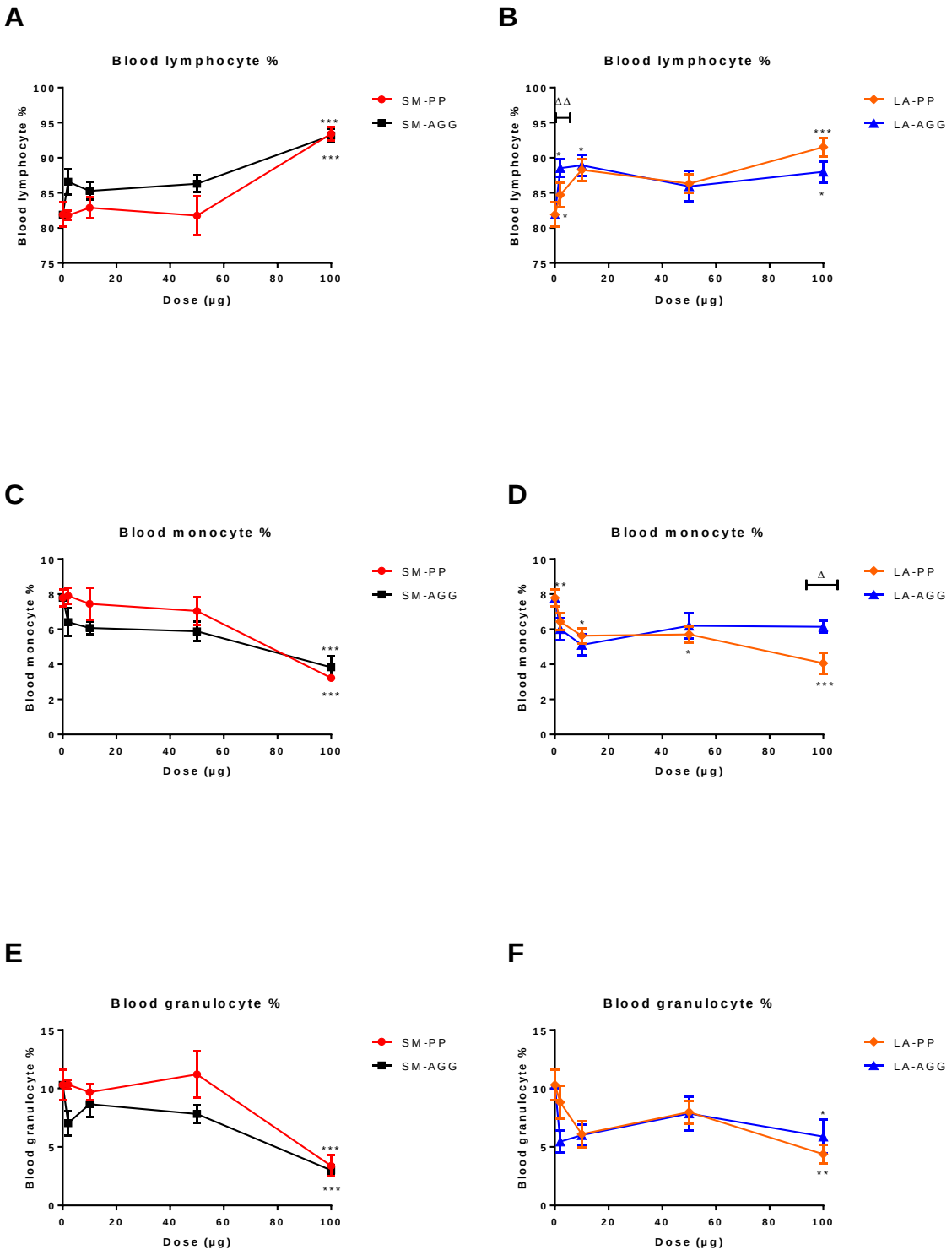

Figure 5.2.17: Effect on systemic inflammation in mice aspirated 3d before with different doses of TiO_2 dispersions. lymphocytes(A and B), monocytes(C and D) and in granulocytes (E and F) changes in blood following exposure to SM (A, C, E) and LA (B, D, F) dispersions. Two-way ANOVA followed by post-hoc tests were performed to determine statistical significances. Data are expressed as means ± SEM from 4-5 mice each group. $p < 0.05$ (*), $p < 0.01$ (**) and $p < 0.001$ (***) represents significant difference compared to control.

Genotoxicity and Oxidative stress

Figure 5.2.18 indicates the results of genotoxicity in blood and BAL, and oxidative stress in the lung of mice aspirated with different doses of TiO_2 dispersions.

SM-TiO_2: a dose dependent increase of DNA damage was noticed in blood for PP while AGG induced an effect only at 100 µg, but significantly higher than PP. At 100 µg, similar increases of BAL DNA damage and glutathione depletion were observed for both PP and AGG.

LA-TiO_2: No overall dose dependent increase of DNA damage was noticed in blood. At 100 µg, similar increases of BAL DNA damage and lung tissue glutathione depletion were observed for both PP and AGG.

Inflammatory mediators

Twenty-three cytokines were measured in BALF and blood of mice exposed to the highest dose. No significant effect was observed for any of the dispersions (data not shown).

5.2.3.2 Short-term exposure: Gavage

Blood lymphocytes were similarly increased and monocytes/granulocytes decreased by all TiO_2 dispersions in both (figure 5.2.19), Glutathione in liver did not change compared to control. At 500 µg, significant and similar DNA damage were observed for PP and AGG dispersions of SM, while it was only PP of LA TiO_2 which that induced significant damage (figure 5.2.20). No significant effect on blood was observed for any of these dispersions (data not shown). Histopathological analysis indicated that, except a few lymphoid infiltrates in the ileum in both control and treated mice, no alteration or damage of the colon and intestine after TiO_2 treatment were detected (annex figure 9 and 10).

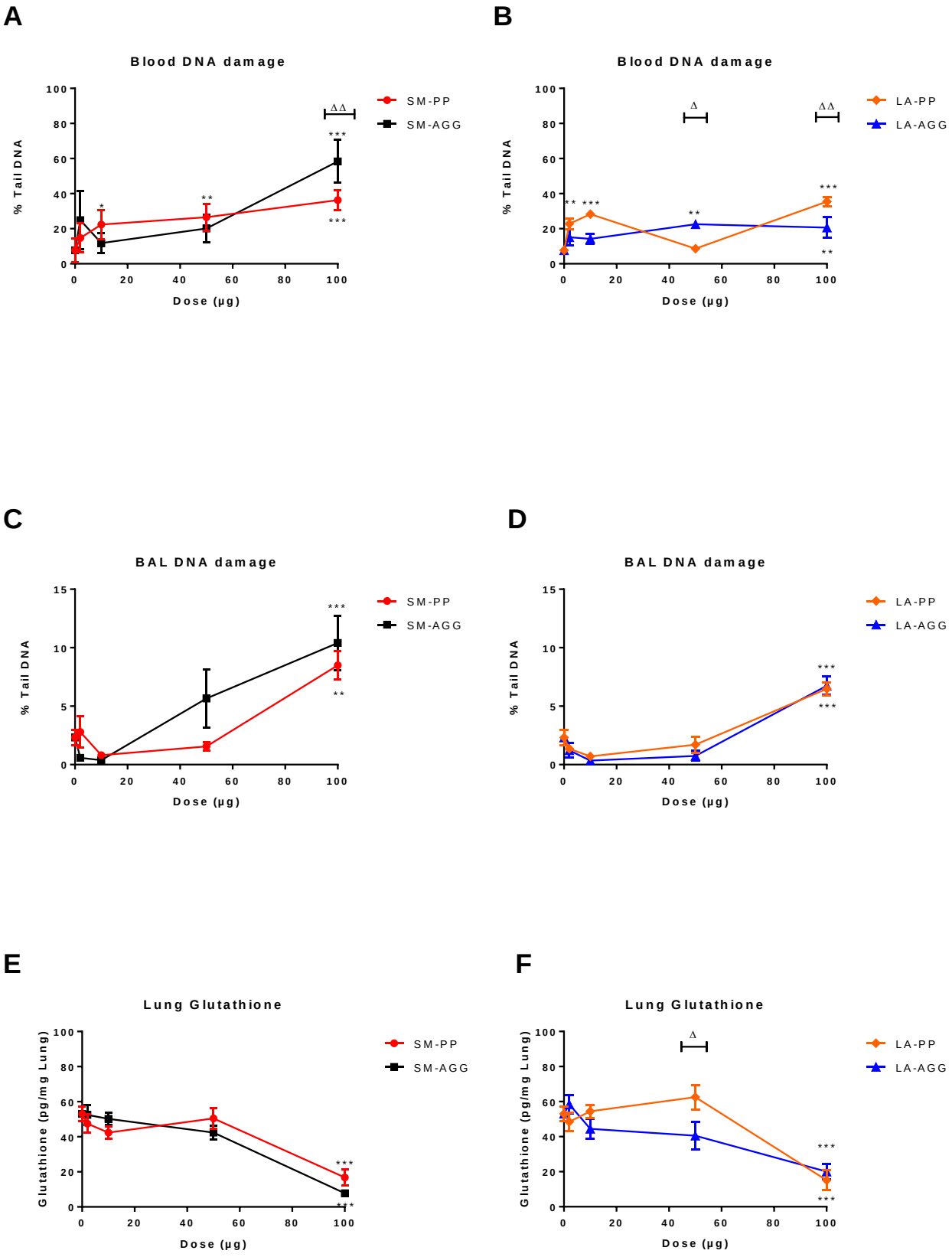

Figure 5.2.18: Effect on genotoxicity and oxidative stress in mice aspirated 3d before with different doses of TiO_2 dispersions. DNA damage in blood (A and B), DNA damage in BAL(C and D) and

glutathione depletion in Lung (E and F) following exposure to SM (A, C, E) or LA (B, D, F) dispersions. Data are expressed as means ± SD from 4-5 mice each group. $p < 0.05$ (*), $p < 0.01$ (**) and $p < 0.001$ (***) represents significant difference compared to control. Two-way ANOVA followed by post-hoc tests were performed to determine statistical significances. $p < 0.05$ (Δ) and $p < 0.01$ (ΔΔ) represents significant difference between PP and AGG at the same mass dose.

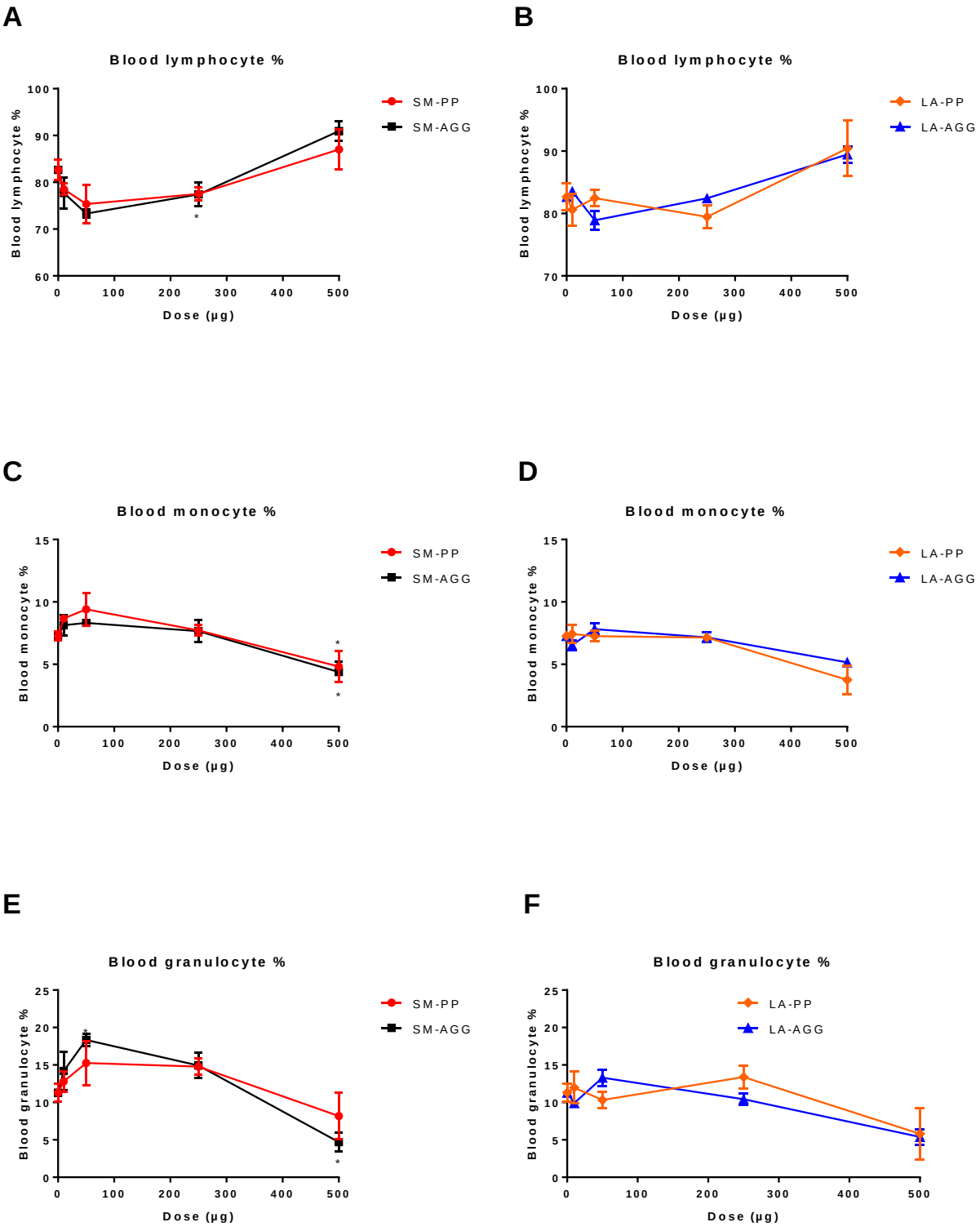

Figure 5.2.19: Effect on systemic inflammation in mice gavaged 3d before with different doses of TiO_2 dispersions. lymphocytes(A and B), monocytes(C and D) and in granulocytes (E and F) changes in

blood following exposure to SM (A, C, E) and LA (B, D, F) dispersions. Data are expressed as means ± SEM from 4-5 mice each group. Two-way ANOVA followed by post-hoc tests were performed to determine statistical significances. $p < 0.05$ (*), $p < 0.01$ (**) and $p < 0.001$ (***) represents significant difference compared to control.

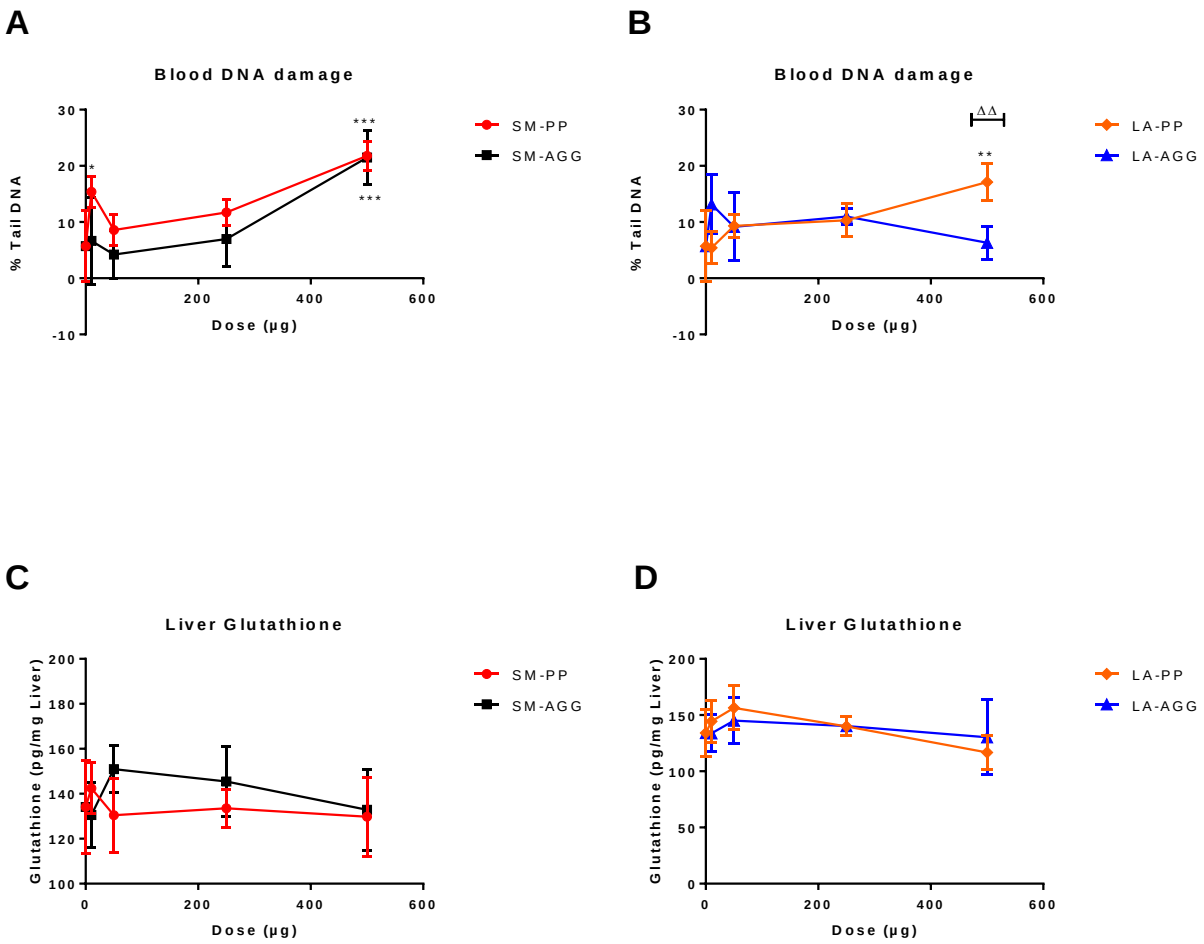

Figure 5.2.20: Effect on genotoxicity and oxidative stress in mice gavaged 3d before with different doses of TiO_2 dispersions (A and B) DNA damage in blood , (C and D) Glutathione depletion in liver following exposure to SM (A,C,E) and LA (B,D,F) dispersions. Data are expressed as means ± SD from 4-5 mice each group. Two-way ANOVA followed by post-hoc tests were performed to determine statistical significances. $p < 0.05$ (*), $p < 0.01$ (**) and $p < 0.001$ (***) represents significant difference compared to control.

Effect on colon and ileum:

Annex figure 9 and 10 shows the images of colon and ileum of mice exposed with 500 µg of different TiO_2 dispersions. Except a few lymphoid infiltrates in the ileum in both control and treated mice, the histopathologist did not observe any alteration or damage of the colon and intestine after TiO_2 treatment.

6 WORK PACKAGE 4: DATA INTEGRATION AND DISSEMINATION

6.1 METHODOLOGY

6.1.1 Statistical analyses

One-way Anova, correlations, Principal Component Analysis (PCA), uni- and multivariate anaylses (regression) were performed using Statistical Software Analysis (SAS) Enterprise Guide 7.1. Statistical analyses were performed with different combinations of dispersions based on our research question.

The database of TiO_2 comprising about 14 descriptive TEM measurands, 3 measurements from other techniques (DLS, PTA) and multiple biological endpoints. For these database, full integration of data could be performed. For silica it was not possible to have all descriptive measurands (issues described in Task 3.2.4), but, only for the DE-AGGR, 6 descriptive measurands could be assessed; therefore it was not meaningful to perform the deep statistical analysis. However, the toxic/biological effects induced by two most important silica (DE-AGGR, SuperN) dispersions were statistically compared (refer figure 5.2.13).

6.2 SCIENTIFIC RESULTS AND RECOMMENDATIONS

6.2.1 Guidelines concerning analytical procedures

The main objective of this task was to classify different measurands (Annex table 1) obtained from descriptive TEM and from other measurements in independent groups of highly correlated parameters such as size, shape and surface topology. We performed PCA analysis to reduce the dimensionality of the data. Table 6.2.1 shows the PCA analysis performed with all the measurands from different dispersions. As expected, many of the measurands strongly correlated to each other. Size related properties are strongly correlated with Principal component (PC) 1 (marked in red in PC1 column) while shape and surface topology related properties (marked in red in PC2 column) are correlated with PC 2. Interestingly, secondary sizes (hydrodynamic diameters) was also highly correlated to PC2. It is feasible to select one representative measurand per group as a nominator/descriptor of size and shape/surface topology/secondary size properties of anatase TiO_2 NMs.

Table 6.2.1: PCA analysis performed with all the measurands from different dispersions. Principal component (PC) 1 and principal component (PC) 2 explains most of the variation in the data. Values in the table represent the correlation coefficient and values in red indicate the measurands that are highly correlated to either PC1 or PC2.

Measurands	PC1	PC2
Size related properties		
Feret maximum	0.303142	-0.03707
Feret minimum	0.301935	-0.05124
Rectangle long side	0.289371	-0.12598
Rectangle short side	0.266136	-0.19777
Maximum inscribed circle diameter	0.289169	-0.09997
Area equivalent diameter	0.300949	-0.06139
Perimeter	0.287439	0.121415
Area	0.275773	-0.16455
Area perimeter	0.298441	-0.06243
Aspect ratio	0.117387	0.360836
Shape related properties		
Elongtion	0.01549	0.407585
Circle	0.154857	-0.34663
Surface topology related properties		
Convexity	-0.19067	-0.31566
Secondary size related properties		
Equivalent circle diameter in cell culture medium	0.228069	0.269571
Hydrodynamic size (PTA)	0.290018	0.121121
Hydrodynamic size (DLS)	0.168138	0.339699
Hydrodynamic size in cell culture medium (DLS)	-0.04119	0.403343

6.2.2 Construction of database

Data collected in all experiments/analyses are stored in **BOX** allowing each partner to access, to add data and to use the database at any time from the start of the project.

6.2.3 Integration the data

Question1: According to the nanotoxicity paradigm, ***the smaller the particle size the greater the toxicity***. To verify this paradigm, we compared the biological effects induced by SM (feret min ~34 nm) and LA (feret min~122 nm) in their dispersed state (PP dispersion). The analyses were performed only at the highest concentration tested as significant effects observed mostly at this concentration. *In vitro*, an analysis of genotoxic effects and glutathione (GSH) depletion was perfomed independent of cell type while the effect of TEER were analysed separately as the TEER values are cell type dependent. Figure 6.2.1 (*in vitro*) and 6.2.2 (*in vivo*) show the comparison of different biological effects induced by SM-PP and LA-PP performed using one-way ANOVA.

Significant difference between dispersions was observed only *in vitro* (figure 6.2.1). Interestingly, LA-PP showed significantly higher DNA damage than SM-PP (see fig 6.2.1A). In contrast to genotoxic effects, SM-PP decreased the TEER significantly compared to LA-PP only in HBE (figure 6.2.1C).

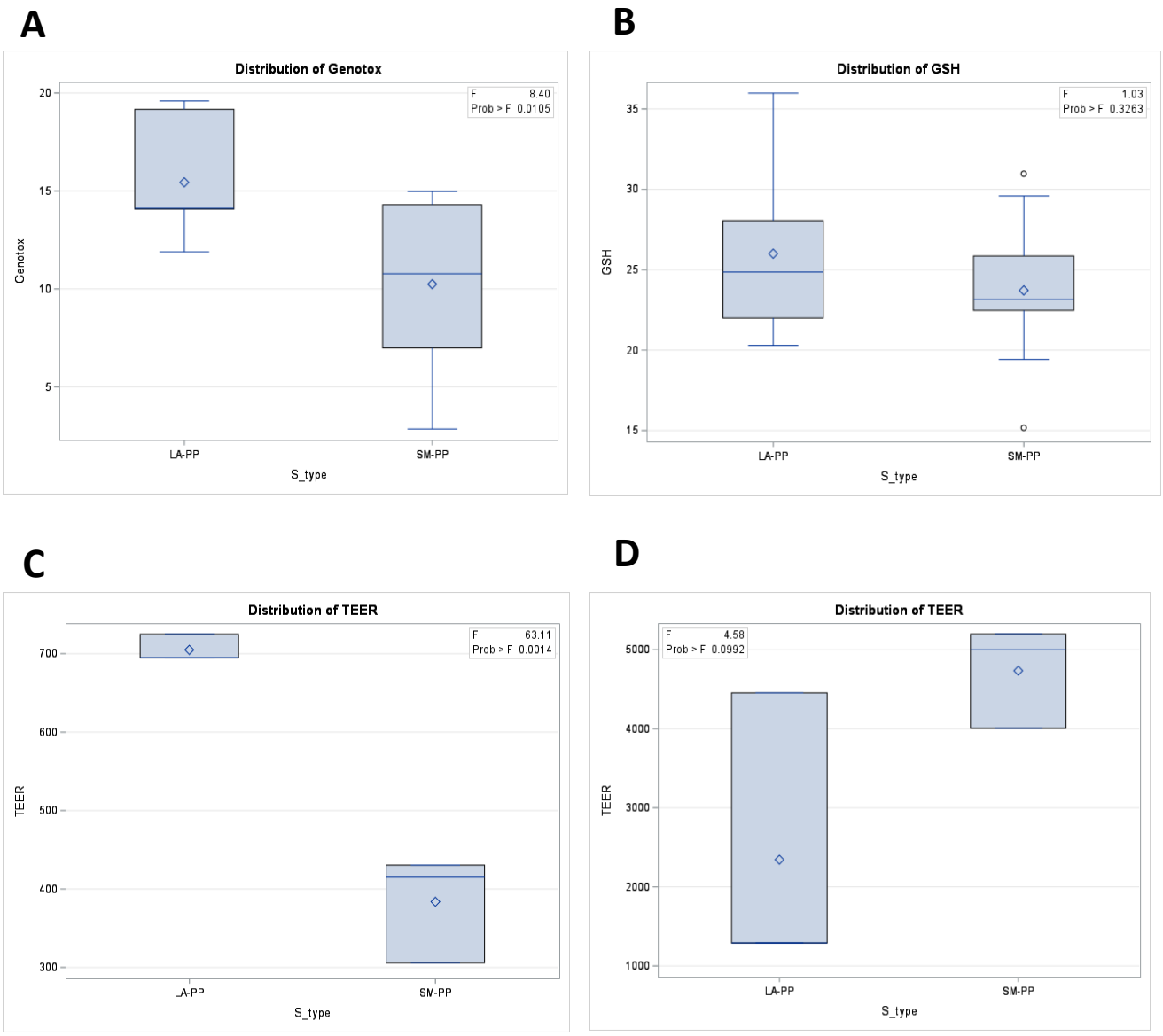

Figure 6.2.1: Comparison of *in vitro* biological endpoints after 24h exposure to SM-PP and LA-PP at 256 µg/ml. DNA damage (A), Glutathione depletion (B), TEER in HBE (C) and TEER in Caco2 (D). Significant differences between LA-PP and SM-PP were considered at $p<0.05$; The lines at the end of the box are upper and lower quartiles; The lines at the end of whisker are minimum and maximum extremes; vertical line in the middle-median; diamond symbol - mean. F-F value; Prob-P value.

In in *vivo* (figure 6.2.2), except DNA damage, no significant difference between dispersions was noticed. In contrast to *in vitro*, SM-PP induced significantly higher DNA damage than the LA-PP in gavaged mice (figure 6.2.2E) but not in aspirated mice (figure 6.2.2A). Taking all into account, the results suggest that exposure models and exposure routes influence the effect of agglomeration on genotoxicity. The nanotoxicity paradigm is not straightforward and needs to be investigated on a case by case basis.

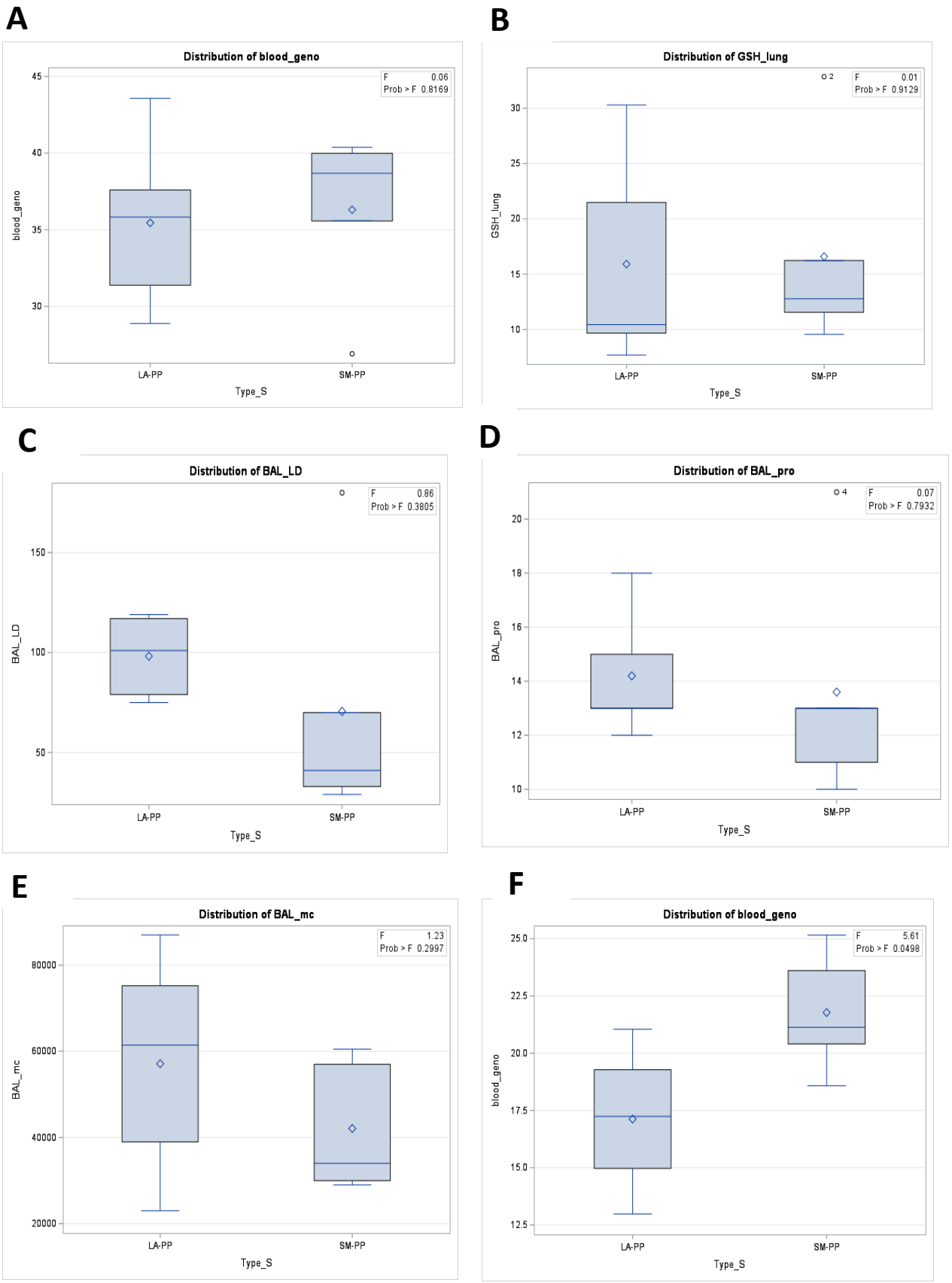

Figure 6.2.2: Comparison of *in vivo* biological endpoints 3d after exposure to SM-PP and LA-PP at 100 µg aspiration (A-E) or 500-µg gavage (F). Blood DNA damage in aspirated mice(A), Lung glutathione(B), BALF LDH (C), BALF proteins(D) , BAL macrophages (E) and Blood DNA damage in gavaged mice(F) . Significant differences between LA-PP and SM-PP were considered at $p<0.05$. The lines at the end of the box are upper and lower quartiles; The lines at the end of whisker are minimum

and maximum extremes; vertical line in the middle-median; diamond symbol - mean. F-F value; Prob-P value.

Question 2: According to EU definition, unbound particles or agglomerates of **size < 100 nm could be considered as nanomaterials** but not unbound particles or agglomerates with size >100. Therefore, we compared the biological effects induced by dispersion with feret min size < 100 (SM-PP) compared with dispersions altogether with feret min size >100 nm (SM-AGG, LA-PP, LA-AGG). Figures 6.2.3 and 6.2.4 show the grouping of dispersions based on size for different biological endpoints *in vitro* and *in vivo* respectively. Significant differences between dispersions were observed only *in vitro* (figure 6.2.3). Dispersions with size greater than 100 nm showed significantly higher genotoxic potential than those with size < 100 nm (figure 6.2.3A). In contrast to genotoxic effects, size<100 nm dispersion decreased the TEER only in HBE (figure 6.2.3C) significantly compared to size>100 nm but no difference found in Caco2 (figure 6.2.3D). For *in vivo* (figure 6.2.4), no significant difference between the sizes were noticed for the compared biological endpoints. These results suggest that TiO_2 unbound particles or agglomerates with size > 100 nm could be potentially toxic as nano sized TiO_2 (size<100 nm).

A

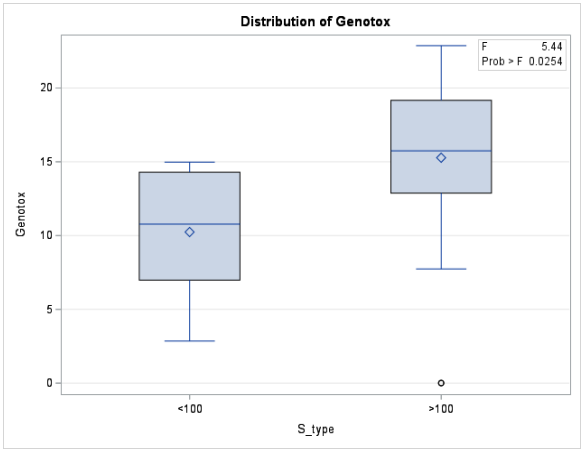

B

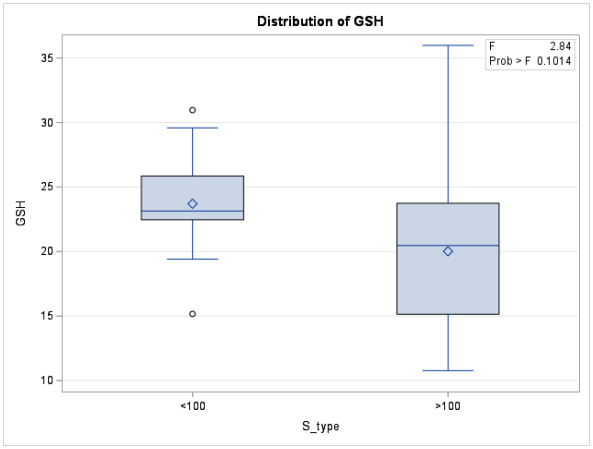

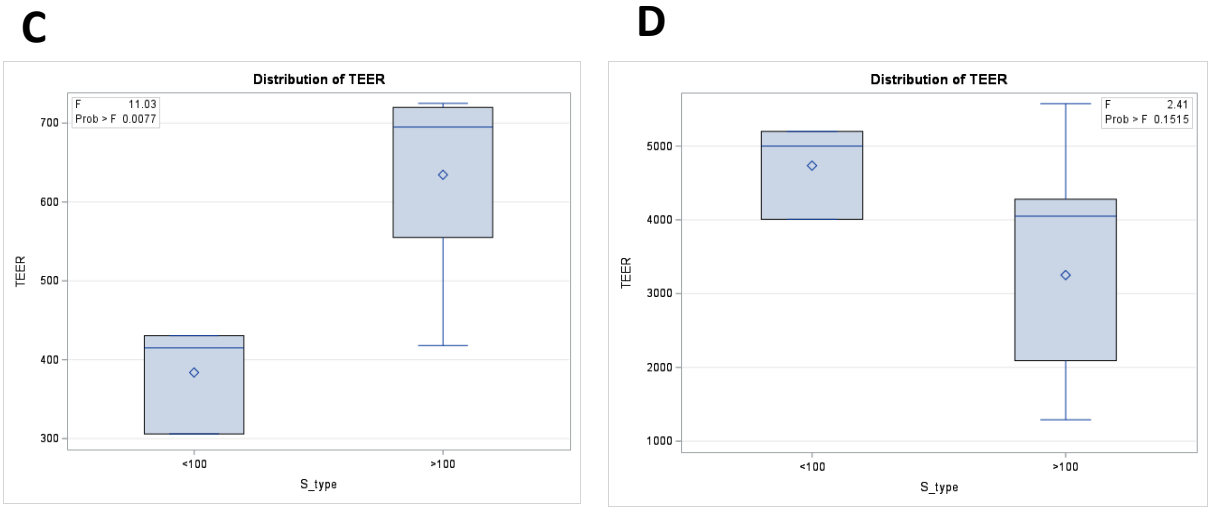

Figure 6.2.3: Grouping of dispersions based on size and comparison of *in vitro* biological endpoints observed at 256 µg/ml. DNA damage(A), Glutathione(B), TEER in HBE (C) and TEER in Caco2(D). Significant differences between LA-PP and SM-PP were considered at p<0.05. The lines at the end of the box are upper and lower quartiles; The lines at the end of whisker are upper and lower extremes; vertical line in the middle-median; diamond symbol - mean. F-F value; Prob-P value.

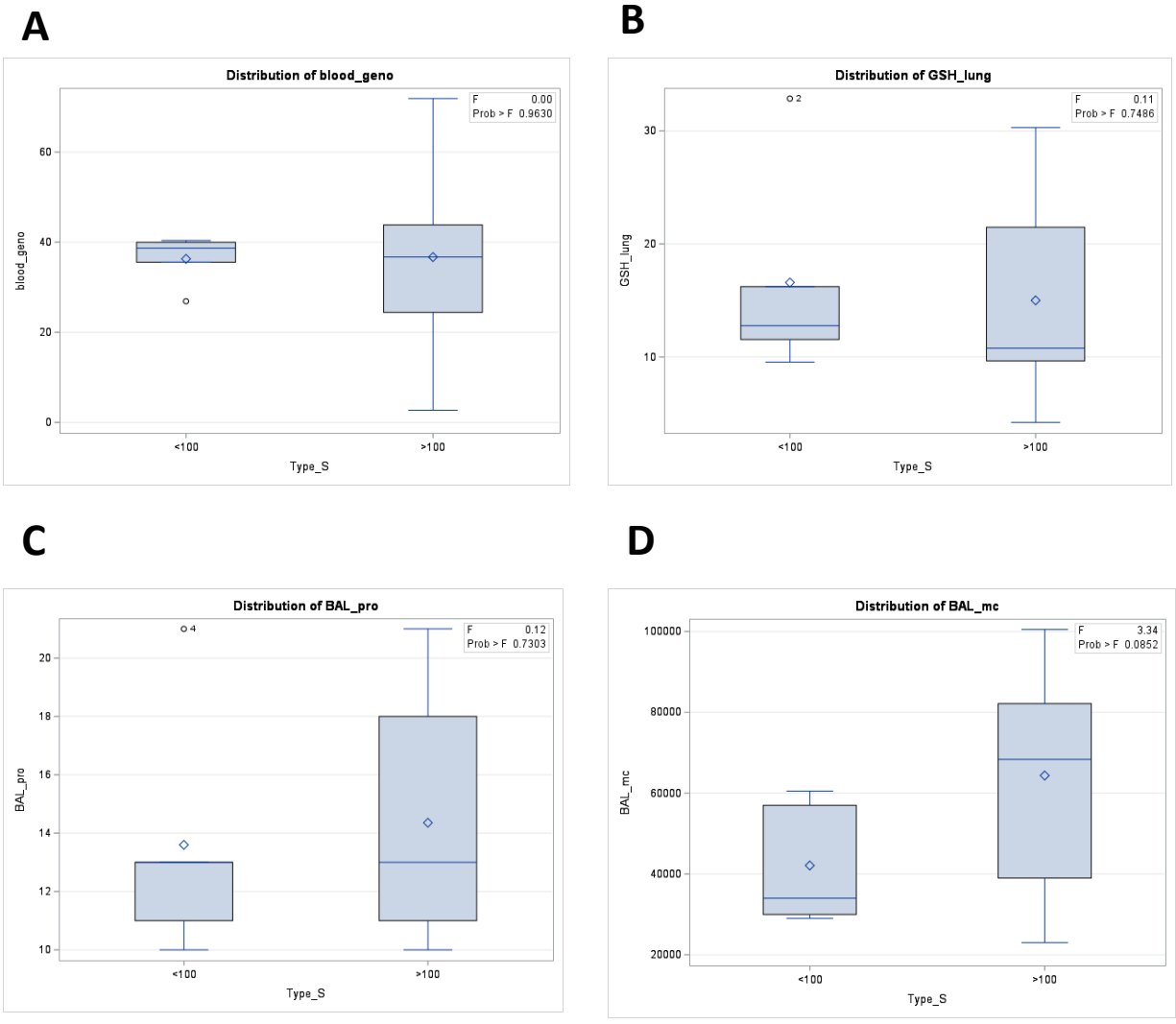

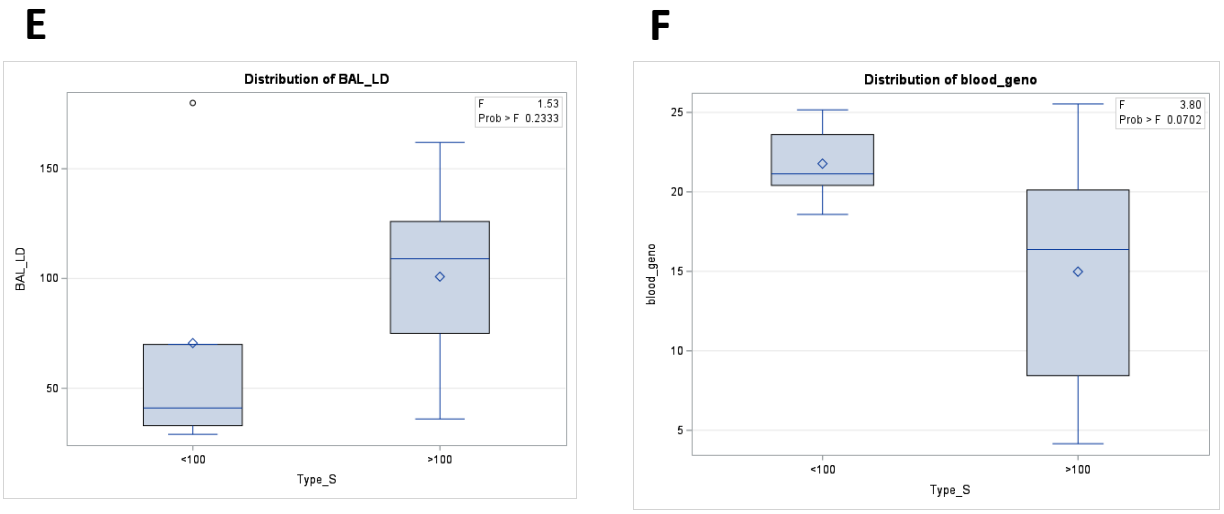

Figure 6.2.4: Grouping of dispersions based on size and comparison of different *in vivo* biological endpoints 3d after at 100 µg aspiration (A-E) or 500 µg gavage (F). Blood DNA damage in aspirated mice (A), Lung glutathione (B), BALF proteins(C), BAL macrophages (D), BALF LDH (E) and Blood DNA damage (F) in gavaged mice. Significant differences between LA-PP and SM-PP were considered at $p<0.05$. The lines at the end of the box are upper and lower quartiles; The lines at the end of whisker are minimum and maximum extremes; vertical line in the middle-median; diamond symbol - mean. F-F value; Prob-P value.

Question 3: To verify the extent of **variability in toxicity/biological responses observed in different cell lines**, principal component analysis (PCA) was used. Figure 6.2.5 shows PCA analysis performed for different biological endpoints in different cell lines including dose as a variable. The results show that all the dispersions grouped very close to each other for HBE and Caco2. For THP-1, LA-PP induced somewhat distinct effects compared to other dispersions that are grouped together (6.2.5C). HBE and Caco2 are adherent cells but THP-1 is a suspension cell type and professional phagocytes. Therefore, cell type might contribute to the observed differences.

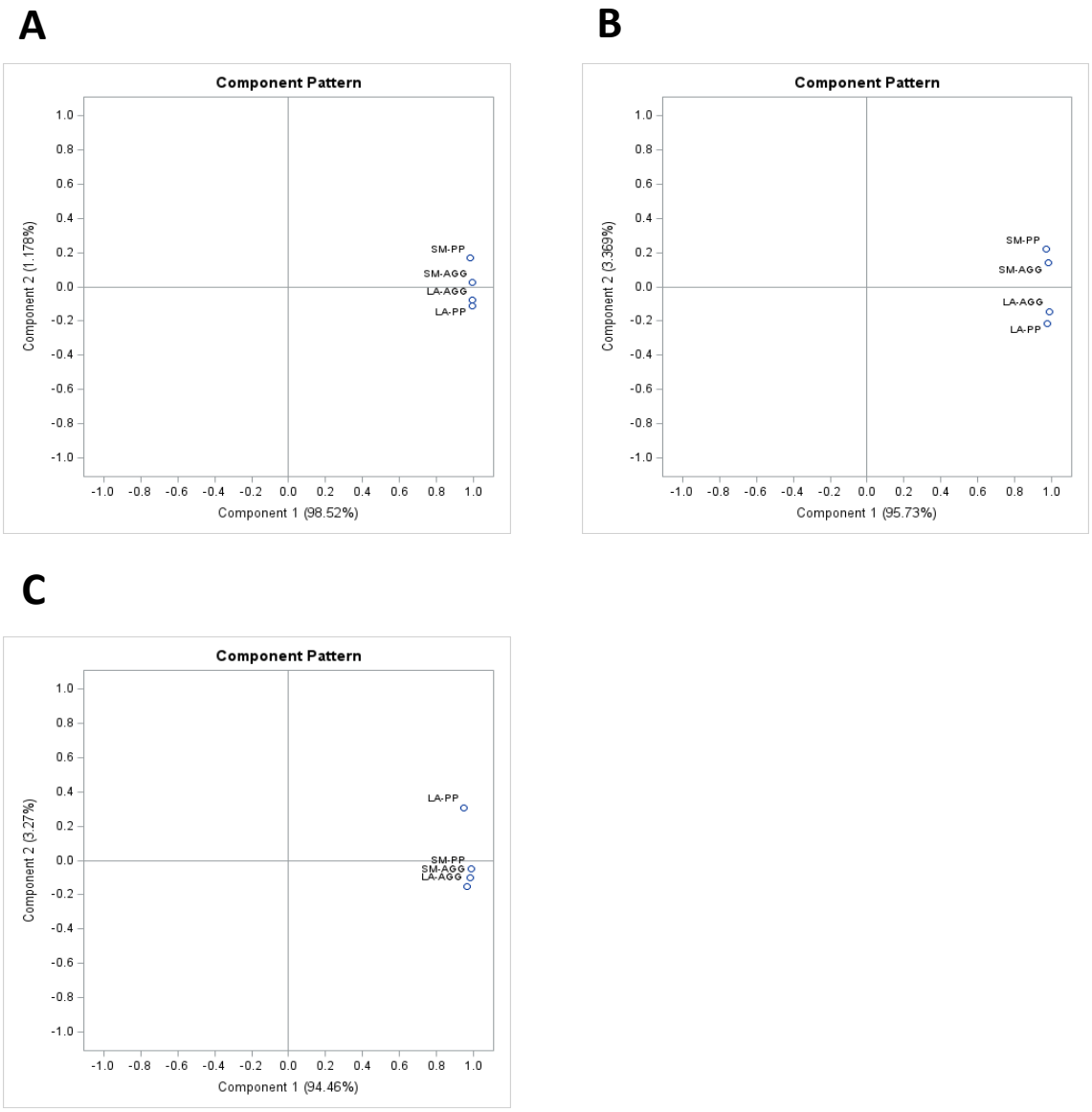

Figure 6.2.5: PCA analysis performed with all biological endpoints in three different cell lines. HBE (A), Caco2 (B) and THP1 (C).

Question 4: Which **physical characteristics (different measurands) are associated with toxicity.** As shown in table 6.2.1, size related properties are strongly correlated to Principal component (PC) 1 (marked in red in PC1 column) while shape/surface topology/secondary size related properties (marked in red in PC2 column) are correlated in PC 2. Therefore, with PC 1 and PC 2, linear regression analyses were performed and such analyses was controlled for dose (also cell type *in vitro*). Table 6.2.2 and 6.2.3 shows regression analysis performed for *in vitro* and *in vivo* respectively. For *in vitro*, PC 1 i.e size related properties are associated with GSH depletion, genotoxicity and IL6 while PC2 associated with IL8. For aspiration *in vivo* (Table 6.2.3A), it is only blood genotoxicity which showed significant relationship with PC1 while BAL genotoxicity, lung glutathione and Ti biodistribution significantly associated only with dose. For gavage *in vivo* (Table 6.2.3B), its only blood genotoxicity which showed significant relationship with PC1.

Table 6.2.2: Linear regression analysis performed with PCs and *in vitro* biological endpoints. Biological endpoints that are significantly associated with either PC1 (Size related properties) or PC2 (Shape/topology/secondary size) related properties) or concentration (conc) was only shown in the table. R^2 - regression coefficient indicating how close the data are to the fitted regression line.

Biological endpoints	PC1	PC2	conc
	R^2	R^2	R^2
Glutathione depletion	0.5445	-	-
IL8	-	0.7484	-
Trans-epithelial electrical resistance	-	-	0.8266
IL6	0.9519	-	-
Genotoxicity	0.6859	-	-

Table 6.2.3: Linear regression analysis performed with PCs and biological endpoints *in vivo.* Biological endpoints that are significantly associated with either PC1 (Size related properties) or PC2 (Shape/topology/secondary size) related properties) or concentration (conc) was only shown in the table. R^2 - regression coefficient indicating how close the data are to the fitted regression line.

A

Biological endpoints	PC 1	PC 2	Dose
	R^2	R^2	R^2
Blood genotoxicity	0.3770	-	-
BAL genotoxicity	-	-	0.5412
Lung glutathione	-	-	0.6270
Ti in lung tissue	-	-	0.6697

B

Biological Endpoints	PC 1	PC 2	Dose
	R^2	R^2	R^2
Blood genotoxicity	0.248509	-	-

6.2.4 Dissemination of the findings

Please refer section 9 for dissemination

7 DISCUSSION \ RECOMMENDATIONS

The main objective of this project was to address the influence of AA on the toxic activity of MNM and to verify how these parameters can be characterized analytically in a precise, repeatable and operational manner. Our results suggest that (i) Adaptation of the conditions of the dispersion protocols allowed to reproducibly generate different AA states (ii) agglomeration state of TiO_2 NMs and aggregation state of silica NMs can influences the toxicity and biological activity.

Compared to other existing protocols (Lankoff et al. 2012)(Magdolenova et al. 2012)(Zook et al. 2011), our dispersion protocol generated different TiO_2 agglomeration status with no/minimal changes in the dispersants and thus more reliable to study the influence of TiO_2 agglomeration on toxicity. Further, the vortexed dispersion (AGGR, SuperN and PREC) of silica used in this study could be more realistic in terms of exposure than dispersion protocols aiming for the most dispersed state (such as DE-AGGR), as the former represents the silica aggregates as manufactured and as applied in products.

Size distribution is the key to classify nanomaterial according the EU definition. The TEM based methodology (De Temmerman et al. 2012) applied in this study allowed to characterize the number-based size distribution of the AA in dispersion quantitatively. DLS and PTA measurements were shown to be less accurate compared to TEM based methods to characterize the size distribution of AA. Due to the manner of assessment, DLS and PTA measurements are biased when few large AA are present. Combining the developed and validated SOPs for dispersion and characterization of the constituent particles of silica and TiO_2 particles by TEM allowed to implement the EC definition. Measurements were most precise when the highest degree of dispersion was obtained.

The *in vitro* dosimetry protocol used in this study (Deloid et al. 2014) is very reproducible and can be used to identify whether the delivered dose was a confounder, when determining the influence of AA on toxicity. The conclusion of our study is that differential sedimentation of the different TiO_2 and silica preparations is unlikely to significantly confound the results of the present investigations.

We observed that the influence of agglomeration state on toxicity was primary particle size, cell type (*in vitro)* (as observed in Rabolli et al. 2010) or exposure route dependent (*in vivo)*. This indicates that these parameters must be taken into consideration when assessing the influence of agglomeration on toxicity. For silica, aggregation state influences the *in vitro* toxicity depending on the size distribution of the aggregated fraction. For instance, very big aggregates in PREC did not exhibit any biological activity while SuperN comprised of relatively smaller aggregates exhibited toxic effects.

The nanotoxicity paradigm “the smaller the size the greater the toxicity” is not always true and is biological endpoint-dependent. For instance, *in vitro*, SM-PP induced stronger oxidative stress, altered barrier integrity and pro-inflammatory responses compared to LA-PP but we found that LA-PP is relatively more genotoxic compared to SM-PP. *In vivo*, SM-AGG induced stronger lung damage and inflammation compared to SM-PP. For silica, aggregates

in superN fractions showed similar toxic potential compared to unbound particles/smaller aggregates in DE-AGGR.

Genotoxicity is an important endpoint to classify nanomaterials according to their hazardous nature. In this study, we found that the TiO_2 agglomerates of small nanoparticles (SM-AGG) and primary large particles (LA-PP) with feret min size ~ 120 nm could be potentially genotoxic (both *in vitro* and *in vivo*) compared to SM-PP with feret min size ~30 nm. Precipitated silica is non-genotoxic as observed in many other *in vitro* studies (Murugadoss et al. 2017) and its aggregation state does not influence this.

For silica NMs, the most intriguing is the comparison between DE-AGGR and SuperN. Dispersions with the same mass doses revealed that both suspensions induced similar effects; indicating that there is a fraction of particles/aggregates (feret min size>100 nm) in their manufactured form that could be potentially hazardous as nano-sized silica (feret min size<100 nm).

Our statistical analysis indicate that the biological effects (*in vitro* and *in vivo)* observed in this study are mostly associated with size related properties of TiO_2. Thus, size remain the best parameter to define nanomaterials with regard to hazard.

8 CONCLUSIONS

The EC Recommendation on the definition of nanomaterial (2011/696/EU) clearly states that the definition in this Recommendation should be used as a reference for determining whether a material should be considered as a 'nanomaterial' for legislative and policy purposes in the European Union. The definition of the term 'nanomaterial' in European Union legislation is based solely on the size of the constituent particles of a material, without regard to hazard or risk.

The observations of this project - although limited to two case studies - indicate that agglomerates and aggregates with size > 100 nm exhibited similar (or in some cases even stronger) toxic potential compared to their nanocounterparts (size<100 nm). This illustrate clearly that 100 nm threshold in the current EU definition is not appropriate to classify nanomaterial with regard to hazard because (i) (nano) scale phenomena do not change abruptly at a size larger than 100 nm, (ii) AA results in size greater than 100 nm but still the surface of primary particles are held together and exposed externally. This is clearly recognised in nanomaterial definitions adopted by Health Canada and Taiwan Council of labors (Boverhof et al. 2015) and AA of size larger than 100 nm is considered in those definitions.

The physicochemical properties of each type of TiO_2 NMs and silica NMs (Napierska et al. 2010) are different and shown to exhibit different biological activity (Di Cristo et al. 2016). Therefore, the results of this study may only be applicable to the anatase TiO_2 and precipitated silica However, dispersion protocols developed in this study can be applied for other types of TiO_2 and silica – and probably also for many other types of particulate materials at a size below 0.5 µm in diameter.

9 DISSEMINATION AND VALORISATION

9.1 Poster/conference papers in international conferences

Eurotox (Brussels): **Influence of dispersion method on silica nanomaterial size distribution/aggregation and their chronic toxicity *in vitro***. Sivakumar Murugadoss, Sybille Van Den Brule ,Dominique Lison, Lode Godderis, Jan Mast, Frederic Brassinne, Noham Sebaihi and Peter Hoet; Toxicology Letters 280:S190. September 2018; https://doi.org/10.1016/j.toxlet.2018.06.906; Journal impact factor (2016) – 3,858

Eurotox (Brussels): **Characterization of the TiO2 E171 food additive**. Frédéric Brassinne, Sandra De Vos, Eveline Verleysen, Pieter-Jan De Temmerman, Marina Ledecq, Jan Mast ; Toxicology Letters 280:S190. September 2018;

Society of Toxicology (San Antonio, United States): **Influence of Titanium-di-oxide nanomaterials agglomeration on toxicity and biological responses *in vitro***. S. Murugadoss, S. Van Den Brule, N. Sebaihi, F. Brassinne, J. Mast, L.Godderis, D. Lison and P. Hoet. San Antonio, Texas,. March 10th to 15^{th,} 2018.

Beltox (Leuven): **Cytotoxicity of silica nanoparticles: comparison between nanofractions and their micron-sized aggregates**; Sivakumar Murugadoss, Dominique Lison, Lode Godderis, Sybille Van Den Brule, Jan Mast, Frederic Brassinne, Noham Sebaihi, Peter H. Hoet; Beltox Annual meeting; December 1st, 2017; Leuven, Belgium.

Eurotox (Bratislava, Slovakia): **Toxicity and biological responses (in vitro) influenced by aggregation and agglomeration of manufactured nanomaterials**; Sivakumar Murugadoss, Sybille Van Den Brule ,Dominique Lison, Lode Godderis, Jan Mast, Frederic Brassinne, Noham Sebaihi and Peter Hoet; Toxicology Letters 280:S190. October 2017; DOI: 10.1016/j.toxlet.2017.07.535; Journal impact factor (2016) – 3,858

Conférence Internationale de Métrologie (Paris): To^{2}DeNano : Towards a toxicologically-relevant definition of nanomaterials. N. Sebaihi, B. De Boeck, M. Coenegrachts, J. Pétry, F. Brassinne, J. Mast, S. Murugadoss, S. Van Den Brule, D. Lison, L. Godderis, P. Hoet. Paris, France, September 2017.

9.2 Oral presentation in international conferences

in-vitro and in-vivo genotoxicity of titanium-di-oxide nanomaterials influenced by its dispersion state. Sivakumar Murugadoss, Sybille Van Den Brule ,Dominique Lison, Lode Godderis, Jan Mast, Frederic Brassinne, Noham Sebaihi and Peter Hoet. 6th International conference on Health and Safety issue related to nanomaterials for a socially responsible approach; Nanosafe 2018.

10 PUBLICATIONS

10.1 Article in peer review journals

Toxicology of silica nanoparticles: an update; Sivakumar Murugadoss, Dominique Lison, Lode Godderis, Sybille Van Den Brule, Jan Mast, Frederic Brassinne, Noham Sebaihi, Peter H. Hoet; Archives of Toxicology, DOI 10.1007/s00204-017-1993-y; Journal impact factor (2016)- 6.6

10.2 Article in preparation/submitted soon

Testing the relevance of the EU definition of nanomaterials with synthetic amorphous silica nanoparticles. Sivakumar Murugadoss, Sybille Van Den Brule, Jan Mast, Frederic Brassinne, Noham Sebaihi and Lode Godderis, Dominique Lison and Peter Hoet.

Testing the toxicological relevance of the EU definition of nanomaterials with titanium-di-oxide agglomerates. Sivakumar Murugadoss, Sybille Van Den Brule, Jan Mast, Frederic Brassinne, Noham Sebaihi and Lode Godderis, Dominique Lison and Peter Hoet.

Comparison of validated TEM, DLS and PTA methods to characterize precisely and accurately the primary particles and the aggregates and agglomerates. Frédéric Brassinne, Eveline Verleysen, Pieter-Jan De Temmerman, Jan Mast.

10.3 Other valorisation

The results of TEM, DLS and PTA characterization methods are presented in the test environment of Belgian Nanoregister. This was used to demonstrate to the Belgian authority that it is possible to make a complete physicochemical characterization of nanomaterials according to the Royal Decree of the 27th May 2014 which request the registration of full physicochemical characterization of the nanomaterials brought on the Belgian market.

11 ACKNOWLEDGEMENTS

We would like to acknowledge

1. BELSPO and Brain-be program for funding this project. Our special thanks to Mrs. BOURGEOIS Emmanuèle.
2. Our follow up committee **(**Gert Roebben, Alain Piette, Linda Wouters, Evelien Frijns, Carine Gorrebeeck, Agnieszka Dobra, Xavier Van Huffel, Wendie Claeys, Valérie Vromman, Benjamin DELCOURT) for the meetings and suggestions
3. Joint Research Commission (JRC) for providing TiO_2 and SiO_2 NMs

12 BIBLIOGRAPHY

Bouwmeester H, Lynch I, marvin HJP, et al (2011) Minimal analytical characterization of engineered nanomaterials needed for hazard assessment in biological matrices. Nanotoxicology 5:1–11. doi: 10.3109/17435391003775266

Boverhof DR, Bramante CM, Butala JH, et al (2015) Comparative assessment of nanomaterial definitions and safety evaluation considerations. Regul Toxicol Pharmacol 73:137–150. doi: 10.1016/J.YRTPH.2015.06.001

Brasil A., Farias T., Carvalho M., Koylu U. (2001) Numerical characterization of the morphology of aggregated particles. J Aerosol Sci 32:489–508. doi: 10.1016/S0021-8502(00)00097-5

Brasil AM, Farias TL, Carvalho MG (1999) A RECIPE FOR IMAGE CHARACTERIZATION OF FRACTAL-LIKE AGGREGATES. J Aerosol Sci 30:1379–1389. doi: 10.1016/S0021-8502(99)00026-9

De Temmerman P-J, Van Doren E, Verleysen E, et al (2012) Quantitative characterization of agglomerates and aggregates of pyrogenic and precipitated amorphous silica nanomaterials by transmission electron microscopy. J Nanobiotechnology 10:24. doi: 10.1186/1477-3155-10-24

De Temmerman PJ, Verleysen E, Lammertyn J, Mast J (2014) Semi-automatic size measurement of primary particles in aggregated nanomaterials by transmission electron microscopy. Powder Technol 261:191–200. doi: 10.1016/j.powtec.2014.04.040

Deloid G, Cohen JM, Darrah T, et al (2014) Estimating the effective density of engineered nanomaterials for in vitro dosimetry. Nat Commun 5:3514. doi: 10.1038/ncomms4514

Di Cristo L, Movia D, Bianchi MG, et al (2016) Proinflammatory effects of pyrogenic and precipitated amorphous silica nanoparticles in innate immunity cells. Toxicol Sci 150:40–53. doi: 10.1093/toxsci/kfv258

Drobne D (2007) Nanotoxicology for Safe and Sustainable Nanotechnology. Arch Ind Hyg Toxicol 58:471–478. doi: 10.2478/v10004-007-0040-4

EU (2011) Commission recommendation of 18 October 2011 on the definition of nanomaterial (2011/696/EU)

Gaté L, Disdier C, Cosnier F, et al (2017) Biopersistence and translocation to extrapulmonary organs of titanium dioxide nanoparticles after subacute inhalation exposure to aerosol in adult and elderly rats. Toxicol Lett 265:61–69. doi: 10.1016/j.toxlet.2016.11.009

Guiot C, Spalla O (2013) Stabilization of TiO2 nanoparticles in complex medium through a pH adjustment protocol. Environ Sci Technol 47:1057–1064. doi: 10.1021/es3040736

Hoet PH, Brüske-Hohlfeld I, Salata O V (2004) Nanoparticles – known and unknown health risks. J Nanobiotechnology 2:12. doi: 10.1186/1477-3155-2-12

Kreyling WG, Hirn S, Schleh C (2010) Nanoparticles in the lung. Nat Biotechnol 28:1275–1276. doi: 10.1038/nbt.1735

Lankoff A, Sandberg WJ, Wegierek-Ciuk A, et al (2012) The effect of agglomeration state of silver and titanium dioxide nanoparticles on cellular response of HepG2, A549 and THP-1 cells. Toxicol Lett 208:197–213. doi: 10.1016/j.toxlet.2011.11.006

Linsinger T, Roebben G, Gilliland D, et al (2012) Requirements on measurements for the implementation of the European Commission definition of the term “nanomaterial”. Publications Office

Lison D, Vietti G, van den Brule S (2014) Paracelsus in nanotoxicology. Part Fibre Toxicol 11:35. doi: 10.1186/s12989-014-0035-7

Luyts K, Napierska D, Nemery B, Hoet PHM (2013) How physico-chemical characteristics of nanoparticles cause their toxicity: complex and unresolved interrelations. Environ Sci Process Impacts 15:23–38. doi: 10.1039/C2EM30237C

Magdolenova Z, Bilaničová D, Pojana G, et al (2012) Impact of agglomeration and different dispersions of titanium dioxide nanoparticles on the human related in vitro cytotoxicity and genotoxicity. J Environ Monit 14:455. doi: 10.1039/c2em10746e

Mast J, Verleysen E, De Temmerman P-J (2015) Physical Characterization of Nanomaterials

in Dispersion by Transmission Electron Microscopy in a Regulatory Framework. In: Advanced Transmission Electron Microscopy. Springer International Publishing, Cham, pp 249–270

Maynard AD (2007) Nanotechnology: The next big thing, or much ado about nothing? Ann. Occup. Hyg. 51:1–12

Murugadoss S, Lison D, Godderis L, et al (2017) Toxicology of silica nanoparticles: an update. Arch Toxicol 91:2967–3010. doi: 10.1007/s00204-017-1993-y

Napierska D, Thomassen LCJ, Rabolli V, et al (2009) Size-Dependent Cytotoxicity of Monodisperse Silica Nanoparticles in Human Endothelial Cells. Small 5:846–853. doi: 10.1002/smll.200800461

Nel A, Xia T, Mädler L, Li N (2006) Toxic potential of materials at the nanolevel. Science (80-.). 311:622–627

Oberdörster G, Oberdörster E, Oberdörster J (2005) Nanotoxicology: An Emerging Discipline Evolving from Studies of Ultrafine Particles. Environ Health Perspect 113:823–839. doi: 10.1289/ehp.7339

OECD (2010) OECD Environmental, Health and Safety Publications - Series on the safety of manufactured nanomaterials. Env/Jm/Mono(2010)46 1–16. doi: ENV/JM/MONO(2007)10

Potočnik J (2011) Commission recommendation of 18 October 2011 on the definition of nanomaterial (2011/696/EU). Off J Eur Union. doi: 10.2777/13162

Pujalté I, Dieme D, Haddad S, et al (2017) Toxicokinetics of titanium dioxide (TiO2) nanoparticles after inhalation in rats. Toxicol Lett 265:77–85. doi: 10.1016/j.toxlet.2016.11.014

Rabolli V, Thomassen LCJ, Princen C, et al (2010) Influence of size, surface area and microporosity on the *in vitro* cytotoxic activity of amorphous silica nanoparticles in different cell types. Nanotoxicology 4:307–318. doi: 10.3109/17435390.2010.482749

Rasmussen K, Mast J, Temmerman P-J De, et al (2014) Titanium Dioxide, NM-100, NM-101, NM-102, NM-103, NM-104, NM-105: Characterisation and Physico- Chemical Properties

Rasmussen K, Mech A, Mast J, et al (2013) JRC SCIENTIFIC AND POLICY REPORTS

SCENIHR (2010) Scientific Basis for the Definition of the Term " Nanomaterial ." Sci Comm Emerg New Identified Heal Risks 1–43. doi: 10.2772/ND-The

Warheit DB, Sayes CM, Reed KL, Swain KA (2008) Health effects related to nanoparticle exposures: Environmental, health and safety considerations for assessing hazards and risks. Pharmacol Ther 120:35–42. doi: 10.1016/j.pharmthera.2008.07.001

Zook JM, MacCuspie RI, Locascio LE, et al (2011) Stable nanoparticle aggregates/agglomerates of different sizes and the effect of their size on hemolytic cytotoxicity. Nanotoxicology 5:517–530. doi: 10.3109/17435390.2010.536615

(2014) KONINKLIJK BESLUIT BETREFFENDE HET OP DE MARKT BRENGEN VAN STOFFEN GEPRODUCEERD IN NANOPARTICULAIRE TOESTAND [C-2014/24329]. BELGISCH Staatsbl 76184

(2008) Nanotechnologies-Terminology and definitions for nano-objects-Nanoparticle, nanofibre and nanoplate Nanotechnologies-Terminologie et définitions relatives aux nano-objets-Nanoparticule, nanofibre et nanoplat Provläsningsexemplar / Preview